ASSESSMENT OF THE EFFECTS OF CARBON DIOXIDE INJECTION ON THE RESERVOIR FORMATION, CAPROCK AND WELLBORE INTEGRITY

A THESIS SUBMITTED TO
THE GRADUATE SCHOOL OF NATURAL AND APPLIED SCIENCES
OF
MIDDLE EAST TECHNICAL UNIVERSITY

BY

ABDIRIZAK ALI OMAR

IN PARTIAL FULFILLMENT OF THE REQUIREMENTS
FOR
THE DEGREE OF MASTER OF SCIENCE
IN
PETROLEUM AND NATURAL GAS ENGINEERING

DECEMBER 2019

Approval of the Thesis:

ASSESSMENT OF THE EFFECTS OF CARBON DIOXIDE INJECTION ON THE RESERVOIR FORMATION, CAPROCK AND WELLBORE INTEGRITY

submitted by **ABDIRIZAK ALI OMAR** in partial fulfillment of the requirements for the degree of **Master of Science in Petroleum and Natural Gas Engineering Department, Middle East Technical University** by,

Prof. Dr. Halil Kalıpçılar
Dean, Graduate School of **Natural and Applied Sciences** _____

Assoc. Prof. Dr. Çağlar Sınayuç
Head of Department, **Petroleum and Natural Gas Engineering** _____

Assoc. Prof. Dr. Çağlar Sınayuç
Supervisor, **Petroleum and Natural Gas Eng. Dept., METU** _____

Examining Committee Members:

Prof. Dr. Mahmut Parlaktuna
Petroleum and Natural Gas Engineering Dept., METU _____

Assoc. Prof. Dr. Çağlar Sınayuç
Petroleum and Natural Gas Engineering Dept., METU _____

Assoc. Prof. Dr. Emre Artun
Petroleum and Natural Gas Engineering Dept., METU NCC _____

Date: 25.12.2019

I hereby declare that all information in this document has been obtained and presented in accordance with academic rules and ethical conduct. I also declare that, as required by these rules and conduct, I have fully cited and referenced all material and results that are not original to this work.

Name, Last name: Abdirizak Ali, Omar

Signature:

ABSTRACT

ASSESSMENT OF THE EFFECTS OF CARBON DIOXIDE INJECTION ON THE RESERVOIR FORMATION, CAPROCK AND WELLBORE INTEGRITY

Omar, Abdirizak Ali
M.Sc., Department of Petroleum and Natural Gas Engineering
Supervisor: Assoc. Prof. Dr. Çağlar Sınayuç

December 2019, 111 pages

Climate change is currently one of the most serious issues affecting the planet earth and its population. The continuously increasing concentration of carbon dioxide (CO_2) in the atmosphere is a major culprit. In efforts to mitigate climate change, Carbon Capture and Storage (CCS) projects have been initiated whereby CO_2 is captured and injected into deep geological formations. However, a major point of concern is the safety and risk involved in the geological sequestration of CO_2. To reduce this risk, it is important to characterize the formations and understand the effects of CO_2 injection on them.

This study aims to understand the effects of CO_2 injection on the reservoir, caprock and wellbore cement integrity. TOUGHREACT is used for numerical simulation of CO_2 injection into a hydrocarbon and a geothermal reservoir. The effect of CO_2 on wellbore cement is also modeled. Results showed that in the carbonate hydrocarbon reservoir, the injected CO_2 was mainly stored by seal trapping and solubility trapping. There was a reduction in the caprock porosity and permeability indicating an improvement in its seal properties. In the geothermal reservoir, injected CO_2 was mainly stored via solubility trapping and mineral trapping. There was some free CO_2 in cases of high injection rates which was stored by seal trapping. The modeling of the cement plug showed that CO_2 presence caused cement degradation. In the presence of a micro-silica additive, CO_2 penetrated less into the plug and there was relatively less degradation. Under high temperature conditions, the degradation was more prominent. However, it was noted that in general, the cement degradation is a very slow process due to its self-inhibiting nature.

Keywords: climate change, CO_2 storage, sequestration, caprock integrity, cement integrity, TOUGHREACT

ÖZ

KARBONDIOKSİT ENJEKSİYONUN REZERVUARA, ÖRTÜ KAYACA VE KUYU BÜTÜNLÜĞÜNE ETKİLERİNİN DEĞERLENDİRİLMESİ

Omar, Abdirizak Ali
Yüksek Lisans, Petrol ve Doğal Gaz Mühendisliği Bölümü
Tez Yöneticisi: Doç. Dr. Çağlar Sınayuç

Aralık 2019, 111 sayfa

İklim değişikliği şu anda dünya gezegenini ve içinde yaşayan nüfusu etkileyen en ciddi konulardan biridir. Atmosferdeki sürekli artan karbondioksit (CO_2) konsantrasyonu bu durumun önemli bir sebebidir. İklim değişikliğini hafifletme çabaları kapsamında, CO_2'in yakalandığı ve derin jeolojik oluşumlara enjekte edildiği Karbon Yakalama ve Depolama (CCS) projeleri başlatıldı. Bu konu ile alakalı olarak büyük bir endişe kaynağı CO_2'in jeolojik depolanması ile ilgili güvenlik ve risktir. Bu riski azaltmak için, oluşumları karakterize etmek ve CO_2 enjeksiyonunun bunlar üzerindeki etkilerini anlamak önemlidir.

Bu çalışma, CO_2 enjeksiyonunun rezervuar, örtü kayaç ve kuyu çimento bütünlüğü üzerindeki etkilerini anlamayı amaçlamaktadır. TOUGHREACT, bir hidrokarbon ve bir jeotermal rezervuar içine CO_2 enjeksiyonunun sayısal simülasyonu için kullanıldı. Bunun yanında CO_2'in kuyu içi çimentosu üzerindeki etkisi de modellenmiştir. Sonuçlar, karbonat hidrokarbon rezervuarında enjekte edilen CO_2'in esasen hapsetme ve çözünürlük kapanı ile depolandığını göstermiştir. Örtü kayaç gözenekliliğinde ve geçirgenliğinde azalma olmuştur ve bu depolama özelliklerinde bir iyileşme olduğunu gösterir. Jeotermal rezervuarında enjekte edilen CO_2, genel olarak çözünürlük kapanı ve mineral kapanı yoluyla depolandı. Yüksek enjeksiyon oranlarında hapsetme sebebiyle CO_2'in serbest bir faz olarak depolandığı durumlar da gözlendi. Çimento tapasının modellenmesi CO_2 varlığının çimento bozulmasına neden olduğunu göstermiştir. Bir mikro-silika katkı maddesinin varlığında, CO_2 tapanın içine daha az nüfuz etmiştir ve nispeten daha az bozulma olmuştur. .Yüksek sıcaklık koşullarında çimento tapasındaki bozulma daha

belirgindi. Bununla birlikte, genel olarak, çimento bozulmasının, kendi kendini sınırlandırıcı doğası nedeniyle çok yavaş bir süreç olduğu da gözlemlendi.

Anahtar Kelimeler: iklim değişikliği, CO_2 depolanması, ayrılma, örtü kayaç bütünlüğü, çimento bütünlüğü, TOUGHREACT

To My Parents

ACKNOWLEDGEMENTS

I would like to express my sincere gratitude to my supervisor Assoc. Prof. Dr. Çağlar Sınayuç for his guidance, advice, support, encouragement, and patience throughout my graduate studies.

I am grateful to TÜBITAK and Assoc. Prof. Dr. Çağlar Sınayuç for awarding me a graduate research scholarship for a portion of my graduate studies.

It is incumbent that I express my gratitude to all my instructors at METU, especially in the Department of Petroleum & Natural Gas Engineering, who have played an important and irreplaceable role in my undergraduate and graduate education.

I would also like to thank my colleague Onur Alp Kaya for his constructive feedback during the preparation of this thesis. Many thanks to Serhat Küçük as well for his helpful advice on modeling using TOUGHREACT.

A special note of thanks to Balqisa Ali Omar who provided help and feedback on the formatting of this document and illustrations herein. Many thanks for her comments of encouragement as well.

I am also grateful to my friends and flatmates for their support, encouragement, and patience throughout the period of the preparation of this thesis.

Finally, I would like to express my deepest thanks and gratitude to my family for their unwavering support and encouragement during my studies. A sincere thank you to my mother, Khadija Mayow Abukar, who has never compromised on my education and always made it a priority regardless of the circumstances. I would like to express my gratitude to my father, Ali Omar Mohamed, as well for his support and encouragement throughout my studies.

TABLE OF CONTENTS

LIST OF TABLES

TABLES

LIST OF FIGURES

FIGURES

CHAPTER 1

INTRODUCTION

1.1 Climate Change

One of the most serious issues currently affecting the planet earth and its inhabitants is climate change. Climate change refers to the range of global phenomena such as increased temperature trends, rise in sea level, loss of ice mass, changes in vegetation blooming, and extreme weather events. These phenomena are predominantly caused by the combustion of fossil fuels which adds heat-trapping gases to the atmosphere. These heat-trapping gases are commonly referred to as greenhouse gases and cause a "greenhouse effect" which implies the entrapment of heat by these gases. This entrapment of heat subsequently causes "global warming" which describes the increasing temperature trends observed since the early twentieth century (NASA, 2019).

1.2 The Effect of Carbon Dioxide on Climate Change

Carbon dioxide (CO_2) is a main product of fossil fuel combustion and one of the main greenhouse gases that causes global warming, which ultimately leads to climate change. The National Oceanic and Atmospheric Administration states that CO_2 levels in the atmosphere have been rising sharply over the past century and are currently at the highest levels ever in the past three million years as shown in figure 1 and 2 (Lindsey, 2018).

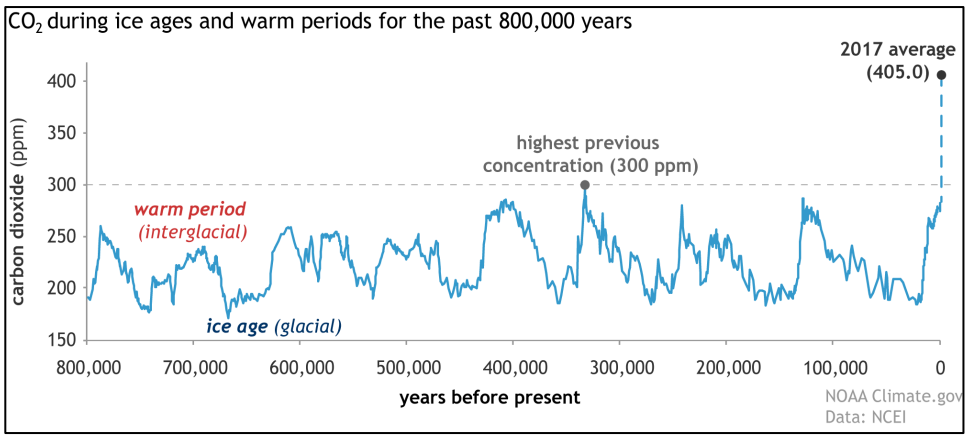

Figure 1. Global carbon dioxide levels over the past 800000 years

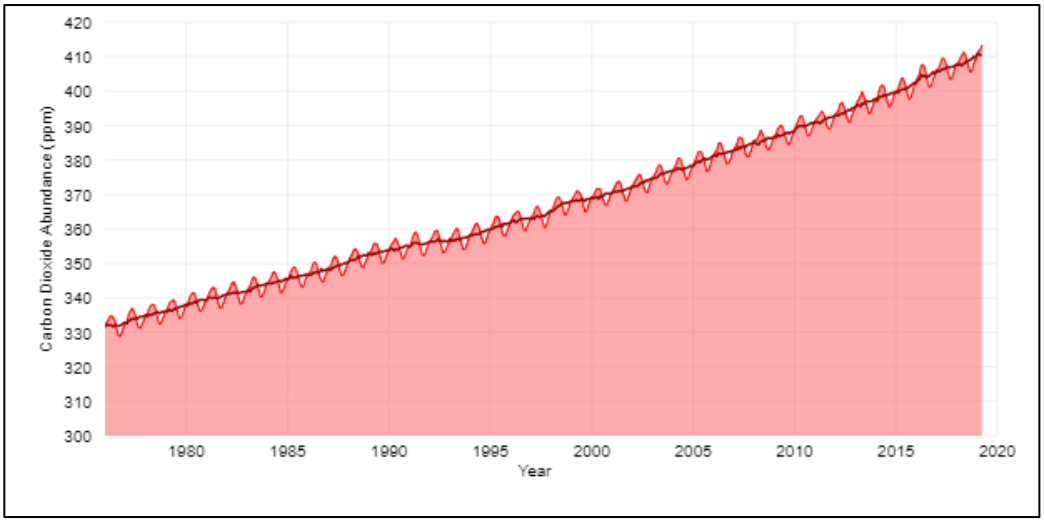

Figure 2. Atmospheric carbon dioxide concentration between 1975 and 2019 (Lindsey, 2018)

Despite CO_2 absorbing less heat per molecule than other greenhouse gases like methane and nitrous oxide, it is of particular importance in the fight against climate change because it is more abundant and lasts much longer in the atmosphere. Water vapor is more abundant than CO_2 in the atmosphere and is also considered a greenhouse gas. However, CO_2 absorbs wavelengths of thermal energy which water vapor does not. Therefore, CO_2 causes a greater imbalance in the total energy causing global warming and is estimated to be responsible for approximately two thirds of the global heating imbalance (Lindsey, 2018). The contribution of different greenhouse gases is shown in figure 3.

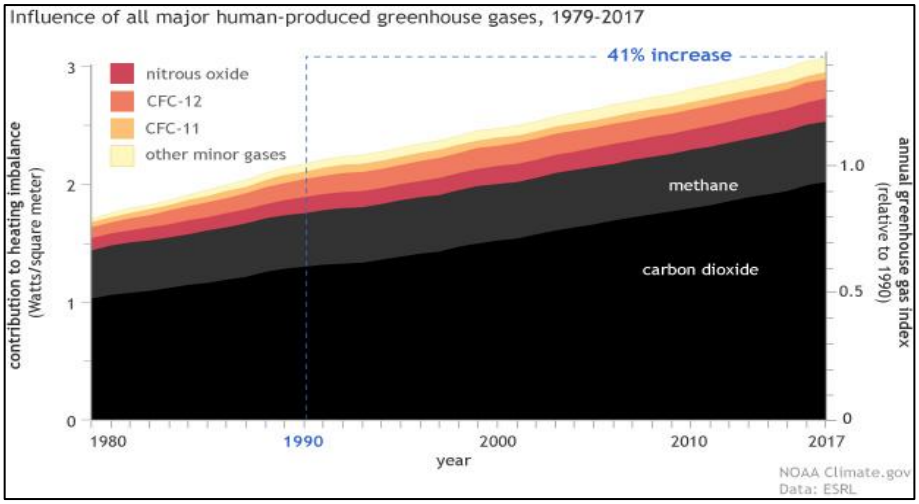

Figure 3. Percentage contribution of major artificial greenhouse gases to global warming

1.3 The Role of Carbon Dioxide in the Mitigation of Climate Change

Being a major culprit in the rise in global warming and adverse effects of climate change, reduction and riddance of CO_2 emissions is an unsurprising solution in the efforts to mitigate climate change. Countries have stepped up efforts to manage and reduce their CO_2 emissions and global atmospheric CO_2 concentrations. These efforts can be seen in the commitment to and ratification of binding agreements such as the Kyoto Protocol and the Paris Agreement (United Nations, 2019b, 2019a).

Bouzalakos et. al suggest that the management of CO_2 emissions is mainly based on three strategies. The first of which is to switch to reliance on renewable and/or alternative sources for primary energy. The second strategy is to improve the efficiency and energy conservation of current fossil fuel sources. The final strategy is to implement the use of Carbon Capture and Storage (CCS) technologies to reduce CO_2 emissions (Bouzalakos & Maroto-Valer, 2010). The advantage of CCS technology is it allows for the continued use of fossil fuels, which are relatively cheap, while simultaneously reducing carbon emissions significantly.

1.4 Carbon Capture and Storage (CCS)

CCS is the separation and capture of CO_2 from major industrial sources/emitters, transport to storage locations, and the long-term isolation of the CO_2 from the atmosphere (IPCC, 2005).

Carbon capture mainly involves the separation of CO_2 to a highly pressurized stream which can be easily transported to storage sites and injected into subsurface formations. The CO_2 is separated at large industrial plants and factories prone to high CO_2 emission rates. Rubin et. al. state that there are three main methods to separate the CO_2 namely; post-combustion, pre-combustion, and oxyfuel combustion systems (Rubin, Mantripragada, Marks, Versteeg, & Kitchin, 2012). These processes are illustrated in figure 4.

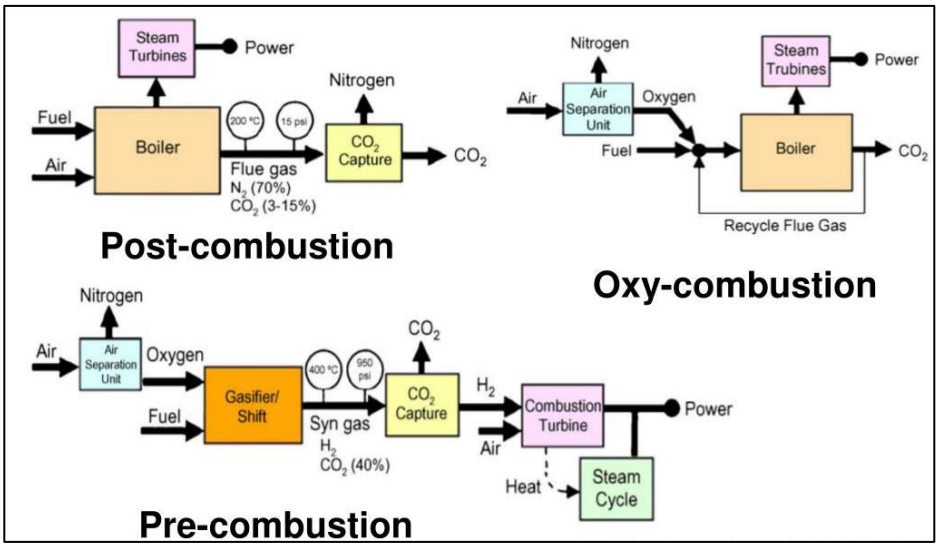

Figure 4. Industrial CO2 separation processes

The CO_2 captured from large-scale emitters can be stored in geological formations such as depleted hydrocarbon reservoirs, coal beds, saline aquifers, and oceans. The long-term storage of CO_2 in such geological formations is referred to as sequestration. Aquifers provide the largest storage capacities but have a disadvantage of being poorly characterized (IPCC, 2005). On the other hand, depleted hydrocarbon reservoirs are well suitable candidates for sequestration because they are usually well characterized.

Furthermore, much of the storage infrastructure is normally already in place. Producer wells can be easily converted to injectors and if there were injectors present, they can almost immediately be used for the injection of the CO_2. Moreover, the petroleum engineering discipline is already well familiar with the concept of CO_2 injection as it has been long used in the industry for enhanced oil recovery in both miscible and immiscible CO_2 floods.

A relatively new concept is the sequestration of CO_2 in geothermal reservoirs (Zhang, Ezekiel, Li, Pei, & Ren, 2014). Geothermal energy recovery results in production of a large amount of CO_2 especially in reservoirs with high CO_2 content dissolved in the brine. Much of this CO_2 is usually released into the atmosphere. However, in efforts to make geothermal energy recovery more environmentally friendly, companies are testing strategies to re-inject the produced CO_2 into the reservoirs either for pressure maintenance or long-term storage. However, this is a concept which relatively novel and not well studied.

The long term storage of CO_2 in geological formations is realized through a combination of processes; in-situ fluids are displaced by the injected CO_2, the CO_2 dissolves in the formation water, and a series of geochemical reactions occur between the injected CO_2 and rock minerals that leads to the formation of stable carbonate compounds. Initially, the displacement of in-situ fluids dominates. However, over longer periods of time spanning hundreds of years, the dissolution of CO_2 into the formation water and the occurrence of geochemical reactions become more significant (Sengul, 2007).

Sengul states that there are four main trapping mechanisms. *Seal trapping or hydrodynamic trapping* which involves the trapping of CO_2 in gaseous or supercritical phase under a low permeability caprock similar to how natural gas exists in reservoirs. *Solubility trapping* which involves the dissolution of the CO_2 into the formation fluids. *Mineralization trapping* which involves the reaction of the CO_2 with the minerals present in the formation rock to form stable compounds. And *phase trapping* which happens when the relative permeability to CO_2 is equal to zero.

1.5 Safety and Risk in Carbon Dioxide Sequestration

The biggest safety concern in the long-term storage of CO_2 in geological formations is the risk of leakage. The sequestered CO_2 could leak into groundwater streams, seep to the surface, and make its way back into the atmosphere. This would be a big drawback in the efforts to mitigate climate change by reducing CO_2 concentrations in the atmosphere. Therefore, it is important to ensure the long-term reliability and safety of CO_2 sequestration sites (Dalkhaa, 2010).

One of the methods through which CO_2 leakage can occur is through caprock failure. This can occur due to geochemical changes in the caprock due to interaction with the CO_2. Dissolution and precipitation reactions occurring can cause significant enough alteration to the caprock to allow for leakage to occur. Ensuring the integrity of the caprock is critical to ensuring the safe geological storage of CO_2. This is because subsurface transport processes and reactions can cause the degradation of seal integrity over time. Therefore, it is crucial to statically and dynamically characterize the caprock to reduce risk of leakage and ensure safe CO_2 sequestration (Olabode & Radonjic, 2013).

Another way through which CO_2 may leak from the formation in which it is stored is through the wellbore. Wells which have not been properly plugged may allow CO_2 to make its way to the surface through cracks or micro-annuli in the space between the cement and the casing or through the cement plug itself. Leakage through the plug is mostly dependent on the permeability of the plug while leakage through the annulus is mostly due to improper bonding of the cement (Vrålstad et al., 2019). The possible leakage pathways for CO_2 in the wellbore are illustrated in figure 5.

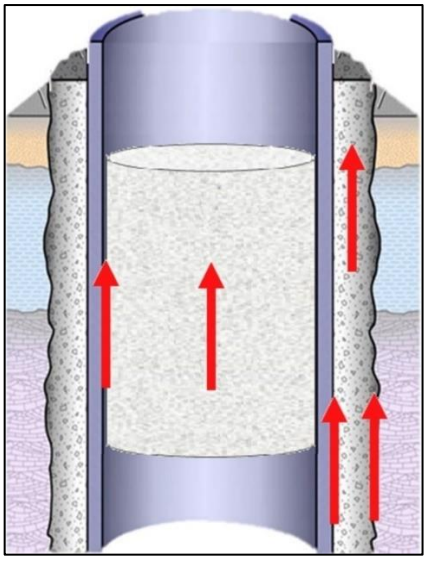

Figure 5. Potential leakage paths for CO2 through the wellbore (Vrålstad et al., 2019)

The contact between CO_2 and the wellbore cement leads to reactions which might cause or accelerate degradation of the cement thus compromising its integrity. To ensure safe storage, it is also important to consider the long-term integrity of wellbore cement in addition to caprock integrity.

This study focuses on modeling the effect of CO_2 on the reservoir formation, caprock integrity and wellbore integrity during long-term CO_2 sequestration. The novelty of this study lies in its exploration of the effects of temperature on changes in the caprock and cement porosity and permeability at a field scale. It compares scenarios of CO_2 sequestration under both low-temperature and high-temperature conditions. It also investigates the effect of additives proposed to mitigate cement degradation in CO_2-rich environments. Furthermore, it compares the effects of CO_2 injection in geothermal reservoirs under different injection rates. The modeling is done using the reactive transport code TOUGHREACT in conjunction with PETRASIM which serves as a pre- and post-processor for TOUGHREACT.

CHAPTER 2

LITERATURE REVIEW

2.1 CO_2 Injection

Currently, apart from enhanced oil recovery, one of the most prevalent reasons for the injection of CO_2 into subsurface formations is for long-term storage in efforts to mitigate climate change. Before being injected into the subsurface formation, the CO_2 is compressed into a supercritical state. This is advantageous because supercritical CO_2 can behave like a gas and easily diffuse through pores. On the other hand, it also behaves like a liquid by occupying less space than a free gas (British Geologic Survey, 2019). CO_2 behaves like a supercritical fluid above its critical temperature of 31.1 degrees Celsius (87.98 degrees Fahrenheit) and critical pressure of 7.39 MPa (1071 psi). There is a critical depth for injection to ensure the injected CO_2 remains in supercritical phase. Based on the physical properties of CO_2, this depth lies at about 0.8 km in formations with normal pressure and temperature gradients (Međimurec, 2018). The change in density of CO_2 with change in pressure and temperature is illustrated in figure 6.

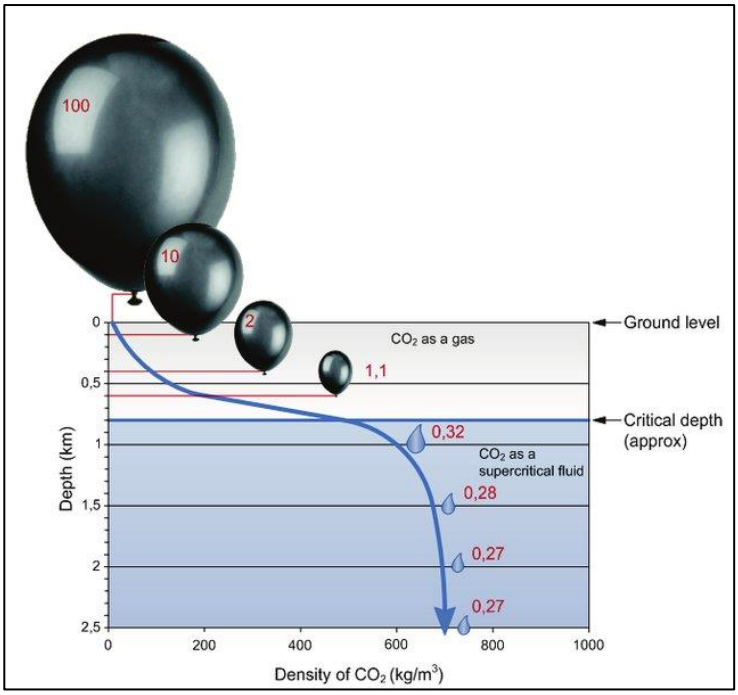

Figure 6. Density profile of CO2 with depth (Međimurec, 2018)

The introduction of CO_2 into the subsurface geosystem affects the chemical composition of the formation water and rock minerals and increases the reactivity of the system. The chemical composition of formation water and minerals is a product of different hydrogeological processes like dissolution and precipitation, mixing, and interaction with bacteria and organic material. (Dalkhaa, 2010). Gaus et. al. postulate that the safety and success of CO_2 storage is largely dependent on understanding the interaction between the CO_2 and the formation water and minerals over the long term. Furthermore, it has been shown that the injected CO_2 travels upwards under favorable vertical permeability and buoyancy conditions, and accumulates under the overlying caprock within a few years of injection (Gaus et al., 2008; Gaus, Azaroual, & Czernichowski-Lauriol, 2005). Therefore, it is also crucial to understand the effect of the geochemical interaction between CO_2 and the caprock.

Injected CO_2 also causes alterations in the wellbore cement when it comes into contact with it either in supercritical phase or as a dissolved phase. Thus, it is also of crucial

importance to understand the effects of the geochemical reaction between CO_2 and wellbore cement.

Geochemical CO_2 interaction after injection over the long term can be considered from the following perspectives:

- CO_2 – Water interaction
- CO_2 – Water – Rock interaction
- CO_2 – Cement interaction

2.2 CO_2 – Water Interaction

The injected CO_2 moves upwards towards the base of the caprock. When it reaches the base, it dissolves in the formation water and diffuses upwards through the caprock. This causes acidization of the caprock formation water (Lagneau, Pipart, & Catalette, 2005). The equations describing the dissolution and speciation process are:

$$CO_2(sc) \rightarrow CO_2(aq)$$

$$CO_2(aq) + H_2O \rightarrow H_2CO_3(aq)$$

$$H_2CO_3(aq) \rightarrow H^+ + HCO_3^-$$

$$HCO_3^- \rightarrow H^+ + CO_3^{2-}$$

The equations above are all homogenous reactions since they only involve aqueous components. Furthermore, the speciation of CO_2 is highly dependent on pH.

The solubility of CO_2 is affected by factors such as temperature, pressure, and salinity. Its solubility decreases with an increase in temperature and salinity, but increases with increasing pressure as shown in figures 7 and 8 respectively (Duan & Sun, 2003).

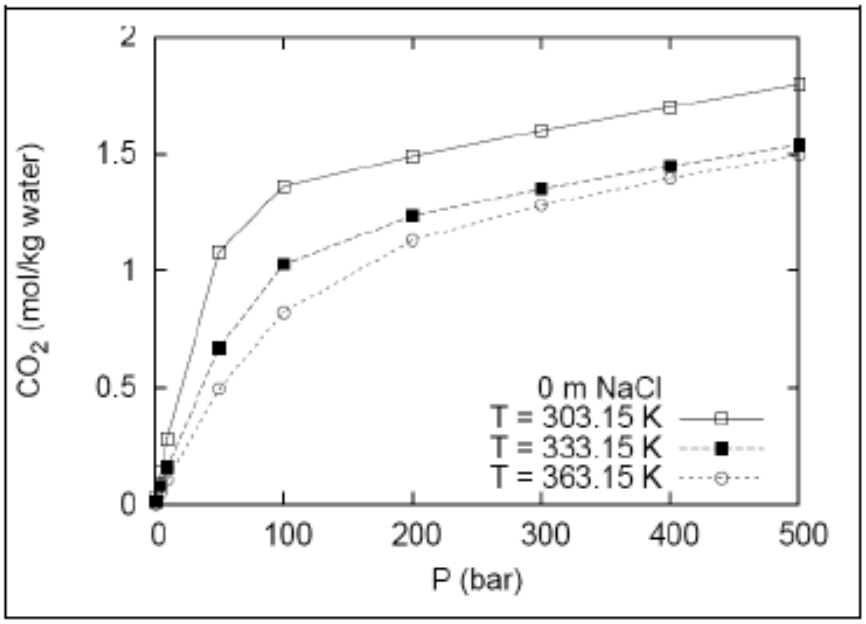

Figure 7. Solubility of CO2 in pure water: Effect of pressure and temperature (Duan & Sun, 2003)

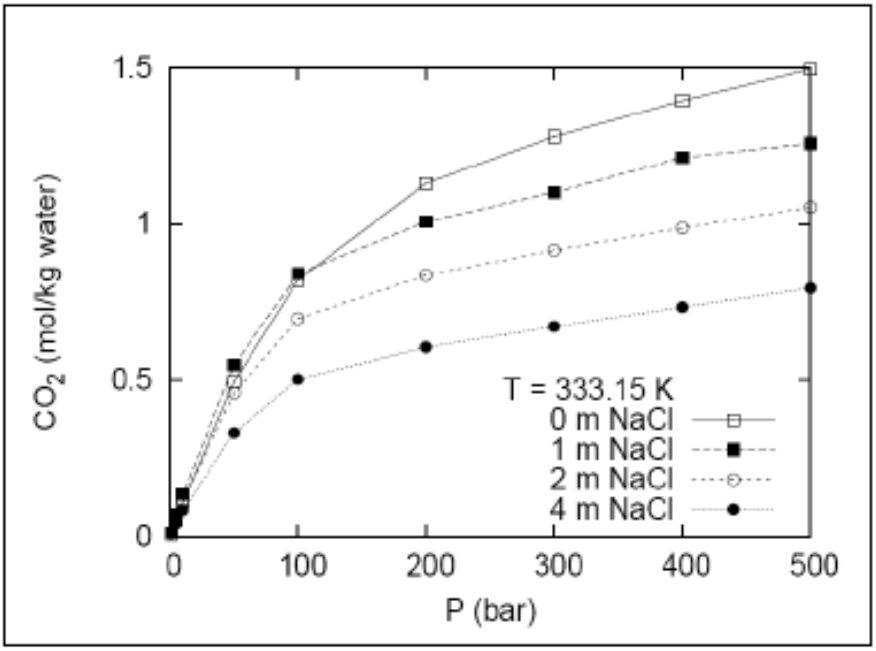

Figure 8. Solubility of CO2 at 60 degrees Celsius: Effect of pressure and salinity (Duan & Sun, 2003)

The viscosity of CO_2 is also an important property that affects its transport and distribution in subsurface formations after injection. The dynamic viscosity of CO_2 increases with an

increase in temperature. The effect of pressure on dynamic viscosity is more significant at lower temperatures. At very high temperatures, the effect of pressure becomes quite small and the viscosity is mainly controlled by the temperature as shown in figure 9. (Engineering ToolBox, 2018).

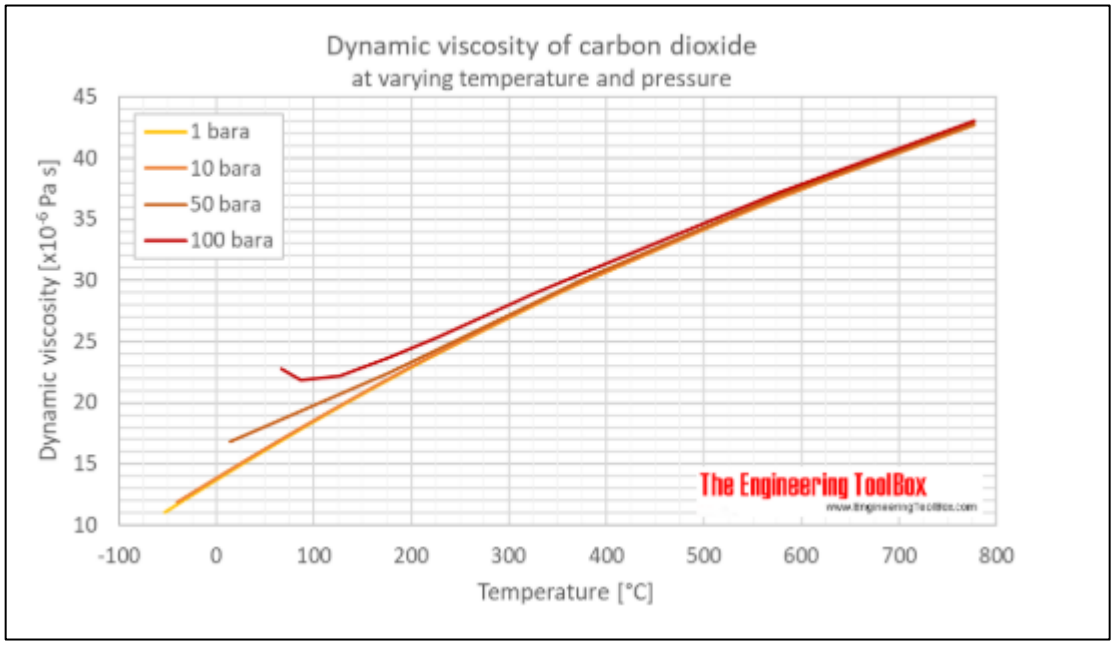

Figure 9. Dynamic Viscosity of CO2 (Engineering ToolBox, 2018)

2.3 CO_2 – Water – Rock Interaction

The acidification of formation water due to dissolution of CO_2 leads to geochemical reactions with the minerals present in the rock. The carbonate ion reacts with cations present to precipitate carbonate minerals. The reactions that occur depend on the mineral composition of the rock. The most common of these reactions are:

$$CO_3^{2-} + Ca \rightarrow CaCO_3\ (Calcite)$$

$$2CO_3^{2-} + Ca + Mg \rightarrow CaMg(CO_3)_2\ (Dolomite)$$

$$CO_3^{2-} + Fe \rightarrow FeCO_3\ (Siderite)$$

Several studies have shown that the occurrence of geochemical reactions due to the interaction of dissolved CO_2 with the minerals in the caprock can cause significant enough alterations to rock properties such as porosity and permeability. The dissolution of CO_2 in the formation water causes it to get acidized. Initially, a porosity increase might be observed due to dissolution of primary (initially present) caprock minerals by the acidized formation water. However, over time, a porosity decrease might occur due to precipitation of secondary minerals. A porosity increase in the caprock is not desired because it might allow for leakage of the sequestered CO_2. On the other hand, a decrease in porosity is a positive consequence as it helps to improve the sealing capacity of the caprock (Gaus et al., 2008, 2005; Olabode & Radonjic, 2013).

2.4 CO_2 – Cement Interaction

The interaction between CO_2 and wellbore cement has the potential to cause alteration in cement properties and lead to formation of leakage pathways in plugged wells (Cao, Karpyn, & Li, 2013). The alterations that might occur are largely dependent on the type of cement used. In the oil industry, Portland Cement is the most commonly type of cement used.

Under API specifications for wellbore cementing, there are several classes of cements ranging from A to H. A, B, and C class cements were originally adapted from the construction industry without any alterations specific to the oil industry. The difference between them was simply based on their reactivity and component materials. After the drilling of deeper wells subject to higher temperature and pressure conditions commenced, there was a need for cements that were resistant to these conditions and did not set very quickly. This led to API classes D, E, and F cements to be developed. These cements have delayed thickening times and are relatively resistant to higher temperatures and pressures compared to the first three classes. Later, specialized cements for general oil well application were developed and came to be known as API classes G and H. These two classes are essentially the same in composition with the only difference in the fineness of

the material. Class G cement is typically finer than class H cement. These two classes are now the most widely used cements in the petroleum industry (Vrålstad et al., 2019).

Khalifeh et al. summarize other materials apart from cement used in plugging wells. Some of these include:

a) Blast furnace slag
b) Bentonite
c) Low melting point metal alloys
d) Thermosetting polymers
e) Unconsolidated sand slurries
f) Thermite
g) Geopolymers.

However, most of these materials are emerging and have not proven their capability to ensure proper sealing of abandoned wells like Portland cement has (Khalifeh, Hodne, Saasen, & Vralstad, 2013).

The major components of Portland cement are; tricalcium silicate, dicalcium silicate, tricalcium aluminate, and tetracalcium aluminoferrite (Vrålstad et al., 2019). These are the basic mineral phases present; however, Portland cement is rarely used without additives which individually serve special purposes. Some of these additives include:

a) Barite or hematite to increase cement slurry density.
b) Bentonite or pozzolans to decrease slurry density.
c) Micro-silica or latex to make the cement gas tight.
d) Silica flour to make the cement resistant to very high temperature.
e) Flexible particles to reduce stiffness.

The most essential properties of the cement used to plug a well are its ability to ensure long-term integrity, permeability, compatibility with casing, mechanical strength, and its resistance to chemicals and substances such as hydrogen sulfide and carbon dioxide.

When exposed to CO_2, Portland cement undergoes a sequence of reactions and changes which affect the sealing integrity of the cement plug. Kutchko et al. describe this sequence

as a mainly two-step degradation of the Portland cement. Initially, the CO_2 is dissolved into the aqueous phase to form a carbonic acid.

$$CO_{2(aq)} + H_2O \rightarrow H_2CO_{3(aq)}$$

This carbonic acid diffuses into the cement matrix and dissolves portlandite to release calcium ions.

$$Ca(OH)_{2(s)} \rightarrow Ca^{2+}_{(aq)} + 2OH^{-}_{(aq)}$$

The calcium ions react with bicarbonate and hydroxide ions to form calcium carbonate.

$$Ca^{2+}_{(aq)} + OH^{-}_{(aq)} + HCO^{-}_{3(aq)} \rightarrow CaCO_{3(aq)} + H_2O_{(aq)}$$

The formation of calcium carbonate causes a decrease in porosity and permeability in the cement matrix. This first step is referred to as carbonation (Kutchko, Strazisar, Dzombak, Lowry, & Thauiow, 2007)

When portlandite gets depleted, dissolution of the relatively less soluble calcium carbonate begins. This indicates the beginning of the second step referred to as bi-carbonation.

$$CaCO_{3(s)} + H^{+}_{(aq)} \rightarrow Ca^{2+}_{(aq)} + HCO^{-}_{3(aq)}$$

This dissolution of calcium carbonate causes an increase in porosity and permeability. However, the degradation of cement is a diffusion-driven process and largely depends on the reaction kinetics. The degradation process can end up being a self-inhibiting process. The decrease in permeability from the first step can significantly slow down the rate of the second step and thus inhibit the overall degradation of the cement. Thus the complete degradation of a cement plug that spans tens of meters can be an extremely slow process and take a very long time (Carroll et al., 2016).

2.5 Caprock Integrity

There have been several studies conducted to investigate the caprock integrity of possible CO_2 sequestration sites. Some of these studies have been carried out experimentally while others have been numerical simulation studies. Each type of study has its merits and demerits. However, Lagneau et. al. suggest that experimental techniques for such studies are limiting in terms of time, space, and experimental conditions. Therefore, although experiments are still important, numerical simulations provide a powerful tool to also predict the effect of CO_2 sequestration in certain geological formations (Lagneau et al., 2005).

Numerical modeling and simulation provide a fast, powerful, and reliable method of analyzing problems such as caprock integrity in CO_2 sequestration. The numerical modeling of CO_2 sequestration problems is generally divided into three types; hydrodynamic, batch geochemical, and reactive transport modeling. Batch geochemical modeling is however less preferred because it simulates geochemical reactions without considering flow effects (Gaus et al., 2008). It is however ideal for modeling static laboratory experiments (Holubnyak et al., 2011).

Research on reactive transport modeling has led to the development of several numerical modeling codes and simulators capable of modeling and simulating CO_2 sequestration and the short-term and long-term effects of this sequestration. These simulators are powerful enough to accurately model static and dynamic conditions, while incorporating effects of parameters such as temperature on the geochemical reactions taking place in the subsurface. Some examples of such codes and simulators are; TOUGHREACT, PHREEQC, and HYTEC.

In a 2005 study, Xu et. al. investigated the effects of CO_2 sequestration in a commonly encountered Gulf Coast sediment of a saline aquifer. Numerical simulations were performed using the reactive transport code TOUGHREACT and the effect of CO_2 immobilization through carbonate precipitation was analyzed. Simulations were run for up to periods of 10000 years and observed that the storage capacity could reach

approximately 60 kg/m^3 of formation through the precipitation of secondary carbonate minerals such as siderite, ankerite, and dawsonite. Furthermore, the injection of CO_2 and precipitation of secondary minerals caused a decrease in porosity. Despite the decrease in porosity being very small, it resulted in a significant permeability decrease (Xu, Sonnenthal, Spycher, & Pruess, 2008)

In a 2007 study Gherardi et. al. modeled CO_2 induced caprock alteration in a depleted gas reservoir. The reactive transport code TOUGHREACT was used to run simulations to understand safety and risk for possible CO_2 sequestration in a gas reservoir. The main focus of the study was the dissolution and precipitation of carbonate minerals due to interaction of CO_2 with in-situ fluids and rock minerals. The researchers observed a self-enhancing phenomenon in the caprock in terms of sealing capacity when CO_2 invaded the caprock in an aqueous phase. This was mainly due to precipitation of secondary minerals, of which calcite was the most significant, which caused a resultant reduction in porosity. On the other hand, if the CO_2 invaded the caprock in a free gaseous phase, low pH values were predicted and there were occurrences of significant calcite dissolution accompanied by porosity enhancement. However, over long periods of time, precipitation dominated dissolution processes and the caprock sealing property was improved (Gherardi, Xu, & Pruess, 2007).

In another study by Gaus et. al., the impact of CO_2 sequestration on the Clayey caprock at Sleipner in the North Sea was investigated. The modeling code PHREEQC was used for batch and reactive transport modeling of CO_2 sequestration and investigation of its effects on the Clayey caprock. The major geochemical reactions between the dissolved CO_2 and formation water and caprock minerals were identified and the impact on the porosity was calculated. It was observed that there was a slight porosity decrease due to the precipitation of secondary minerals. This porosity decrease helps to improve the sealing capacity of the caprock. However, this effect was only observed in the lower meters of the caprock (Gaus et al., 2005).

Bildstein et. al. carried out an integrative modeling of caprock integrity for CO_2 storage in the Paris basin. An assessment of the impact of the CO_2 storage on safety and performance was done. Different scenarios were investigated under different geochemical conditions and pressure regimes. For instance, the supercritical CO_2 plume invading the caprock when the reservoir pressure is higher than the capillary entry pressure, and the CO_2 entering the caprock by diffusion while dissolved in the formation water. The modeling code PHREEQC was used and the results showed there were significant porosity alterations in the part of the caprock close to the reservoir used for sequestration. However, these changes in porosity were not significant enough to allow for leakage of any CO_2 (Bildstein et al., 2010).

Dalkhaa carried out a numerical modeling study to investigate caprock integrity for a potential CO_2 storage site in Turkey. A dynamic core flooding experiment was modeled using the reactive transport modeling code TOUGHREACT. CO_2 injection into a Sayindere core was simulated. CO_2 was injected for 99 days followed by simulation of a 25-year post injection monitoring period. Results showed that the main mineral present, calcite, was dissolved first then reprecipitated. There was a 0.01% decrease in porosity and a 0.03% decrease in permeability. These decreases aided the sealing ability of Sayindere caprock (Dalkhaa, 2010).

2.6 CO_2 Injection into Geothermal Reservoirs

In one of the earliest studies on CO_2 injection into high temperature geothermal reservoirs, Liu et al. conducted experiments simulating CO_2 injection to granite and sandstone rock/hot water systems under temperatures ranging between 100 and 350 degrees Celsius. Results showed that the presence of CO_2 enhanced the dissolution of granite and sandstone, and the precipitation of secondary minerals. The changes in CO_2 volume content coincided with the deposition of aluminum silicate and calcium-aluminosilicate secondary minerals which suggest trapping of CO_2 in the minerals. Liu et al. concluded that capturing CO_2 in high temperature hydrothermal granite/sandstone reservoirs was a

viable option to reduce atmospheric CO_2 concentration (Liu, Suto, Bignall, Yamasaki, & Hashida, 2003).

In a 2014 study, Zhang et al. assessed the feasibility of CO_2 storage in geothermal reservoirs in China. CO_2 storage in different geological formations such as hot dry rock, saline aquifers, and geopressured reservoirs was compared. The best options for storage based on a range of factors such as storage capacity, heat characteristics, and development prospects were analyzed. Comparatively, deep saline aquifers were chosen as the best option for CO_2 storage. The researchers also did reservoir simulation comparing scenarios where geothermal reservoirs were used as pure storage sites and combined storage/heat extraction sites. It was concluded that injecting and using CO_2 for heat extraction was more feasible than simply storing the CO_2 in the reservoirs (Zhang et al., 2014).

Randolph and Saar also investigated the feasibility of coupling CO_2 storage in geothermal reservoirs with using CO_2 as the working fluid. It was suggested that CO_2 could potentially transfer heat more efficiently than water; especially in lower temperature reservoirs which were deemed unfeasible for geothermal energy recovery. Furthermore, it was demonstrated that coupling storage with energy recovery is more feasible than simply injecting the CO_2 for sequestration purposes. The researchers stated that this coupling of purpose significantly aids the large-scale implementation of the CO_2 storage technology which is a critical challenge in terms of economic viability (Randolph & Saar, 2011).

Güleç and Hilton studied some geothermal fields in Turkey as natural analogues for CO_2 storage sites. The geochemistry involved and CO_2 trapping mechanisms in different reservoirs was investigated. It was observed that in high temperature reservoirs, calcite precipitation accompanies dissolution of primary minerals and can trap up to 80% of the injected CO_2 in some cases. It was observed that in general, the relative contribution of calcite precipitation to CO_2 storage was less than dissolution. In most of the reservoirs studied, the major sink for CO_2 was dissolution with calcite precipitation as a minor sink (Güleç & Hilton, 2016).

A field pilot for CO_2 injection was tested in Umurlu geothermal field in Turkey. The project was implemented with the aim of improving reservoir performance and energy extraction. It was observed that CO_2 injection had a significant effect on the behavior of reservoir pressure around the pilot wells. This study however did not investigate the CO_2 – mineral interaction and the researchers recommended this as a next step in studying the effect of CO_2 injection in Umurlu geothermal field (Yücetaş, Ergiçay, & Akın, 2018).

2.7 Wellbore Cement Integrity

The effect of CO_2 on wellbore cements has been investigated in some studies published in literature. Majority of these studies are experimental investigations of the degradation of cement used in CO_2 injection wells or abandonment plugs. These studies have investigated the reaction between wet CO_2 and cement, and CO_2 saturated brine and cement. Some studies have taken sample cement cores from abandoned fields which previously underwent CO_2 injection. These cores have been tested for mechanical integrity and degradation extent.

In a 2013 study, Cao et al. designed a dynamic flow-through experiment to investigate the alterations in wellbore cement integrity due to geochemical reactions in CO_2 – rich environments. Composite sandstone-cement cores were synthesized and continuously flooded with CO_2 – saturated brine. Continuous gaps were created in the cement sections to represent malformities such as fractures and voids in the cement matrix. The volumetric and structural alterations in the cement zone were monitored using CT imaging. It was observed that the gaps increased in aperture size in the cement zone due to degradation while the sandstone sections remained unaffected. The changes were more significant and occurred faster in the early stages of the experiment compared to the later stages. The CO_2 – saturated brine flowed preferentially through the apertures and the zones of the cement which were most degraded were those closest to the apertures (Cao et al., 2013).

Kutchko et al. conducted experiments in 2007 to investigate the durability of cements used in wells penetrating formations that were potential candidates for geological storage of CO_2. The effect of cement curing conditions on the longevity of the cement and resistance

to CO_2 attack was tested. Experiments were run at 50 degrees Celsius and 30.3 MPa, and 20 degrees Celsius and 0.1 MPa. It was observed that the samples cured at 50 degrees Celsius and 30.3 MPa were more resistant to CO_2 attack and had a well-defined carbonated zone. This relatively better resistance was attributed to the more optimal carbonation conditions compared to very low-temperature and low-pressure conditions (Kutchko et al., 2007).

In a study to investigate the performance of oil well cement after long-term CO_2 exposure, Carey et al. obtained a core sample including casing, cement, and shale caprock from a formation subject to a 30-year CO_2 – flooding operation. The permeability of the recovered sample was in the range of a tenth of a millidarcy suggesting that the cement had maintained its integrity. However, there was a layer of carbonate precipitate adjacent to the casing. This suggested CO_2 migration along the cement-casing interface. The cement adjacent to the shale also showed signs of carbonation suggesting interaction with CO_2. Carey et al. concluded that the integrity of the cement-casing and cement-formation interfaces were the most integral to prevention of CO_2 leakage in the field case study (Carey et al., 2007).

Carey et al. took their study one step further by creating a numerical simulation model to understand the carbonation process and try to develop a predictive model for cement degradation. Cement – CO_2 interaction was simulated using the reactive transport code FLOTRAN. The problem was reduced to a two-dimensional flow problem consisting of a column of shale with CO_2 – saturated brine in contact with a CO_2 – free cement. It was concluded that the main controlling variables for the transport and reaction of the CO_2 were the tortuosity and porosity of the cement, and reaction rates of the minerals (Carey et al., 2007).

In 2010, Duguid and Scherer conducted a series of experiments to investigate how CO_2 – saturated brine reacts with wellbore cement when equilibrated under conditions present in sandstone and carbonate reservoirs. API class H cement was tested under temperature conditions ranging between 20 and 50 degrees Celsius which are representative of shallow

sequestration at depths of up to 1 kilometer. The cement samples exposed to CO_2 – saturated brine were analyzed using techniques such as optical microscopy and x-ray diffraction. Results showed that there was no detectable attack when the carbonated solution was pre-equilibrated with calcium carbonate which is characteristic of conditions present in a limestone formation. However, there was significant degradation of the outer layer of the cement when the carbonated solution was pre-equilibrated under sandstone-like conditions. It was concluded from the experiments that the rate of cement degradation was primarily controlled by the rate of dissolution of the carbonated layer, and the rate of diffusion through the degraded layers (Duguid & Scherer, 2010).

Huerta et al. designed a series of experiments to investigate effects of flow of carbonated brine along fractures in cement along a leaky wellbore. A carbonic acid with pH ranging between 2.0 and 3.15 acting as an analog was injected at constant flowrates ranging between 0.3 and 9.4 cm/s. The pressure difference across the core samples and resultant pH of the exiting fluid was measured. It was observed that the reaction between CO_2 and the cement occurred mostly on the surface of the fractures within the cement. This reaction caused leaching of calcium and induced precipitation of minerals. An interesting observation was made in that even in leaky cement, the flow of CO_2 – saturated water was a self-inhibiting phenomenon. Monitoring of the pressure difference across the core samples showed that the precipitation of minerals caused by reaction with CO_2 was enough to inhibit the flow itself. Huerta et al. suggested that the leakage of CO_2 – saturated fluids may eventually cause sealing of the leakage channels if the apertures are small and enough time passes for precipitation of minerals to occur (Huerta, Hesse, Bryant, Strazisar, & Lopano, 2013).

Lowry and Dzombak conducted a study to determine the effect of carbonated brine and supercritical CO_2 on hydrated class H well cement. It was observed that the alteration of cement exposed to supercritical CO_2 was similar to cement in contact with atmospheric CO_2. On the other hand, the degradation of cement exposed to CO_2 – saturated brine was similar an acid attack on cement. The supercritical CO_2 penetrated further into the cement cores compared to the CO_2 – saturated brine. Nonetheless, the researchers concluded that

the results suggest that degradation significant enough to heavily impact the integrity of class H well cement requires a time scale greater than several decades. Therefore, it is unlikely that cement exposure to CO_2 under normal sequestration conditions will lead to severe leakage (Lowry & Dzombak, 2008).

In their review of the role of mechanics, transport, and chemistry on well integrity in CO_2 storage, Carrol et al. state that much of the studies that have been done on the integrity of wellbore cements during CO_2 storage have been conducted only at lab scales. They however underline the importance of carrying out field scale studies through the use of simulation techniques to understand the effect of CO_2 on field scale cement plugs and compare these results against experimental results.(Carroll et al., 2016)

CHAPTER 3

STATEMENT OF THE PROBLEM

The sequestration of CO_2 in subsurface geological formations has been identified as one of the methods to reduce CO_2 concentration in the atmosphere and achieve the bigger goal of climate change mitigation. However, a factor of concern in the sequestration of CO_2 in such geological formations is the eventual risk of leakage back to the atmosphere.

One of the methods CO_2 leakage can occur is through failure of the caprock to properly seal the sequestration formation. This cap rock failure can occur due to rock alteration as a result of interaction between the injected CO_2 and in-situ water and rock minerals. Furthermore, leakage might occur through the wellbore. Reaction between CO_2 and wellbore cement might cause significant enough degradation to the cement to allow formation of leakage pathways in the cement plugs used to seal the well.

The aim of this research is to analyze the effects of CO_2 on the reservoir formation, caprock and wellbore integrity of potential CO_2 sequestration sites and comment on the CO_2 storage mechanisms, and related safety and risk involved in the sequestration of CO_2 at these sites. Numerical modeling and simulation are used to understand the effects of CO_2 storage in hydrocarbon and geothermal reservoirs, and the effect of injection under different temperature conditions. The reactive transport code TOUGHREACT is used with PETRASIM as a pre- and post-processor to carry out the modeling and simulation.

CHAPTER 4

METHODOLOGY

This study uses numerical modeling to understand the effect of geochemical reactions induced by CO_2 on the reservoir formation, caprock, and wellbore cement. The modeling of these CO_2 – reservoir, CO_2 – caprock and CO_2 – cement interactions is done using the reactive transport code TOUGHREACT. PETRASIM is used as a pre- and post-processor for TOUGHREACT.

4.1 TOUGHREACT

TOUGHREACT is a "simulation program for non-isothermal multiphase reactive geochemical transport in variably saturated geologic media" (Xu et al., 2008). TOUGHREACT is applicable to a wide range of subsurface conditions, and chemical and physical heterogeneities. It can be used to model 1-dimensional, 2-dimensional, and 3-dimensional problems. TOUGHREACT gives priority to temperature dependence of reactions over pressure dependence because the equilibrium constants are not as sensitive to pressure as they are to temperature. The main criteria for heat flow and fluid flow in TOUGHREACT are (Xu et al., 2008);

1. Fluid flow in all phases occurs under pressure, viscous, and gravity forces.
2. Relative permeability and capillary pressure curves are used to represent the interaction between flowing phases.

3. Convection and conduction govern flow of heat.
4. Gas phases and water vapor undergo diffusion processes.

TOUGHREACT solves problems using a sequential iteration approach. Systems of mixed-equilibrium kinetic chemical reaction equation are solved by Newton-Raphson iteration on a grid-block by grid-block basis. The equations are iteratively solved until convergence is achieved (Xu et al., 2008).

TOUGHREACT is also capable of calculating porosity and permeability changes during the simulation. Porosity change is calculated from the changes in mineral volume fractions. The related permeability changes are calculated using a simple cubic law (Gherardi et al., 2007).

The calculation of porosity is governed by the equation below.

$$\emptyset = 1 - \sum_{m=1}^{n} V_{fr-m} - V_{fr-nr}$$

Where;

$$n = number\ of\ minerals$$
$$V_{fr-m} = Volume\ fraction\ of\ mineral\ in\ the\ rock$$
$$V_{fr-nr} = Volume\ fraction\ of\ non-reactive\ minerals\ in\ the\ rock$$

Permeability is calculated from porosity using the cubic equation below.

$$k = k_i \cdot \left(\frac{\emptyset}{\emptyset_i}\right)^3$$

Where;

$$k_i = initial\ permeability$$
$$\emptyset_i = initial\ porosity$$

TOUGHREACT provides several EOS (Equation of State) modules and it is upon the user to select the appropriate one for the problem being modeled. The EOS modules available are (Xu et al., 2008):

a) EOS1 – for water with frequent application to hydrothermal problems.
b) EOS2 – for multiphase mixtures of CO_2 and water with some applications to hydrothermal problems.
c) EOS3 – for multiphase mixtures of water and air with frequent application to problems concerning nuclear waste disposal.
d) EOS4 – this module has the same capabilities as EOS3 but incorporates vapor pressure lowering effects due to capillary pressure.
e) EOS9 – for single phase water with typical application to geochemical transport problems at ambient pressure and temperature conditions.
f) ECO2N – for multiphase mixtures of water, CO_2, and NaCl with frequent application to problems concerning CO_2 disposal in brine aquifers.

The problem of CO_2 sequestration in geological formations is best modeled using the ECO2N module which is appropriate for multiphase mixtures of CO_2 and water with typical applications in CO_2 disposal in saline aquifers (Xu et al., 2008). ECO2N module accurately models thermophysical properties of CO_2 in both gas and liquid phases but does not distinguish between the two phases in flow calculations (Pruess, 2005). Furthermore, ECO2N does not account for an oil phase. There is presence of an oil phase in the reservoir and it is inevitable that some of the CO2 will dissolve in or interact chemically with the oil.

It is of critical importance however, to understand the limitations of each EOS module depending on the problem being modeled. For instance, ECO2N module can only be used up to temperatures of 110 degrees Celsius. To model CO_2 disposal problems at higher temperatures, it is required to use the EOS2 module which is capable of handling simulations at much higher temperatures.

4.2 PETRASIM

PETRASIM is a pre- and post-processor for the TOUGH family of codes. It allows for the quick building of models and viewing of results after simulations (Thunderhead Engineering, 2017). It allows the user to quickly create a code compatible with the TOUGH family of simulators, an otherwise cumbersome process. The general steps followed in using PETRASIM and TOUGHREACT in tandem to run a simulation are outlined below.

1. Specify the TOUGH code and version to be used for the simulation (TOUGHREACT for this case).
2. Select the correct EOS module to be used.
3. Define the global simulation properties.
4. Define the material properties.
5. Set the initial conditions.
6. Set the solver parameters and output options in the TOUGHREACT tab in PETRASIM.
7. Specify the chemical components.
8. Define geochemical zones.
9. Create the model boundary and grid.
10. Define boundary conditions.
11. Define solution and output controls.
12. Associate geochemical zones with the grid.
13. Save the model.
14. Run the simulation.
15. View results.

The steps defined above are not a linearly rigid procedure but rather an iterative one where the user goes back and forth between some steps until a proper model is built. Some of the actions described in the steps above can be performed before others preceding them in the sequence without affecting the integrity of the model or the reliability of the simulation run.

CHAPTER 5

NUMERICAL MODELING AND SIMULATION

5.1 CO_2 Storage in a Hydrocarbon Reservoir

PETRASIM was used to build a synthetic model representative of a potential CO_2 sequestration site in Turkey (Bati Raman field). A more detailed description of Bati Raman is given in the next section. As much data as is available in public literature was used to construct this model. However, it is to be noted with caution that this study in no way aims to completely model CO_2 sequestration in Bati Raman, but rather aims to create a synthetic model using some of the reservoir and caprock properties of Bati Raman to understand the effect of CO_2 sequestration on the integrity of caprocks with similar properties. Assumptions have been made where data is not publicly available.

5.1.1 Bati Raman Field

Bati Raman field, located in South-East Turkey and discovered in 1961, is the largest oil accumulation in Turkey. It has an estimated initial oil in place of 1.85 billion stock tank barrels.

The main producing formation is Garzan which is a cretaceous aged heterogenous carbonate formation with a gross thickness of 64 meters. The structural trap is a long and partly asymmetric anticline, oriented in the East-West direction, about 17 km long and

varying in width between 2 and 4 km. The field has an average porosity of 18% and a low matrix permeability that ranges from 10 – 100 millidarcies. However, well tests have shown permeability values of up to several darcies thus confirming the existence of secondary porosity. The carbonate formation is also heavily fractured (Arslan, Akin, Karakece, & Korucu, 2007; Babadagli et al., 2008).

The oil from Bati Raman is heavy, viscous oil with an API gravity ranging between 9 and 13. The nature of the oil in Bati Raman and its complex geological characteristics have proved a production challenge. Thus, Bati Raman is the subject of one of the largest immiscible CO_2 flooding operations in the world with the aim of improving recovery (Babadagli et al., 2008). Approximately 40 million scf of CO_2 is injected into Bati Raman daily through 67 injectors. About half of this amount is delivered by pipeline from the nearby Dodan gas field while the rest is recycled gas (Sahin, Kalfa, Celebioglu, Duygu, & Lahna, 2012).

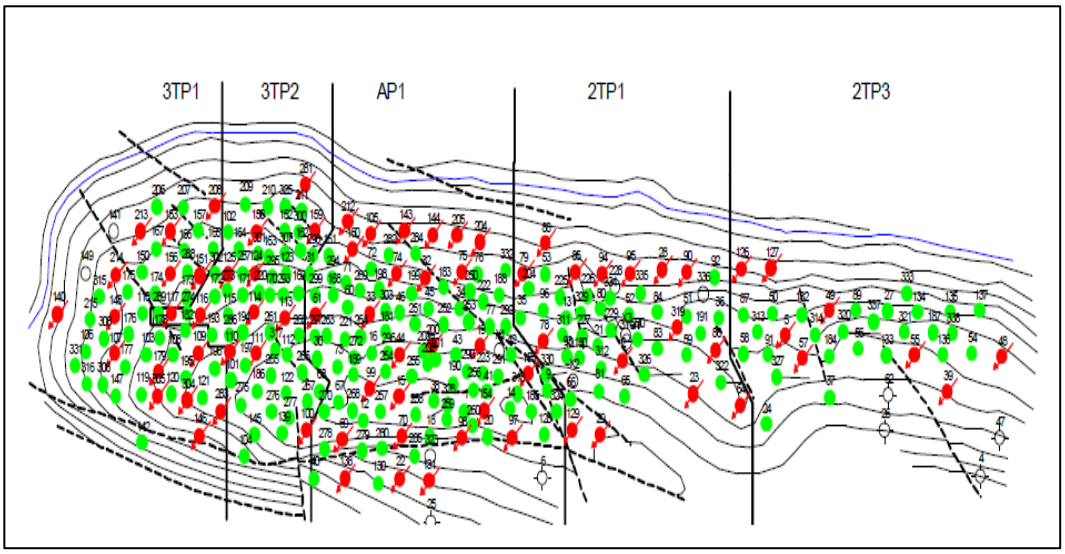

Figure 10. Subsurface structural contour map of Bati Raman (Garzan formation)
(Sahin, Kalfa, Celebioglu, & Corp, 2007)

Germav is the caprock for the main producing formation in Bati Raman – Garzan. Germav formation varies in thickness from 50 to 200 meters and is made up of alternating shale, sandstone, and local conglomerates (Alsharhan & Nairn, 2003).

Germav formation is divided into two distinct units – Lower Germav and Upper Germav. The Lower Germav unit of Upper Cretaceous age is characterized by shale-sandstone alternations which are dark grey in color. The Upper Germav unit of Paleocene age consists of light-grey colored shale, marl, and siltstone-sandstone alternations (Tetiker, Akman, & Yalcin, 2018)

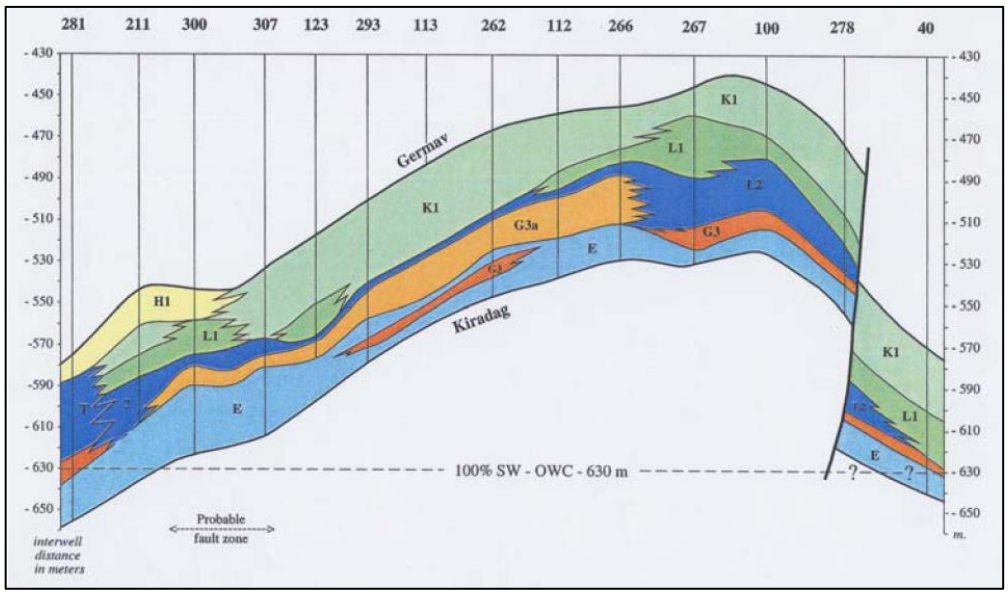

Figure 11. Stratigraphy of Bati Raman field (Babadagli et al., 2008)

Germav formation contains rocks that show different grain size, mineralogical composition, and textural properties. A 2018 study by Tetiker et al. showed the presence of a range of minerals in the rock of Germav formation. Ordered in decreasing abundance; calcite, phyllosilicate/clay (chlorite, C-S, C-V, vermiculite, illite, serpentine, I-C and I-V), quartz, feldspar, dolomite, hematite and goethite. Based on the results of optical microscopy (OM), scanning electron microscope (SEM), and x-ray diffraction (XRD) tests, there are also detrital minerals from metamorphic and ophiolitic units as well as diagenetic minerals. The phyllosilicate/clay minerals with different chemical composition are rich in Al_2O_3, tFe_2O_3 and/or MgO (Tetiker et al., 2018)

5.1.2 Potential for CO_2 Storage in Bati Raman Field

Turkey acceded to the United Nations Framework Convention on Climate Change (UNFCCC) in May 2004 and thus CO_2 capture and storage is being explored as a viable option to reduce anthropogenic CO_2 emissions in Turkey (Dalkhaa & Okandan, 2013). Given Bati Raman's history and success with CO_2 injection as a means of improved oil recovery, it has naturally been considered as a candidate for possible CO_2 sequestration after exhaustion of economic oil recovery. Bati Raman is currently the subject of ongoing projects that look to establish a network of industrial CO_2 emitters and possible sequestration sites. It is geographically close to the Batman refinery which emits a whopping 75 million tonnes of CO_2 per year. Bati Raman is also close to several cement factories which are also major contributors to Turkey's CO_2 emissions.

Being a mature field, Bati Raman's main producing formation (Garzan) is well characterized. However, a detailed review of publicly available literature shows there has been little research done on Germav formation. More precisely, an extensive literature survey shows there have been no previous investigations of the integrity of Germav caprock under CO_2 sequestration conditions.

5.1.3 Model Geometry and Grid

A simplified two-dimensional radial model was built on PETRASIM using some properties of Garzan reservoir and the lower member of Germav caprock. This model was used to simulate CO_2 injection into the reservoir zone and analyze the interaction between CO_2 and the formation water and caprock minerals.

The radial model has a vertical thickness of 100 meters (65 m representing the caprock and 35 m representing the reservoir). This is represented by 100 cells in the Z direction with according division of the reservoir and caprock zones. The model has a symmetric radial extent of 100000 m. In the radial direction, the cells have been divided in an exponentially increasing manner. The size of cells in the radial direction increases towards the radial boundary of the model. This was done to simulate conditions of an infinite boundary.

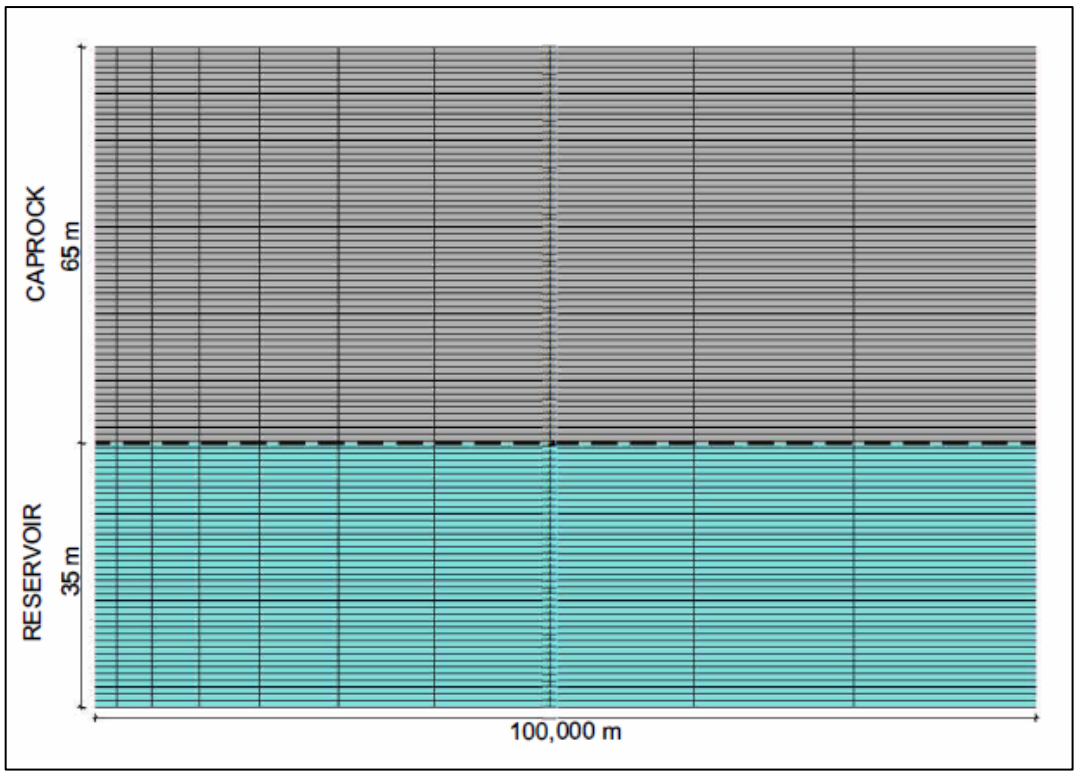

Figure 12. Cross section of the caprock and reservoir radial model

5.1.4 Caprock & Reservoir Properties

The main physical properties of the caprock and the reservoir used in the simulation are presented in table 1.

Table 1. Physical properties of the reservoir and caprock formations

Parameter	**Caprock**	**Reservoir**
Porosity (fraction)	0.1	0.18
Permeability (m^2)	2.264E-17 (0.02 mD)	5.724E-14 (58 mD)
Residual Liquid Sat. (fraction)	0.2	0.2
Residual Gas Sat. (fraction)	0.0	0.0
Rock Grain Density (kg/m^3)	2365	2780

Formation Heat Conductivity (W/m ºC)	2.0	2.0
Rock Grain Specific Heat (J/kg ºC)	1000	1000
Pressure (psi)	-	1750
Temperature (Fahrenheit)	-	150

The rock grain densities were calculated from the weighted averages of the minerals present in the formations. These values fall within the range of rock grain densities of shale and carbonate rocks respectively as stated in literature. The values of formation heat conductivity and rock grain specific heat were used as the default values of the simulation program. The X and Y permeabilities were assumed equal. The Z permeability was taken to be one tenth of the X permeability. The pressure and temperature values were defined at the bottom of the reservoir layer.

The mineralogy of the caprock was adapted from the 2018 study by Tetiker et. al. on the mineralogical properties of Germav formation (Tetiker et al., 2018). Germav formation is divided into two distinct units – upper and lower Germav. The unit of interest for the simulation was lower Germav because it is the caprock directly in contact with Garzan reservoir. The rock mineralogy used in the simulation is given in the table 2. The mineralogy of the reservoir was assumed to be 100 percent calcite because it is a carbonate reservoir.

Table 2. Mineralogy of the caprock and reservoir formation used for modeling

Caprock	Calcite	Calcite	60%
	Phyllosilicate Minerals (Clay)	Chlorite	10%
		Vermiculite	9%
		Illite	9%
	Quartz	Quartz	12%

Reservoir	Calcite	Calcite	100%

To run the simulation, it was required to define the kinetic parameters for kinetic rate law of mineral dissolution and precipitation. The parameters kinetic parameters required were rate constant, reactive surface area, activation energy, and the weighting factor. These parameters were taken from the TOUGHREACT reference manual some of which are given in table 3. It was assumed that the precipitation rate equals the dissolution rate for all minerals (Xu et al., 2008)

Table 3. Kinetic properties of minerals

NO.	Mineral	Reactive surface area (m^2/g)	Neutral mechanism		Acid mechanism			Base mechanism		
			α_{25} ($mol/m^2/s$)	E_a (KJ/mol)	Weighting factor K_{25}	Activation energy	n(H^+) exponet	Weighting factor K_{25}	Activation energy	n(H^+) exponet
1	Albite	0.0483	9.52E-13	69.8	9.87E-11	65.0	0.457	2.512E-16	71.0	-0.572
2	Calcite	1.0E-3	1.55E-9	23.5	5.012E-04	14.4	1.000	1.55E-6	23.5	0.0
3	Illite	0.991	1.66E-13	35.0	1.047E-11	23.6	0.340	3.020E-17	58.9	-0.400
4	K-feldspar	0.0247	3.89E-13	38.0	8.710E-11	51.7	0.500	6.310E-22	94.1	-0.823
5	Quartz	0.0557	1.023E-14	87.7	-	-	-	-	-	-
6	Smectite-Ca	1.52E-2	1.7E-13	35.0	1.047E-11	23.6	0.340	3.020E-17	58.9	-0.400
7	Smectite-Na	1.52E-2	1.7E-13	35.0	1.047E-11	23.6	0.340	3.020E-17	58.9	-0.400
8	Anorthite	1.0E-3	7.6E-10	17.8	3.162E-04	16.6	1.411	2.75E-13	69.8	0.0
9	Pyrite	1.29E-3	-	-	3.02E-8	56.9	n(H^+)=-0.5 n(Fe^{3+})=0.5	2.8184E-5	56.9	n($O_{2(aq)}$)=0.5
10	Chlorite	2.0E-3	3.02E-13	88	7.762E-12	88.0	0.5	-	-	-
11	Magnesite	1.0E-3	4.57E-10	23.5	4.169E-7	14.4	0.5	-	-	-
12	Dawsonite	1.0E-3	1.26E-9	62.76	6.457E-06	36.1	0.5	-	-	-
13	Kaolinite	0.0987	6.61E-14	22.2	4.898E-12	65.9	0.777	8.913E-18	17.9	-0.472
14	Siderite	1.0E-3	1.66E-11	18.6	2.57E-9	18.6	0.28	-	-	-
15	Ankerite	1.0E-3	1.26E-9	62.76	6.46E-4	36.1	0.2	-	-	-

5.1.5 Simulation Scenarios

5.1.5.1 Scenario I

CO_2 was injected into the reservoir formation for a period of 100 years simulating long-period injection. It was first injected at a reservoir temperature and pressure of 150 degrees Fahrenheit and 1750 psi respectively. The CO_2 was injected at a rate of 120 kg/s continuously for the 100-year period. Injection was done at the center of the radial model as shown in figure 13 through the cells in the bottom 10 meters. A post-injection

monitoring period of 1000 years was simulated for both scenarios to observe the movement of the injected CO_2 and understand the geochemical changes caused by the CO_2. This period was also simulated to be able to analyze the alterations in the sealing capacity of the caprock through observing porosity and permeability changes.

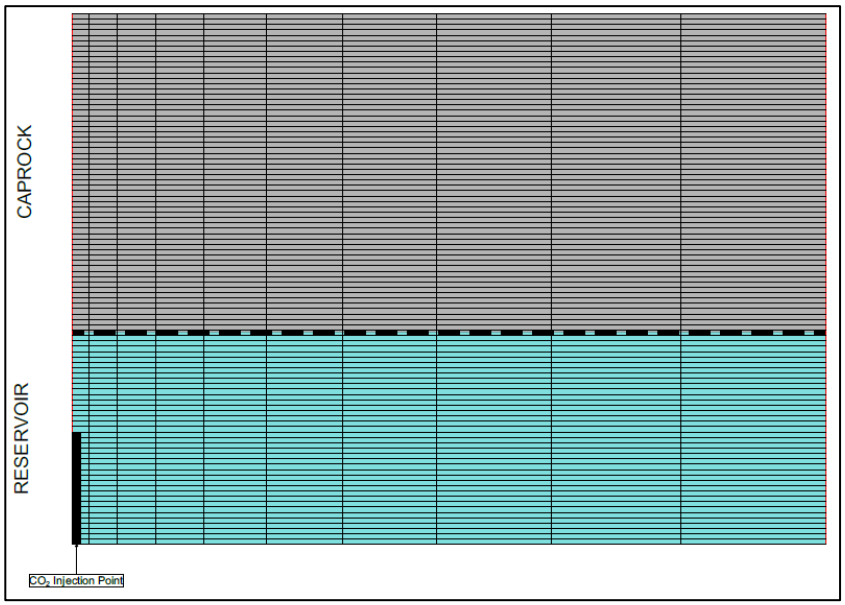

Figure 13. 2-D radial model with CO2 injection point

5.1.5.2 Scenario II

A second simulation was done whereby CO_2 was injected at the same rate but at an elevated temperature of 300 degrees Fahrenheit to observe the differences in results that might occur due to high temperature conditions. Similar to the first scenario, CO_2 was injected for 100 years followed by a post-injection monitoring period of up to 1000 years.

5.2 CO_2 Storage in a Geothermal Reservoir

PETRASIM was used to build a simple two-dimensional radial model of a geothermal reservoir. The properties of this reservoir were chosen to be representative of the reservoir properties of the Iğdecık formation of Kızıldere geothermal field in Turkey. A more detailed description of Kızıldere field is given in the next section. Like the case of CO_2 injection into a hydrocarbon reservoir, as much data as is available in public literature was

used to construct the model with assumptions made where data was not available. However, it is to be noted with caution that this study in no way aims to completely model CO_2 sequestration in Kızıldere, but rather aims to create a synthetic model using some of the reservoir properties of Iğdecık formation to understand the effect of CO_2 sequestration on the reservoir and CO_2 trapping mechanisms in similar geothermal reservoirs.

5.2.1 Kızıldere Field

Kızıldere, located between Denizli and Aydin provinces, was discovered by the Turkish Directorate of Mineral Research and Exploration (MTA) and was the first geothermal field developed for electricity production in Turkey. It was used to produce electricity which was supplied to the national electric grid. Kızıldere was run by the Turkish Electricity Generation Co. Inc. (EÜAŞ) for 24 years before it was privatized in 2008. Zorlu Energy Group acquired the rights to operate Kızıldere and the commercial-scale electricity generation plant it was supplying. Zorlu continued the development of Kızıldere and built 2 more power plants making this field one of the most productive geothermal fields in Turkey and the world in terms of the power generation capacity of the plants it is supplying (Küçük, 2018).

Kızıldere is in the eastern part of the Büyük Menderes Graben with the general stratigraphy of the field mostly composed of Paleozoic metamorphic rocks of Menderes Massifs and Pliocene and Quaternary sedimentary rocks (Bozkurt & Oberhänsli, 2001; Şimşek, Parlaktuna, & Akın, 2009).

Menderes metamorphic rocks form the basement rocks, which mainly consist of marble, quartzite, gneiss, schist, and mica-schist (Karamanderesi, 2013). The upper Pliocene and Quaternary sedimentary rocks are composed of four lithological units namely; Kızılburun Formation, Sazak Formation, Kolankaya Formation, and Tosunlar Formation (Şimşek, 1985). Kızılburun Formation acts as a caprock due to its impermeable nature and forms the boundary between the Paleozoic metamorphic rocks and Pliocene sedimentary rocks.

Sazak Formation forms the shallow reservoir section of Kızıldere and mainly consist of 100 - 250 m thick limestone. The interbedded marble-quartzite-schist section of the upper unit of

the Menderes metamorphic section is called İğdecik Formation, and forms the intermediate level reservoir of Kızıldere field, with thickness ranging between 100 - 300 m. İğdecik Formation has better reservoir characteristics compared to the Sazak Formation and has been proposed to be used for re-injection because it has good enough permeability to successfully reinject fluids. A deeper, third reservoir section, which mainly consists of metamorphic schist and marble has a good production zone but is not suitable for re-injection purposes (Karamanderesi, 2013).

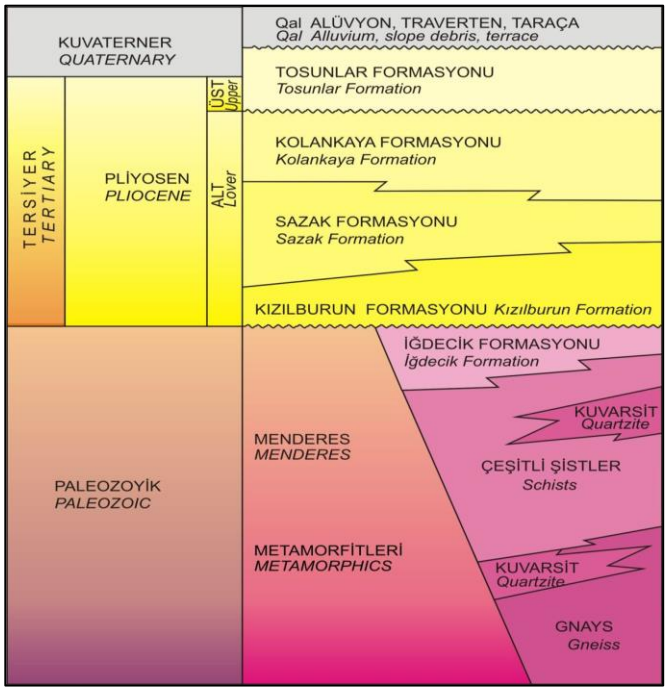

Figure 14. General stratigraphy of Kızıldere field (Şimşek et al., 2009)

5.2.2 Potential for CO_2 Storage in Kızıldere Field

Turkey, one of the biggest geothermal countries has been involved in research concerning injection of CO_2 into geothermal reservoirs. A large-scale project ongoing in Turkey regarding the injection of CO_2 into geothermal fields is the Geothermal Emission Control (GECO) project. This is a joint EU project that aims to lower emissions from geothermal power generation by capturing CO_2 either for reuse or storage (GECO/EU, 2019).

In Turkey, this project focuses on Kızıldere geothermal field, operated by Zorlu energy group. It employs CO_2 injection, field monitoring, and reservoir modeling to investigate

the effects of CO_2 injection on Kızıldere field. This ongoing project has not published results yet but is the first of its kind in Turkey and one of the first few in the world in terms of purpose and scale. It opens a gateway for possible CO_2 sequestration in geothermal reservoirs in Turkey in the future.

Currently, Kızıldere produces a large amount of CO_2 which is not re-injected back into the reservoir. Re-injecting the produced CO_2 back into the reservoir is an option that is being considered to reduce emissions from the field.

5.2.3 Model Geometry and Grid

A simplified two-dimensional radial model was built on PETRASIM using some properties of İğdecik formation. This model was used to simulate CO_2 injection into the reservoir and observe the changes induced by the CO_2 injection and understand the storage potential and mechanisms involved.

The radial model has a vertical thickness of 100 meters represented by 100 cells in the Z direction. The model has a symmetric radial extent of 100000 m. Similar to the previous case, in the radial direction, the cells have been divided in an exponentially increasing manner as shown in figure 15. The size of cells in the radial direction increases towards the radial boundary of the model. This was done to simulate conditions of an infinite boundary.

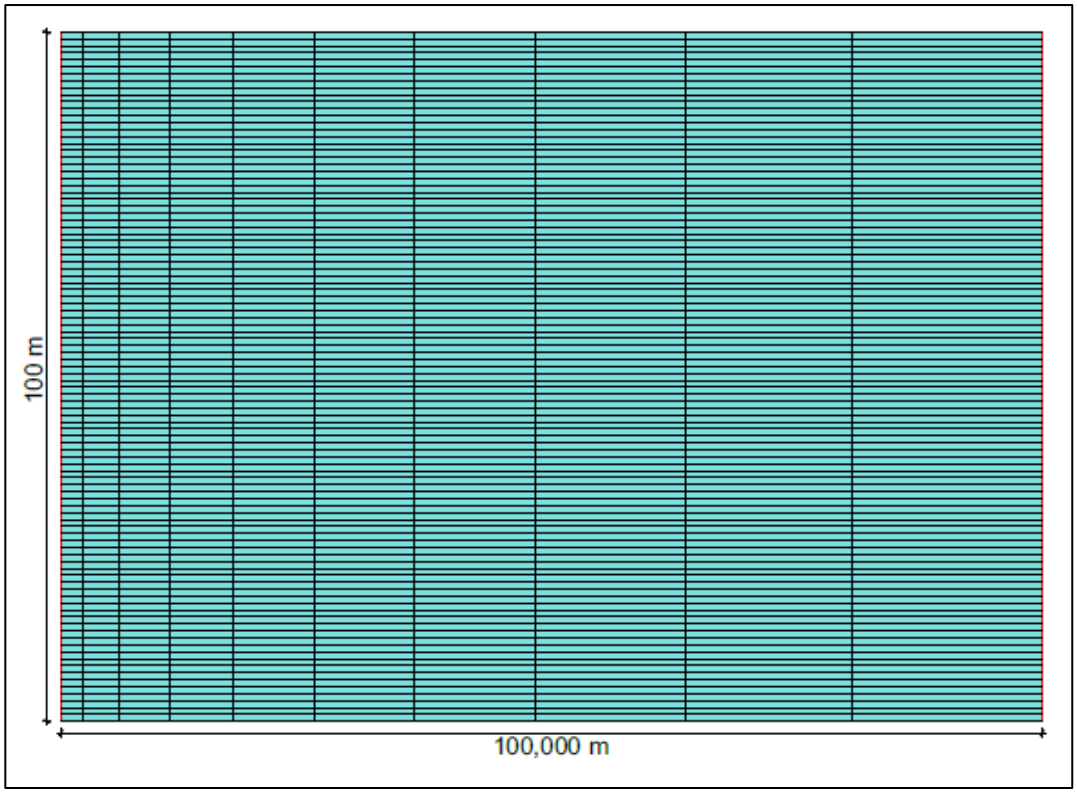

Figure 15. Cross-section of reservoir model

5.2.4 Reservoir Properties

Table 4. Reservoir properties used in the simulation

Parameter	**Value**
Porosity (fraction)	0.05
Permeability (m^2)	4.935E-14 (50 mD)
Dissolved CO_2 (mass fraction)	0.02
Free Gas Sat. (fraction)	0.0
Rock Grain Density (kg/m^3)	2600
Formation Heat Conductivity (W/m ºC)	1.0

Rock Grain Specific Heat (J/kg ºC)	1000
Pressure (psi)	3050
Temperature (Fahrenheit)	468

The properties above were obtained from a detailed simulation study on Kızıldere geothermal field published in a thesis by Küçük (Küçük, 2018). The X and Y permeabilities were assumed equal. The Z permeability was taken to be one tenth of the X permeability.

A detailed mineralogical analysis of the metamorphic rocks of İğdecik formation is not available in any public literature. However, the general rock composition is known, and approximate values were assigned to individual mineral species present as indicated in table 5.

Table 5. Mineralogy of the reservoir formation used for modeling

Marble	Calcite	Calcite	85%
Quartzite	Quartz	Quartz	5%
Schist	Quartz	Quartz	5%
	Mica Minerals	Biotite	1%
		Chlorite	1%
		Muscovite	1%
	Plagioclase	Anorthite	1%
		Albite	1%

The kinetic properties of the minerals such as rate constant, reactive surface area, and activation energy used in the simulation were obtained from the TOUGHREACT manual (Xu et al., 2008)

5.2.5 Simulation Scenarios

5.2.5.1 Scenario I

The first scenario simulated is re-injecting the amount of produced CO_2 back into the reservoir. Kızıldere produces about 6700 tons per hour of water which contains CO_2 ranging between 1.5 and 3% by weight. (Küçük, 2018). Assuming a value of 2%, the amount of CO_2 produced is approximately 134 tons per hour (37.2 kg/s) CO_2 was injected into the reservoir for a period of 100 years at a rate of 37.2 kg/s. This was followed by a monitoring period of up to 1000 years.

5.2.5.2 Scenario II

The second scenario simulated is using the reservoir for CO_2 storage by injecting large amounts of CO_2. CO_2 was injected for a period of 100 years at a rate of 120 kg/s. This was also followed by a monitoring period of up to 1000 years.

5.3 Cement Plug Integrity

PETRASIM was used to build a field-scale model of a cement plug to simulate the degradation of wellbore cement in a CO_2 – rich environment. A two-dimensional linear model was built. The model was built in such a way that the first cell has the properties of a reservoir rock. CO_2 injection is done into this cell at a constant rate. This is done to imitate realistic conditions whereby it is expected the injected CO_2 would interact with reservoir brine and minerals under reservoir conditions first before coming into contact with the wellbore cement.

5.3.1 Model Geometry and Grid

The two-dimensional model of a cement plug has a length of 100 meters and a thickness of 0.5 meters. It has a grid composed of 100 cells. The thickness of the cells is set to increase in an exponential manner away from the point of CO_2 injection as shown in figure 16. This is done to better observe the changes near the CO_2 contact point. Further points

are less likely to be affected as drastically as the points near the point of first contact with CO_2; therefore, those cells can have a greater thickness.

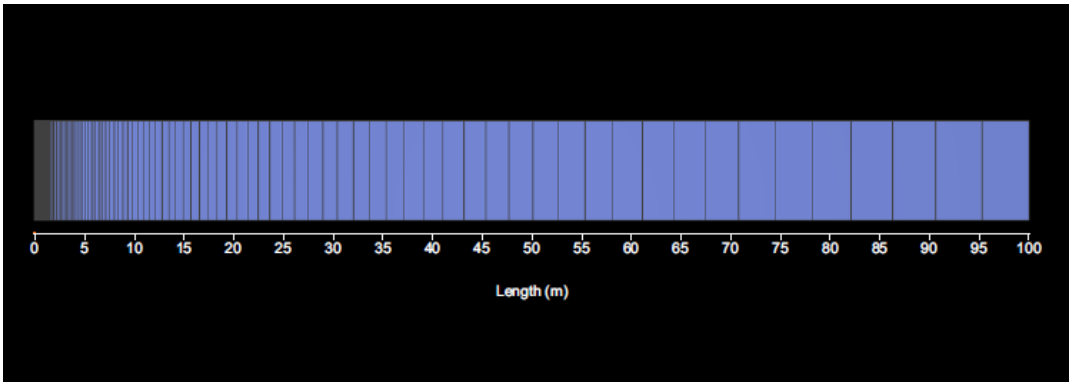

Figure 16. Cross-section of the cement plug model

5.3.2 Cement Plug Properties

The model was constructed based on an API class G Portland oil well cement with the following properties used for the simulation.

Table 6. Cement properties

Parameter	**Value**
Porosity (fraction)	0.2
Permeability (m^2)	1.974E-17
Rock Grain Density (kg/m^3)	3150
Rock Grain Specific Heat (J/kg ºC)	1000

The mineralogic properties of Portland cements have been widely studied and data is readily available in public literature. This data was used to simulate the interaction between CO_2 and wellbore cement. There are four main minerals present in Portland cement shown in table 7. These minerals and the information associated with them is

summarized in table 7 published by Barron and Johnson in Portland Cement in the Energy Industry (Barron & Johnson, n.d.).

Table 7. Portland cement mineral composition (Barron & Johnson, n.d.)

Mineral	Chemical formula	Oxide composition	Abbreviation
Tricalcium silicate (alite)	Ca_3SiO_5	$3CaO.SiO_2$	C3S
Dicalcium silicate (belite)	Ca_2SiO_4	$2CaO.SiO_2$	C2S
Tricalcium aluminate	$Ca_3Al_2O_4$	$3CaO.Al_2O_3$	C3A
Tetracalcium aluminoferrite	$Ca_4Al_nFe_{2-n}O_7$	$4CaO.Al_nFe_{2-n}O_3$	C4AF

Chemical formulae and cement nomenclature for major constituents of Portland cement. Abbreviation notation: C = CaO, S = SiO_2, A = Al_2O_3, F = Fe_2O_3.

Barron and Johnson state that the exact composition might vary depending on the application of the cement. However, typical cements contain between 50 – 70% CS3, 15 – 30% C2S, 5 – 10% C3A, 5 – 15% C4AF, and 3 – 8% other additives.

The formula of each of these minerals can be broken down into the basic calcium, silicon, aluminum, and iron oxides. Schutz et al. present the oxide composition of an API class G cement as summarized in table 8.

Table 8. Chemical composition & density of class G cement (Schütz et al., 2019)

Composition	%
SiO_2	21.25
Al_2O_3	3.95
Fe_2O_3	4.57
CaO	65.07
MgO	2.31
SO_3	2.27
Na_2O	0.25
K_2O	0.33
Density ($g.cm^{-3}$)	3.1

5.3.3 Simulation Scenarios

5.3.3.1 Scenario I

CO_2 was injected into the cell with reservoir-like properties at a constant rate of 0.001 kg/s for a period of 100 years. The reservoir properties were set similar to that of the carbonate hydrocarbon reservoir modeled previously. It was first injected at a pressure of 1750 psi and temperature of 150 degrees Fahrenheit. The transport of the CO_2 and the changes in the cement porosity and permeability due to interaction of the CO_2 with the cement was monitored for this 100-year period.

5.3.3.2 Scenario II

A second simulation was run using the same parameters from the first simulation but with one difference. A micro-silica additive was added to the cement composition to observe its effect on CO_2 interaction with cement. Some studies have postulated that adding micro-silica to cement mixtures makes it gas tight and improves cement resistance to CO_2 attack (Vrålstad et al., 2019). The addition of micro-silica additive to the cement composition was done by including SiO_2 with a micro-scale grain surface area.

5.3.3.3 Scenario III

A third simulation was run by injecting CO_2 into the first cell with reservoir-like properties similar to the geothermal reservoir modeled. CO_2 was injected at a rate of 0.001 kg/s for 100 years. It was injected at a pressure of 3050 psi and temperature of 468 degrees Fahrenheit.

CHAPTER 6

RESULTS AND DISCUSSION

6.1 CO_2 Storage in a Hydrocarbon Reservoir

6.1.1 Scenario I – 150 Degrees Fahrenheit

6.1.1.1 Transport of Supercritical CO_2

The injected CO_2 initially migrated upward due to buoyancy until it was trapped under the caprock and began to form a plume. The plume reached up to a radial extent of 1000 meters after 2 years of CO_2 injection. After 100 years of injection, it had reached up to 4000 meters in radial extent. This can be seen in figures 17 and 18 respectively.

At half of the post-injection monitoring period, the CO_2 plume had extended to approximately 6500 meters. After 1000 years, it reached 7500 meters radially from the point of injection. The farthest radial distances were reached by the top part of the CO_2 plume as shown in figures 19 and 20.

The transport and distribution of supercritical CO_2 at discrete time periods during the injection and monitoring periods is graphically presented in two-dimensional in figures 17 to 20.

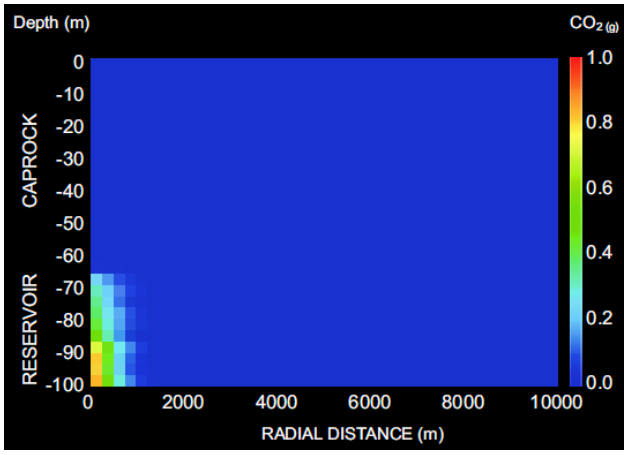

Figure 17. Distribution of supercritical CO_2 (saturation) - 2 years injection period

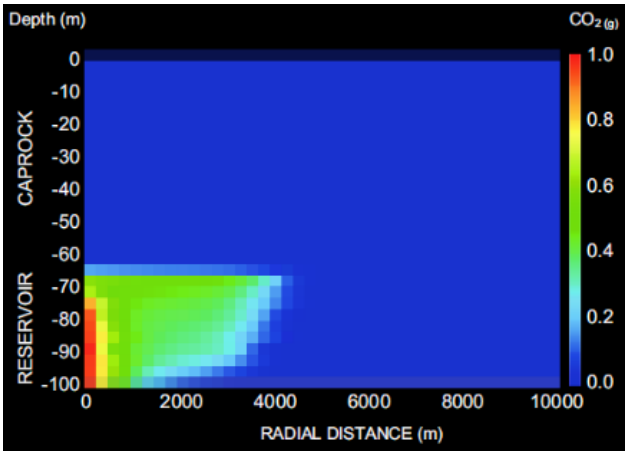

Figure 18. Distribution of supercritical CO_2 (saturation) - 100 years injection period

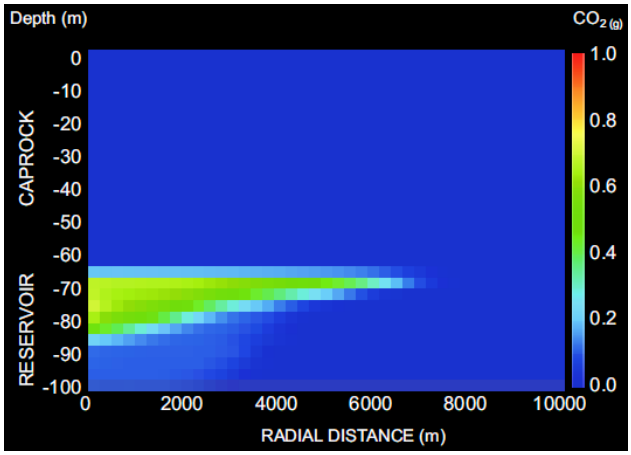

Figure 19. Distribution of supercritical CO_2 (saturation) - 500 years post-injection monitoring period

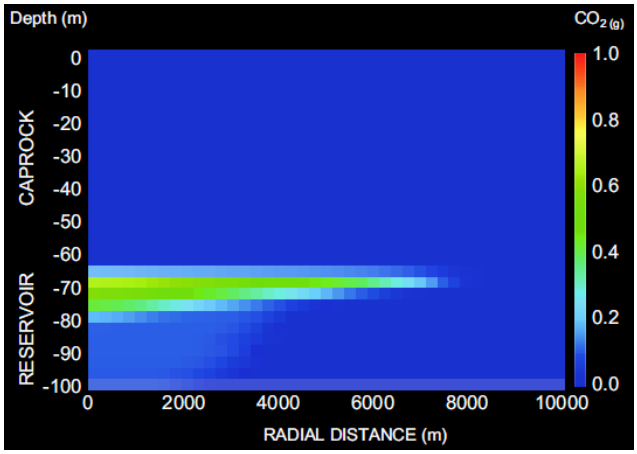

Figure 20. Distribution of supercritical CO_2 (saturation) - 1000 years post-injection monitoring period

6.1.1.2 Dissolution of CO_2

After injection for 2 years, it was observed that the mass fraction of dissolved CO_2 had reached a value of approximately 0.045 in the region just above the injection point as shown in figure 21. The radial extent of dissolved CO_2 after 2 years of injection was approximately 1000 meters. After 100 years of injection, the radial extent had reached 4800 meters. There was also minor vertical diffusion of dissolved CO_2 into the caprock as in figure 21 and 22.

At 500 and 1000 years of post-injection monitoring, the dissolved CO_2 had reached radial extents of 7800 and 8600 meters respectively as shown in figures 23 and 24. Furthermore, the concentration of dissolved CO_2 was reducing as its extent radially increased. This is attributed to mixing and convection of CO_2 saturated and unsaturated formation water.

The distribution of dissolved CO_2 mass fraction at discrete time periods during the injection and monitoring periods is graphically presented in two-dimensional plots in figures 21 to 24.

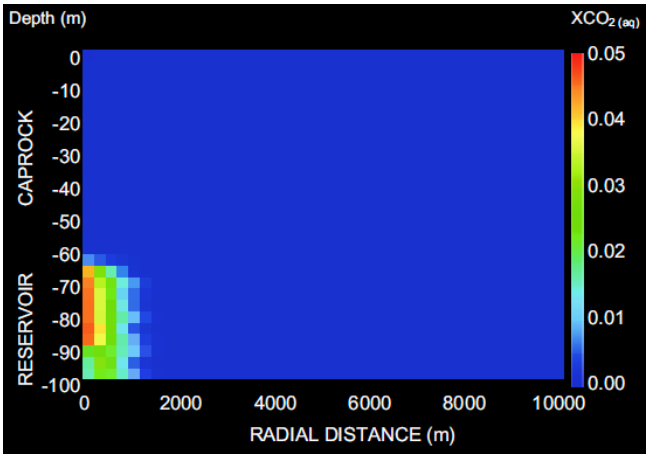

Figure 21. Distribution of dissolved CO_2 (mass fraction) - 2 years injection period

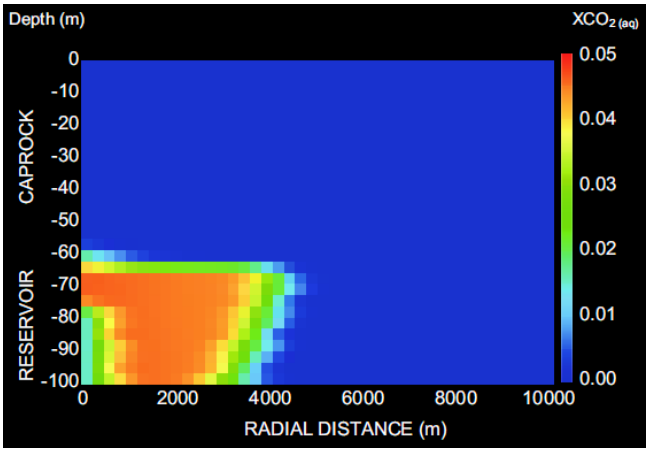

Figure 22. Distribution of dissolved CO_2 (mass fraction) - 100 years injection period

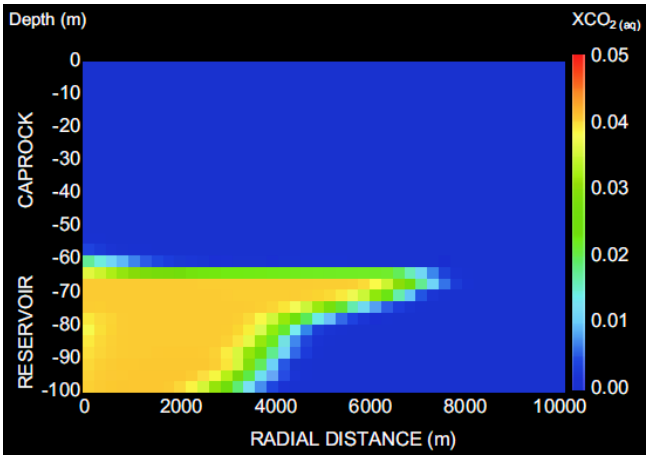

Figure 23. Distribution of dissolved CO_2 (mass fraction) - 500 years post-injection monitoring period

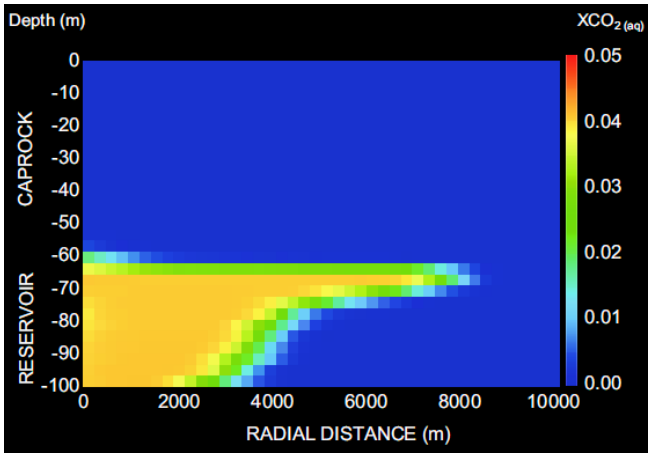

Figure 24. Distribution of dissolved CO_2 (mass fraction) - 1000 years post-injection monitoring period

6.1.1.3 Evolution of Calcite

The biggest observed change in the concentration and distribution of minerals in the reservoir rock and caprock was in the abundance of calcite. There was major dissolution of calcite minerals in the regions swept by the formation water with dissolved CO_2. This is attributed to the acidic brine saturated with CO_2. Most of the calcite dissolution occurred in the reservoir region. There was also minor calcite dissolution in the bottom parts of the caprock which were invaded by formation water with dissolved CO_2.

$$CaCO_3 + H^+ \rightarrow Ca^{2+} + HCO_3^-$$

Due to the dissolution of calcite, there was an increase in abundance of Ca^{2+} and HCO_3^- ions in the regions where calcite dissolution occurred. The changes in the abundance of calcite and Ca^{2+} and HCO_3^- ions due to the presence of CO_2 saturated brine are graphically represented in two-dimensional plots shown in figures 25 to 36.

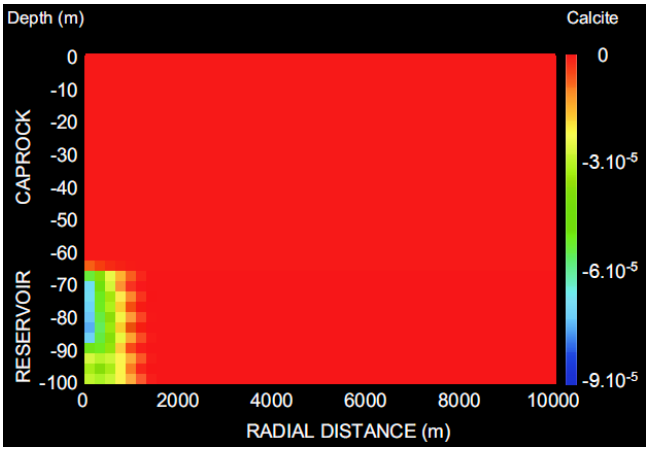

Figure 25. Change in calcite volume fraction - 2 years injection period

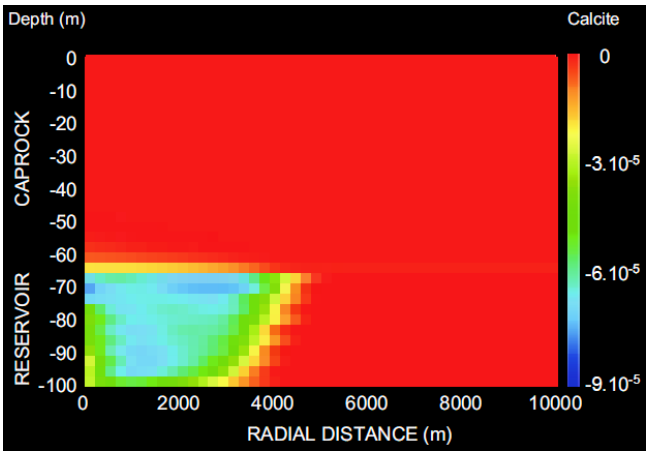

Figure 26. Change in calcite volume fraction - 100 years injection period

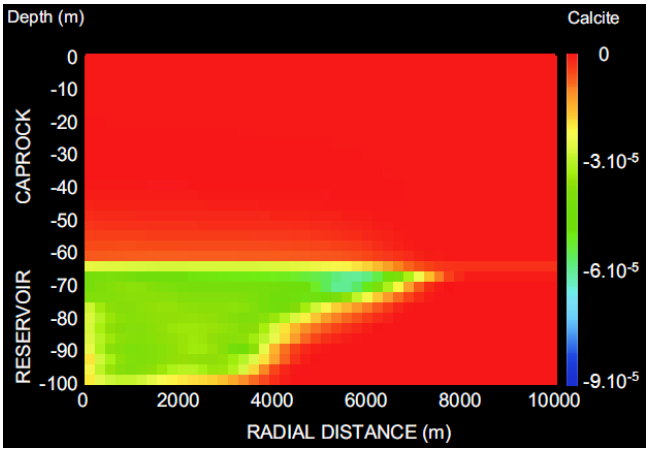

Figure 27. Change in calcite volume fraction - 500 years post-injection monitoring period

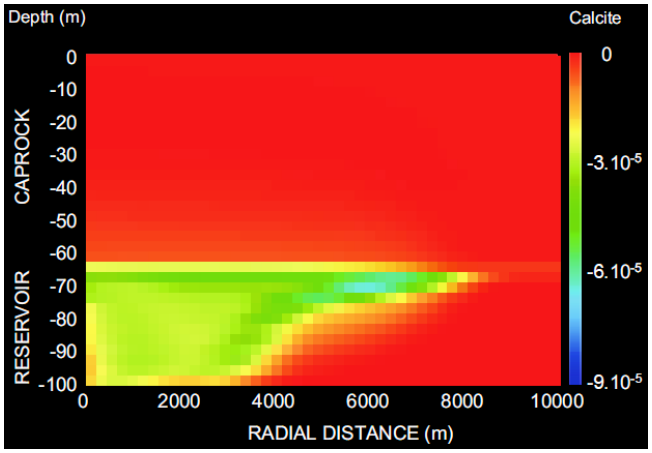

Figure 28. Change in calcite volume fraction - 1000 years post-injection monitoring period

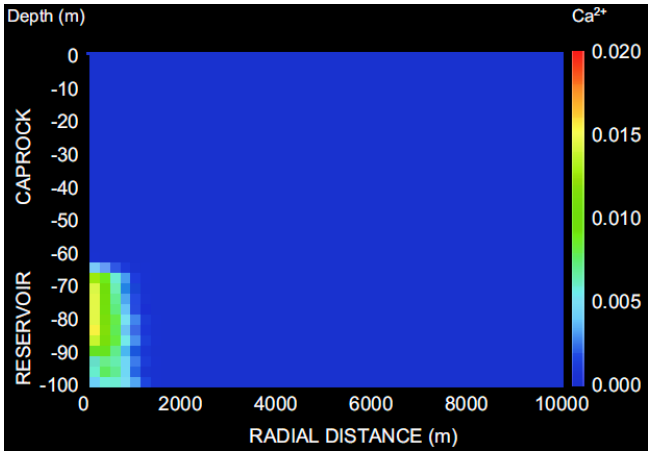

Figure 29. Concentration of Ca ions (mol/kg) - 2 years injection period

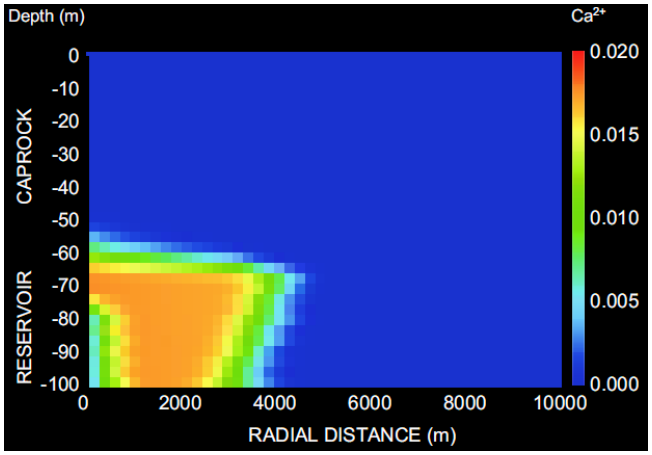

Figure 30. Concentration of Ca ions (mol/kg) - 100 years injection period

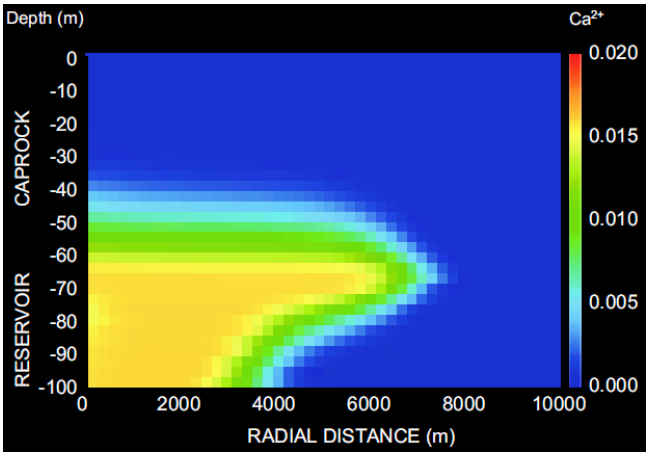

Figure 31. Concentration of Ca ions (mol/kg) - 500 years post-injection monitoring period

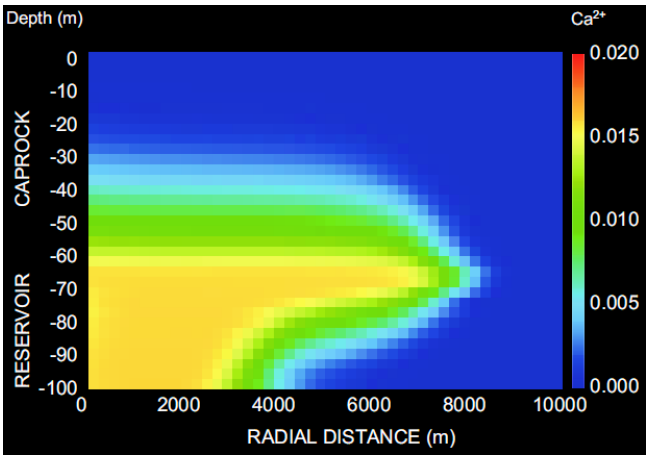

Figure 32. Concentration of Ca ions (mol/kg) - 1000 years post-injection monitoring period

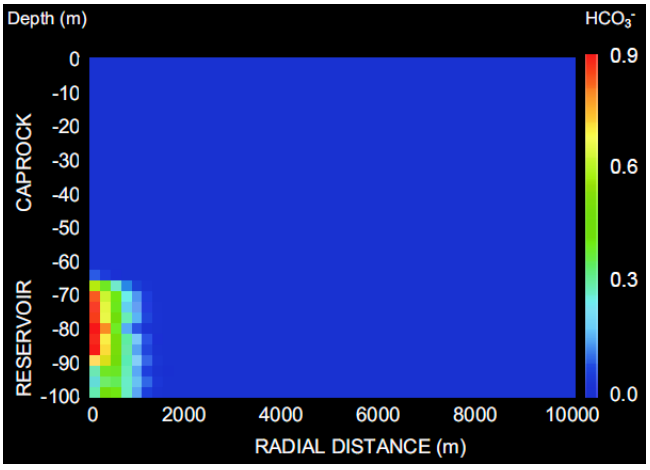

Figure 33. Concentration of HCO_3 ions (mol/kg) - 2 years injection period

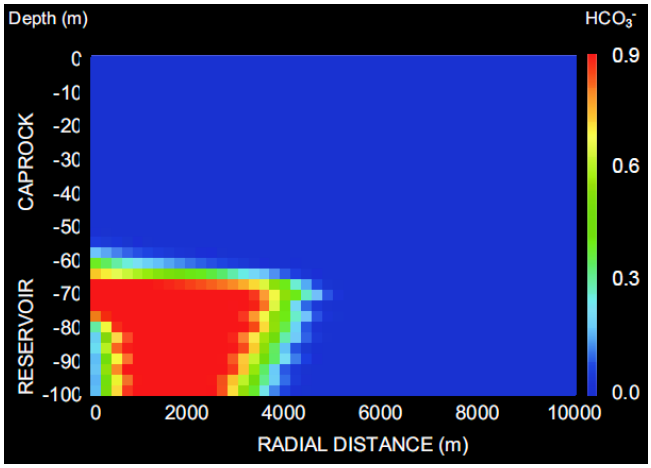

Figure 34. Concentration of HCO_3 ions (mol/kg) - 100 years injection period

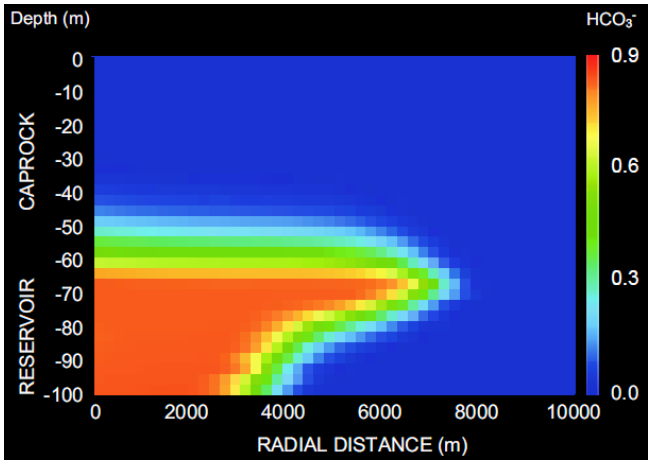

Figure 35. Concentration of HCO_3 ions (mol/kg) - 500 years post-injection monitoring period

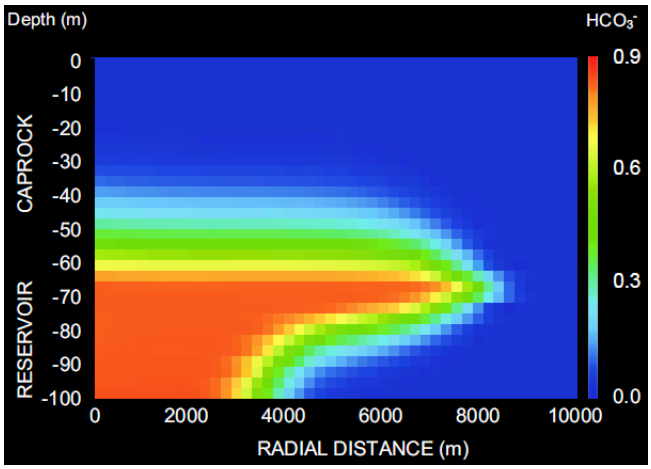

Figure 36. Concentration of HCO_3 ions (mol/kg) - 1000 years post-injection monitoring period

6.1.1.4 Changes in pH

Initially, the caprock formation water pH was a relatively neutral value of 7.2. After the injection of CO_2, the pH of the brine began to gradually decrease until it reached a value of approximately 4.5, in the lower meters, 1000 years after injection as can be seen in figure 40. Similarly, in the reservoir formation, the pH decreased from an initially neutral value of 7.5 to an acidic low of 4.5. The decreases in pH are because of the acidification of formation waters due to dissolution of CO_2. The changes in pH are graphically shown in two-dimensional plots in figures 37 to 40.

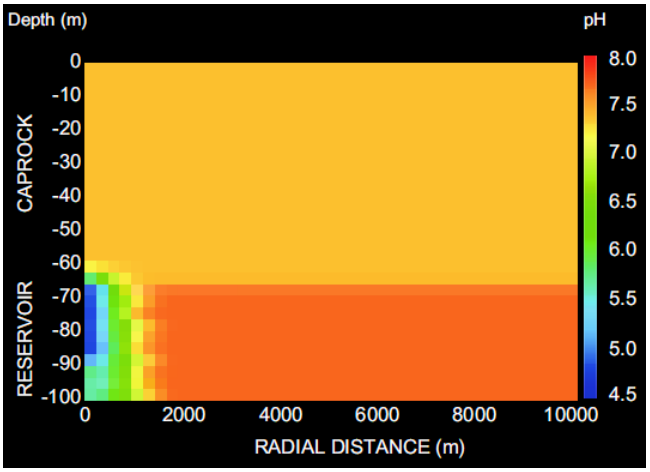

Figure 37. Formation water pH - 2 years injection period

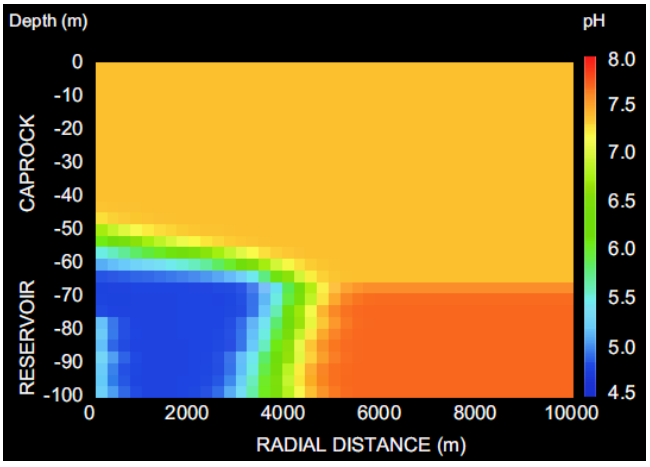

Figure 38. Formation water pH - 100 years injection period

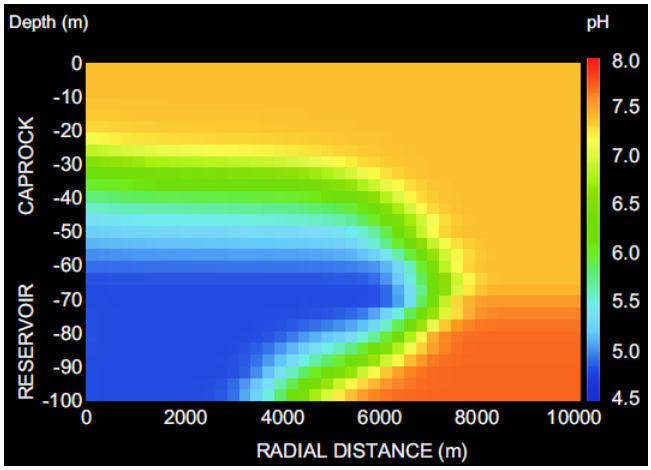

Figure 39. Formation water pH - 500 years post-injection monitoring period

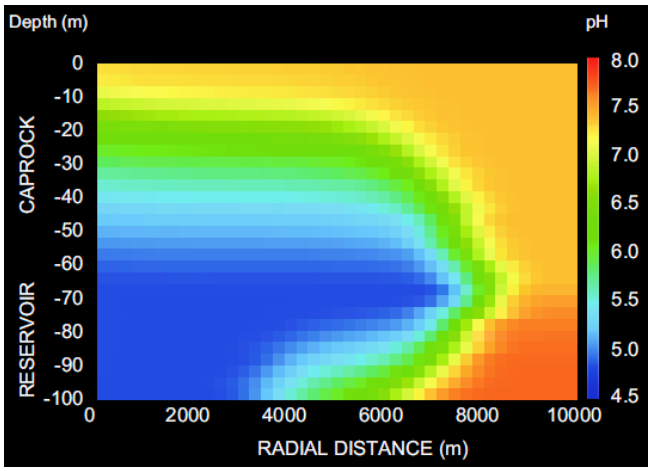

Figure 40. Formation water pH - 1000 years post-injection monitoring period

6.1.1.5 Fate of the Caprock Integrity

There were very minor alterations in the caprock porosity and permeability. The change in permeability is calculated from the change in porosity using a simple cubic expression. Initially, there was a slight increase in porosity. This was due to the dissolution of minerals. However, the precipitation of minerals became dominant over the dissolution and this led to an overall decrease in porosity in the long term. Therefore, over the long term, there was also a resultant decrease in permeability.

Table 9. Maximum changes in caprock porosity and permeability

	Porosity Change (%)	Permeability Change (%)
2	+0.02	+0.230
100	-0.02	-0.239
500	-0.1	-1.86
1000	-0.12	-1.87

The changes in caprock porosity and permeability at discrete times during the simulation are shown in two-dimensional plots in figures 41 to 48.

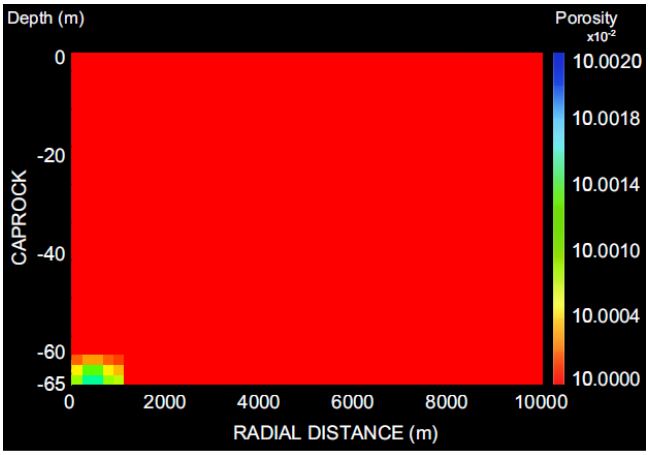

Figure 41. Caprock porosity - 2 years injection period

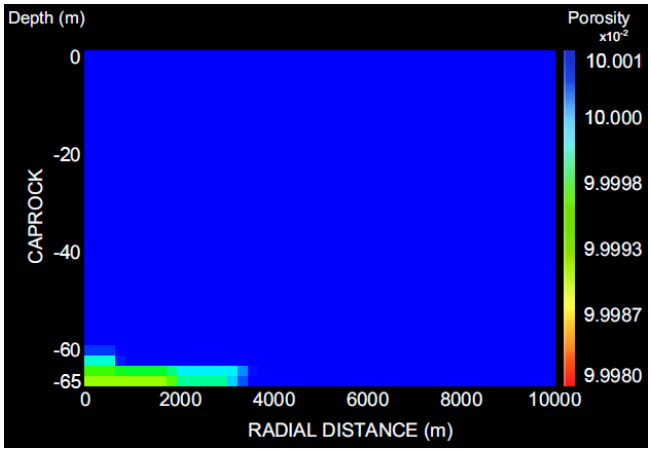

Figure 42. Caprock porosity - 100 years injection period

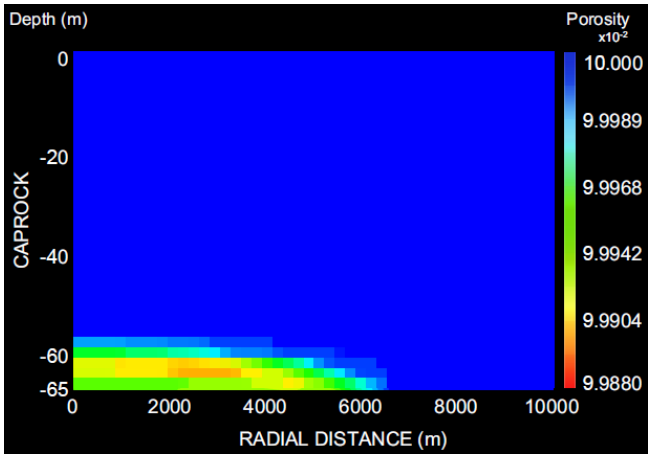

Figure 43. Caprock porosity - 500 years post-injection monitoring period

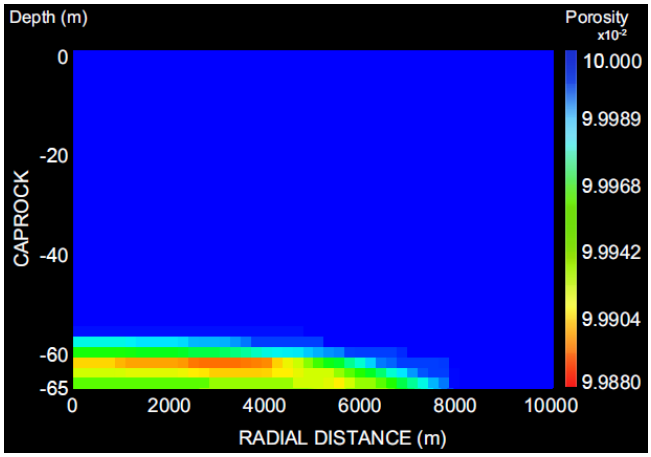

Figure 44. Caprock porosity - 1000 years post-injection monitoring period

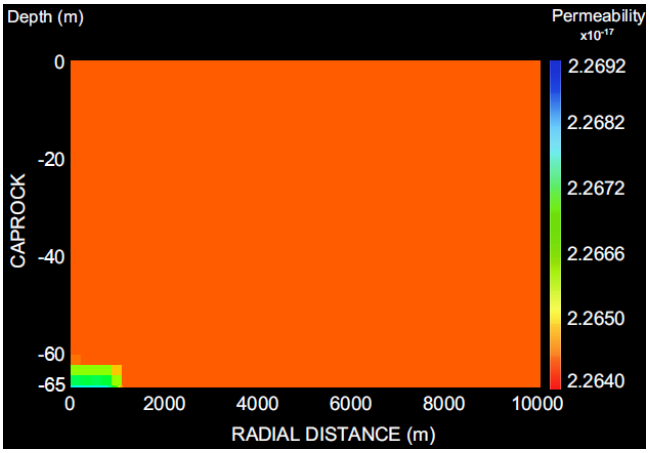

Figure 45. Caprock permeability - 2 years injection period

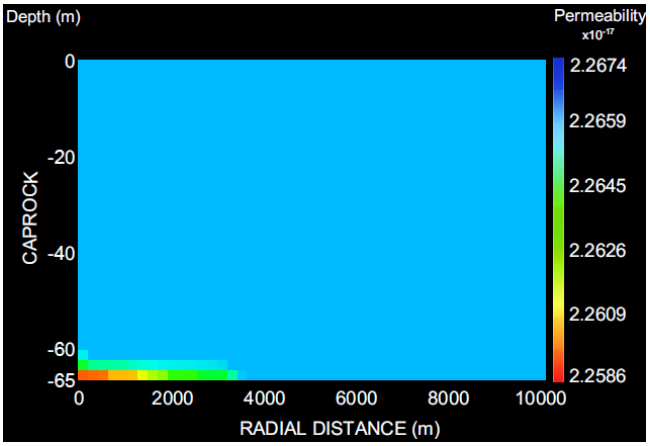

Figure 46. Caprock permeability - 100 years injection period

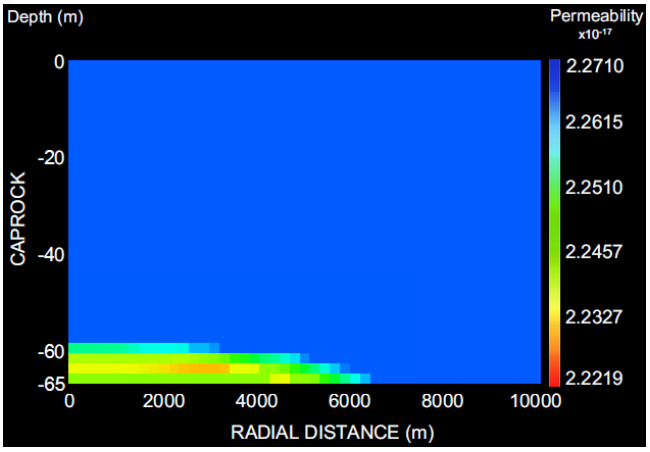

Figure 47. Caprock permeability - 500 years post-injection monitoring period

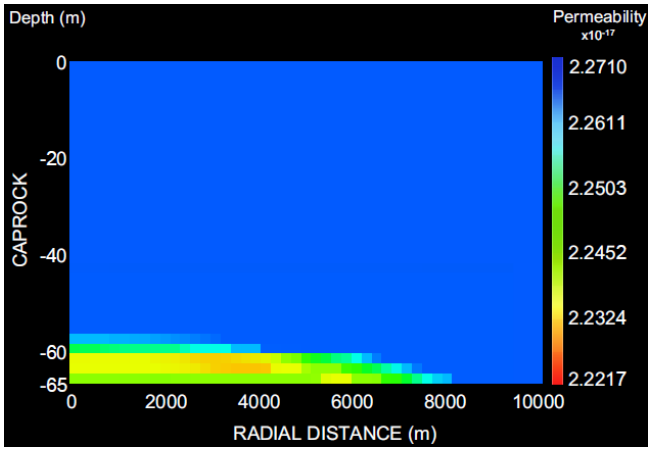

Figure 48. Caprock permeability - 500 years post-injection monitoring period

6.1.1.6 Storage of the Injected CO_2

Most of the injected CO_2 was stored via seal trapping and solubility trapping. Approximately 76% of the injected CO_2 was trapped under the caprock as a free phase while most of the remaining amount was dissolved in the reservoir formation water.

After 1000 years of post-injection monitoring, very minor amounts of the injected CO_2 had diffused into the caprock. Furthermore, the effect of the very small amount that invaded the caprock was mostly evident in the lowest 5 – 10 meters of the caprock. However, the changes in pH in the caprock were observed over a larger area because of convective mixing of the formation water.

6.1.2 Scenario II – 300 Degrees Fahrenheit

The injection of CO_2 at a much higher temperature of 300 degrees Fahrenheit was simulated to observe the effect of high temperatures on CO_2 transport and storage. Results showed that high temperatures seemed to inhibit the transport and storage of the injected CO_2. There was a lesser effect of CO_2 on the reservoir and caprock minerals and integrity. This could be because of the properties of CO_2 in high temperature environments. In the high temperature simulation, there was significantly less spatial transport of CO_2. More of the injected CO_2 remained the injection point compared to the low temperature scenario. Thus there was a higher concentration near the injection point as can be seen in

figure 81. This is because an increase in temperature causes an increase in the viscosity of CO_2. This leads to a reduction in its mobility and thus it does not spread as far as in the low temperature case. Furthermore, there was less dissolution of CO_2 in the high temperature case. This is because the solubility of CO_2 in water decreases with an increase in temperature.

Due to the inhibition of CO_2 spread and dissolution, there was a lesser effect on the reaction with formation minerals. There was less dissolution of calcite compared to the low temperature case. Subsequently there was a smaller increase in the amount of calcium and bicarbonate ions. Moreover, there was less reduction in formation water pH due to less dissolution of CO_2 and less presence of bicarbonate ions.

The caprock porosity and permeability changes in the high temperature case were smaller and occurred over smaller spatial zones. This is because porosity is calculated from the change in mineral volumes and there were relatively less changes in mineral volumes. Permeability is calculated from porosity and it followed a similar trend.

The amount of CO_2 stored by solubility trapping was less than in the low temperature case. Based on the simulation under high temperatures, it is evident that high temperature sedimentary carbonate reservoirs are not ideal for CO_2 storage as the high temperatures inhibit the movement and storage of the injected CO_2.

Plots comparing results from the low temperature and high temperature cases at discrete times during the simulations have been relegated to appendix A.

6.2 CO_2 Storage in a Geothermal Reservoir

6.2.1 Scenario I – 37.2 Kg/s Injection Rate

6.2.1.1 Transport of Supercritical CO_2

In the geothermal reservoir, there was no accumulation of CO_2 as a free phase. All the injected CO_2 was dissolved into the formation water. This was observed throughout the injection period and at the end of the monitoring period as shown in figures 49 and 50.

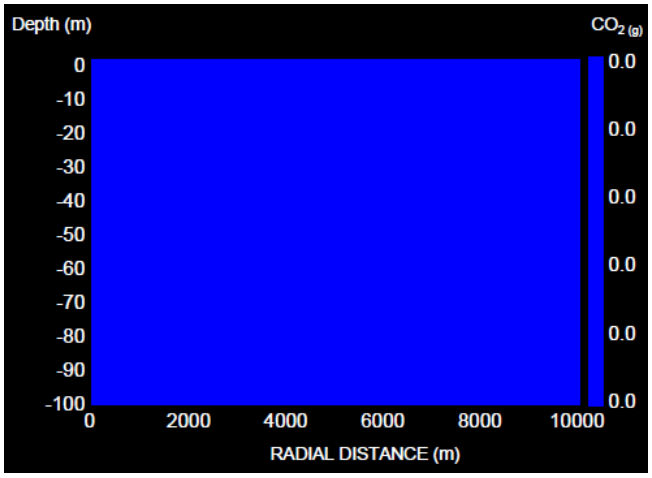

Figure 49. Distribution of supercritical CO_2 (saturation) - 100 years injection period

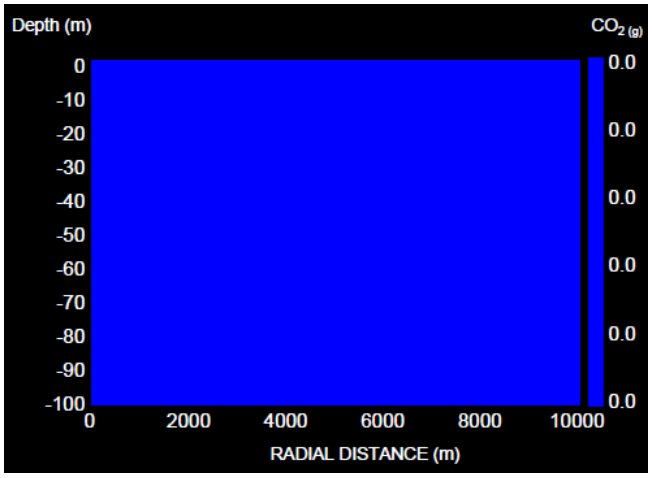

Figure 50. Distribution of supercritical CO_2 (saturation) - 1000 years post-injection monitoring period

6.2.1.2 Dissolution of CO_2

After 2 years of injection, the mass fraction of dissolved CO_2 had increased to a maximum value of 0.045 from the initial value of 0.02. The CO_2 saturated brine spread through the reservoir mixing with other water and causing the mass fraction of dissolved CO_2 to increase. At the end of the 1000-year monitoring period, dissolved CO_2 had spread to an extent of approximately 7500 m from the injection point. The concentration of dissolved CO_2 had reduced after 1000 years. This is due to mixing of CO_2 saturated brine and relatively less concentrated brine as spreading occurred.

The distribution of dissolved CO_2 mass fraction at discrete time periods during the injection and monitoring periods is graphically presented in two-dimensional plots in figures 51 to 54.

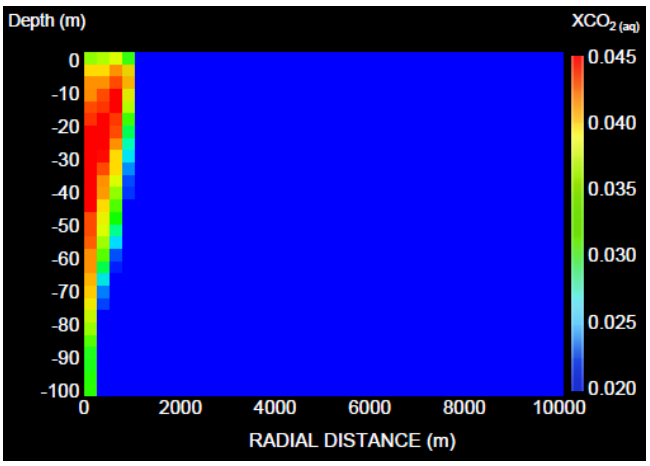

Figure 51. Distribution of dissolved CO2 (mass fraction) - 2 years injection period

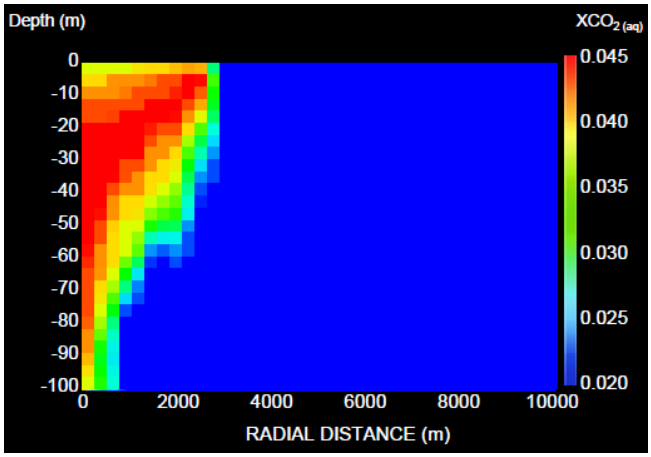

Figure 52. Distribution of dissolved CO2 (mass fraction) - 100 years injection period

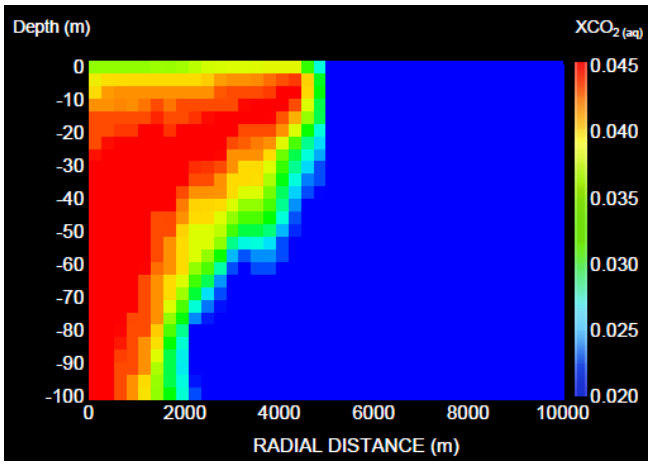

Figure 53. Distribution of dissolved CO2 (mass fraction) - 500 years post-injection period

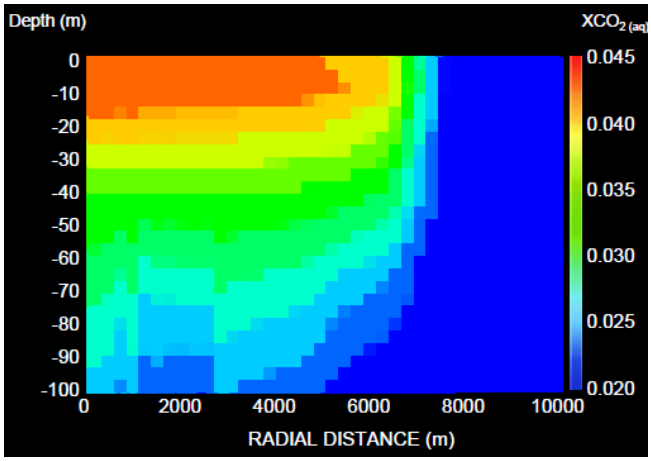

Figure 54. Distribution of dissolved CO2 (mass fraction) - 1000 years post-injection period

6.2.1.3 Evolution of Calcite

There was significant calcite precipitation in the reservoir. The zones of calcite precipitation were mostly those swept by formation water with increased dissolved CO_2 content. The changes in the abundance of calcite due to the presence of CO_2 saturated brine are graphically represented in two-dimensional plots in figures 55 to 58.

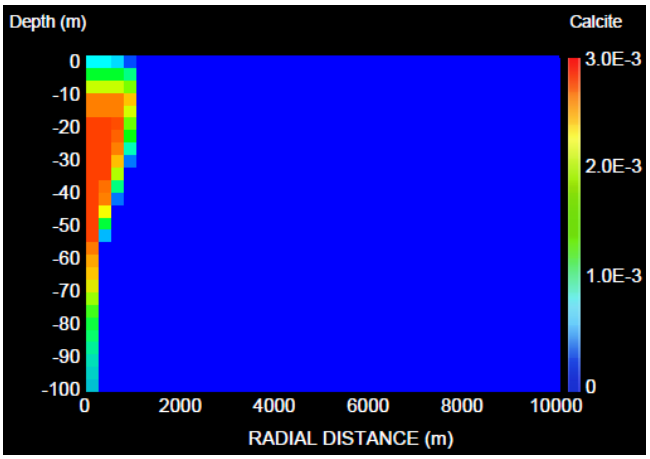

Figure 55. Change in calcite volume fraction - 2 years injection period

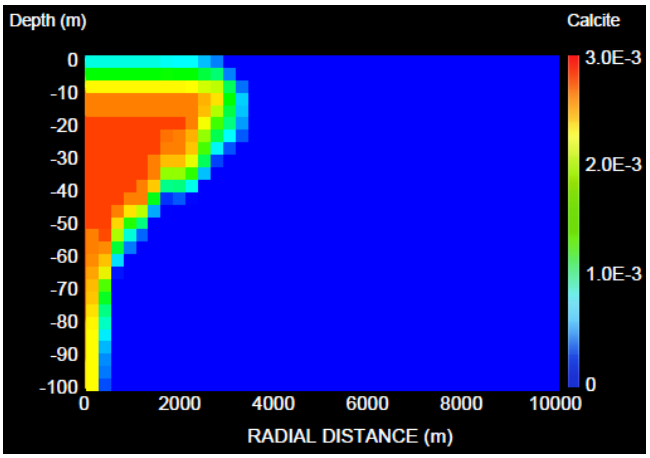

Figure 56. Change in calcite volume fraction - 100 years injection period

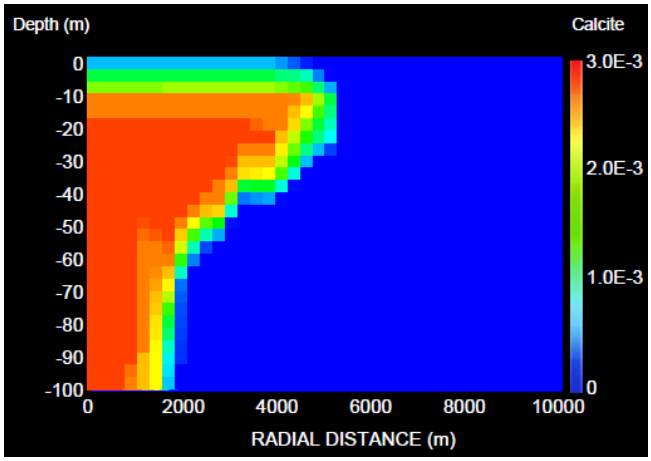

Figure 57. Change in calcite volume fraction - 500 years post-injection monitoring period

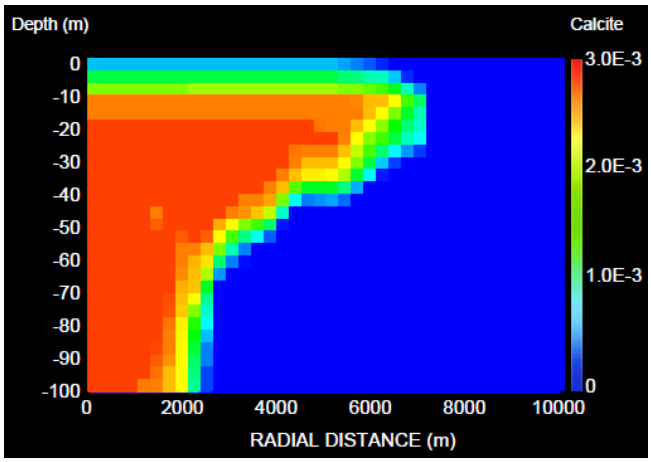

Figure 58. Change in calcite volume fraction - 1000 years post-injection monitoring period

6.2.1.4 Changes in Porosity and Permeability

There were net porosity reductions in the zones of the reservoir where there was calcite precipitation. The precipitated calcite fills up pore volume and thus the overall porosity decreases. Furthermore, TOUGHREACT calculates porosity changes from the changes in mineral volumes and thus the increase in calcite mineral volume directly affects the porosity.

There were also net decreases in permeability following a similar trend to the porosity decrease. This is because TOUGHREACT does not calculate changes in permeability independently but rather using a cubic law correlating changes in permeability to changes

in porosity. Therefore, it is natural that the changes in permeability follow similar trends to the changes in porosity.

The changes in porosity and permeability at discrete times during the simulation are shown in two-dimensional plots in figures 59 to 66.

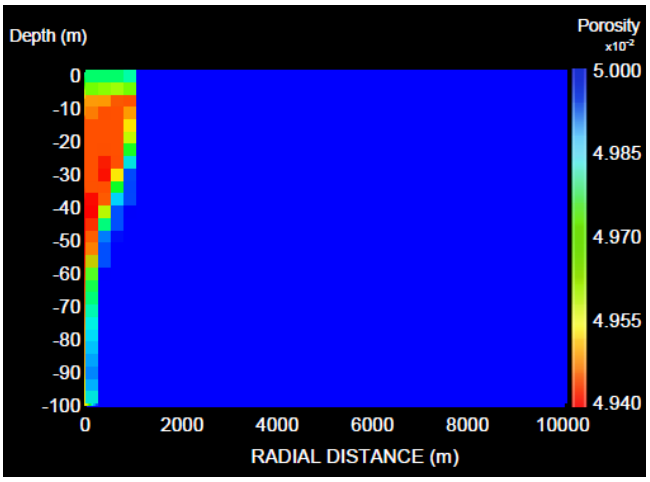

Figure 59. Porosity - 2 years injection period

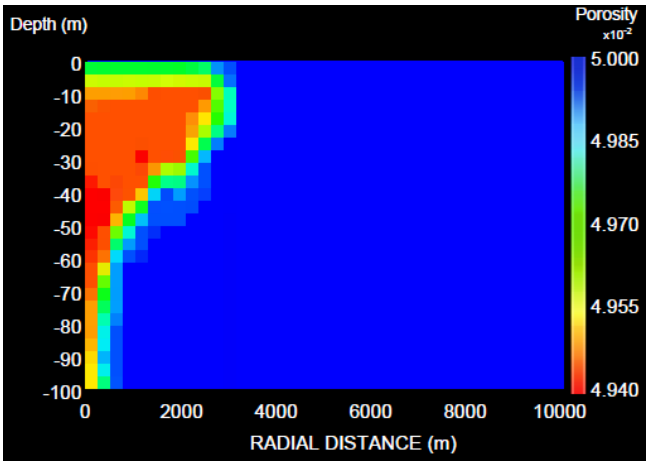

Figure 60. Porosity - 100 years injection period

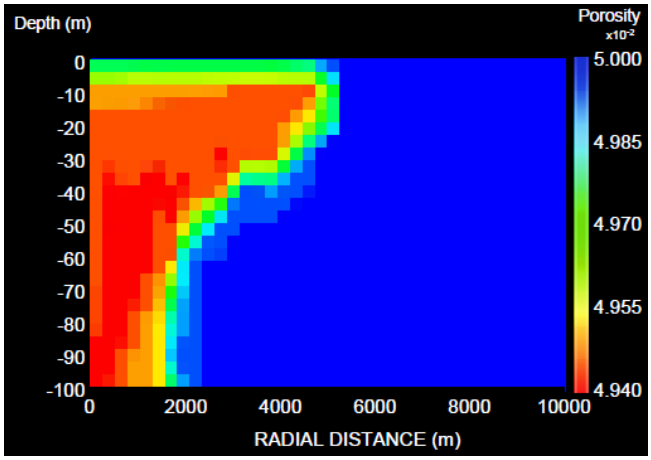

Figure 61. Porosity - 500 years post-injection monitoring period

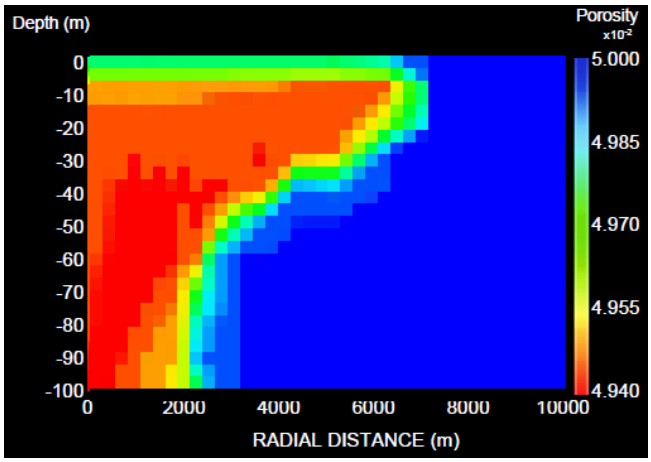

Figure 62. Porosity - 1000 years post-injection monitoring period

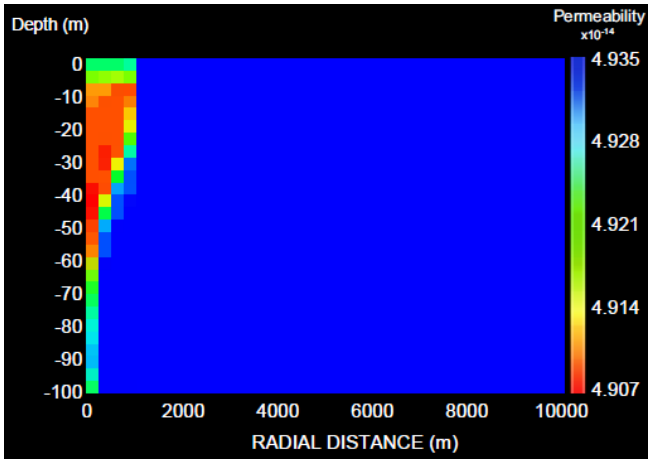

Figure 63. Permeability - 2 years injection period

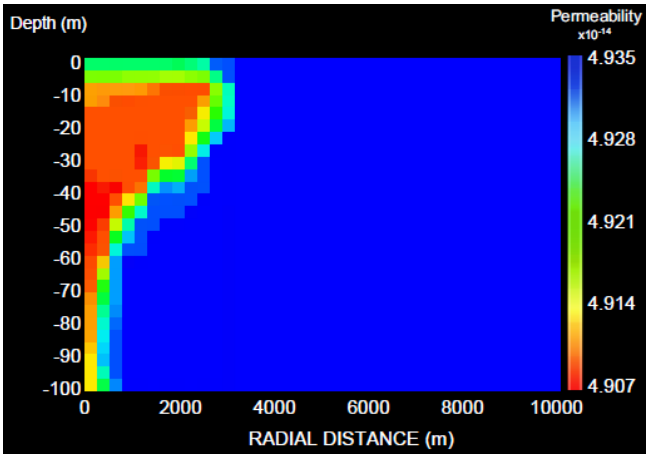

Figure 64. Permeability - 100 years injection period

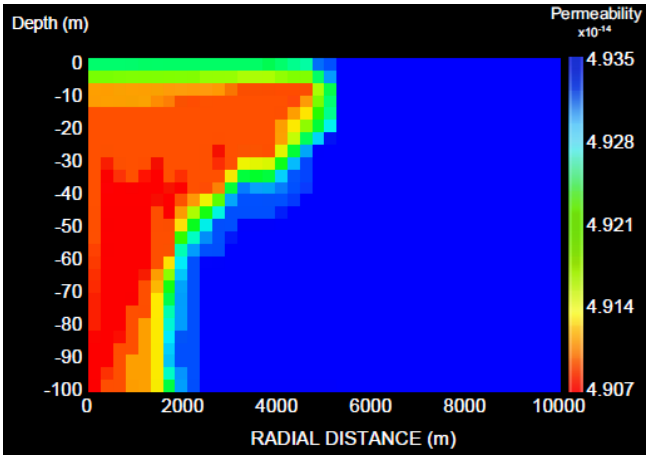

Figure 65. Permeability - 500 years post-injection monitoring period

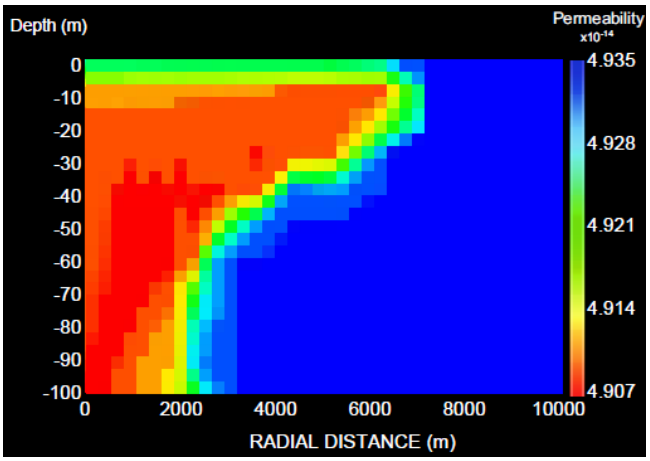

Figure 66. Permeability - 1000 years post-injection monitoring period

6.2.1.5 Storage of the Injected CO_2

The injected CO_2 was stored by solubility trapping and mineral trapping. Approximately 60% of the CO_2 was stored by dissolving into the in-situ brine while the rest was stored through the formation of carbonate compounds such as calcium carbonate signifying mineral trapping.

6.2.2 Scenario II – 120 Kg/s Injection Rate

Some of the injected CO_2 remained as a free phase and migrated upward due to buoyancy and formed a plume. The plume reached up to a radial extent of 1500 meters after 2 years of CO_2 injection as shown in figure 67. After 100 years of injection, it had reached up to 3800 meters in radial extent (figure 68). After 500 years, the CO_2 plume had extended to approximately 5800 meters (figure 69). After 1000 years, it reached 7500 meters radially from the point of injection as shown in figure 70. The transport and distribution of supercritical CO_2 at discrete time periods during the injection and monitoring periods is graphically presented in two-dimensional plots in figures 67 to 70.

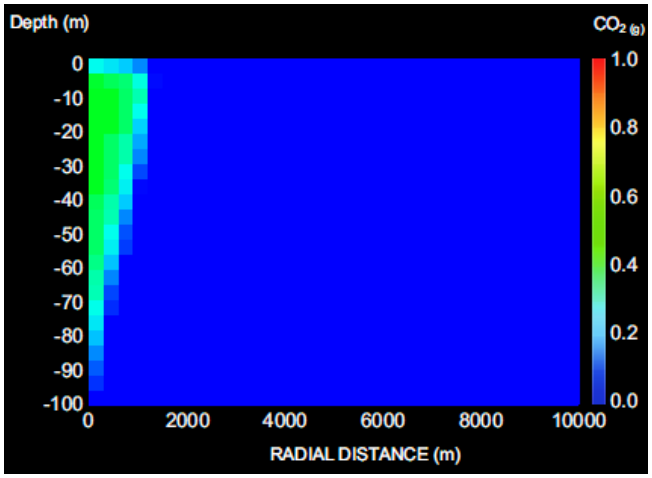

Figure 67. Distribution of supercritical CO2 (saturation) - 2 years injection period

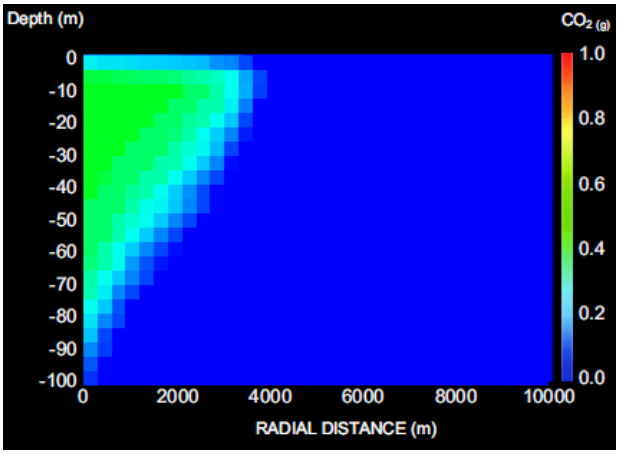

Figure 68. Distribution of supercritical CO2 (saturation) - 100 years injection period

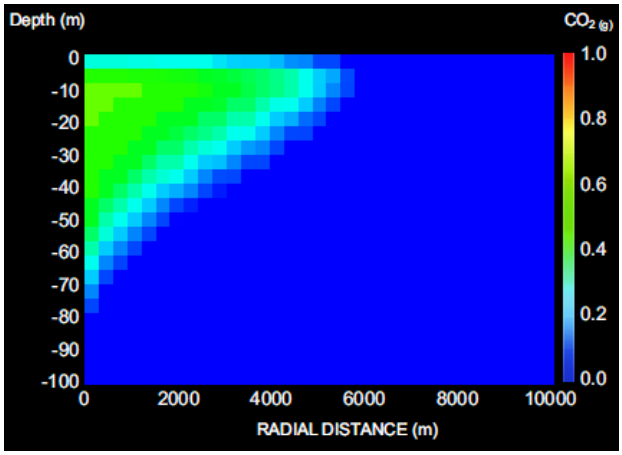

Figure 69. Distribution of supercritical CO2 (saturation) - 500 years post-injection monitoring period

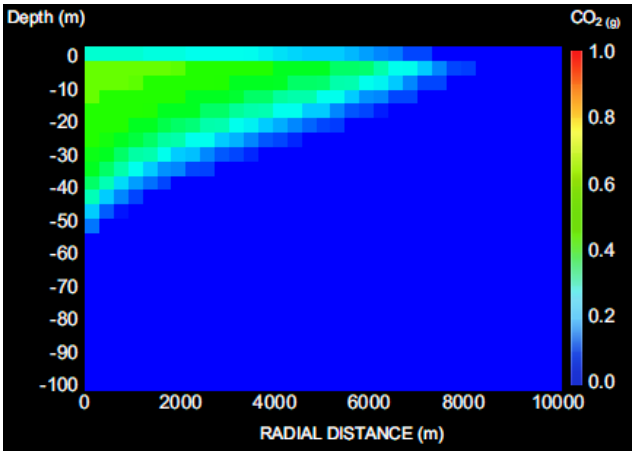

Figure 70. Distribution of supercritical CO2 (saturation) - 1000 years post-injection monitoring period

At a higher injection rate of 120 kg/s, there was a higher mass fraction of dissolved CO_2 compared to the lower injection rate of 37.2 kg/s. Similarly, there were higher volumes of calcite precipitation. Resultantly, there were slightly more decreases in porosity and permeability when CO_2 was injected at a higher rate. Plots comparing the effects of the CO_2 injection at different rates have been relegated to appendix B.

The injected CO_2 was mostly stored via solubility trapping (~55%) while the rest was stored via mineral trapping (~ 25%) and seal trapping (~20%).

It should be noted however that in both sets of simulations, the dynamic nature of geothermal fields was not considered. The production and reinjection of fluids is bound to have an impact on the observations made. Furthermore, the reinjection of colder fluids into the reservoir is likely to affect the storage mechanisms of the CO_2. In this study, the injection temperature of the CO_2 was assumed to be that of the reservoir. However, in real scenarios, the injection temperatures are expected to be lower than that of the reservoir.

6.3 Cement Plug Integrity

6.3.1 Scenario I

CO_2 was injected into a block with reservoir-like properties similar to the sedimentary carbonate reservoir previously simulated. It was injected at a steady rate of 0.001 kg/s for a period of 100 years and a temperature of 150 degrees Fahrenheit. This block was contacted with a 100-meter-long cement plug to see the effect of CO_2 on the degradation of wellbore cement in CO_2-rich environments.

CO_2 – saturated brine had penetrated approximately 19 meters into the cement plug in the 100 years of contact as shown in figure 71.

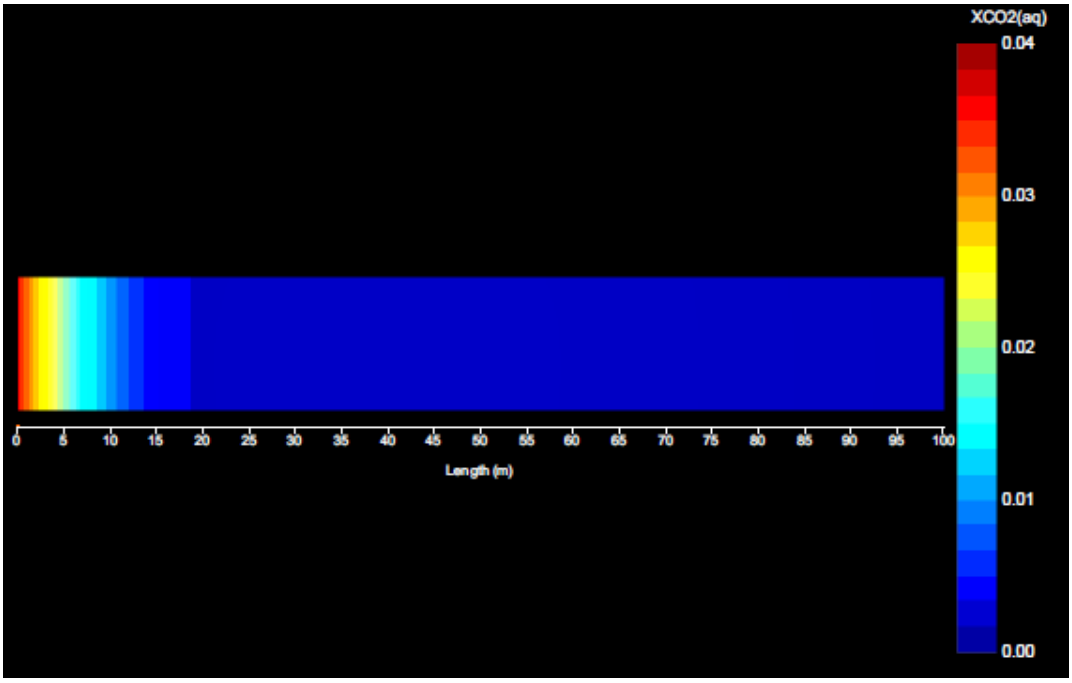

Figure 71. CO2 penetration into the cement plug after 100 years - 150 degrees Fahrenheit

There was a resulting alteration of porosity and permeability in the zones of the cement which were contacted by CO_2 – rich brine. Initially there was a decrease in porosity. This is due to the dissolution of portlandite by the carbonated brine which leads to the release of calcium ions. These ions react with available hydroxide ions which leads to the formation of calcium carbonate. The precipitation of calcium carbonate causes a decrease in porosity and subsequently permeability. This step in the reaction between cement and CO_2 is called carbonation.

This is followed by a reversal in the decrease in porosity and permeability. An increase in these properties of the cement plug is observed after a certain point. This is because when portlandite gets depleted, dissolution of the relatively less soluble calcium carbonate begins. This indicates the beginning of the second step referred to as bi-carbonation. This dissolution of calcium carbonate leads to an increase in porosity and permeability indicating a degradation of the cement. The changes in porosity and permeability are shown in figures 72 and 73. These plots indicate the trends observed in the first grid cell contacted by CO_2 which was affected the most.

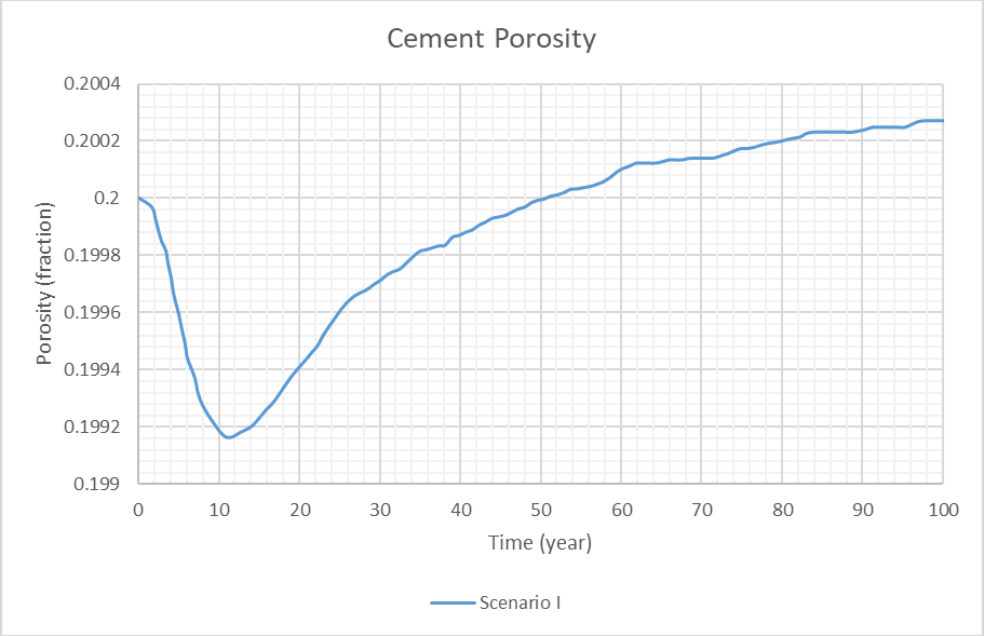

Figure 72. Cement porosity trend – Scenario I (150 degrees Fahrenheit)

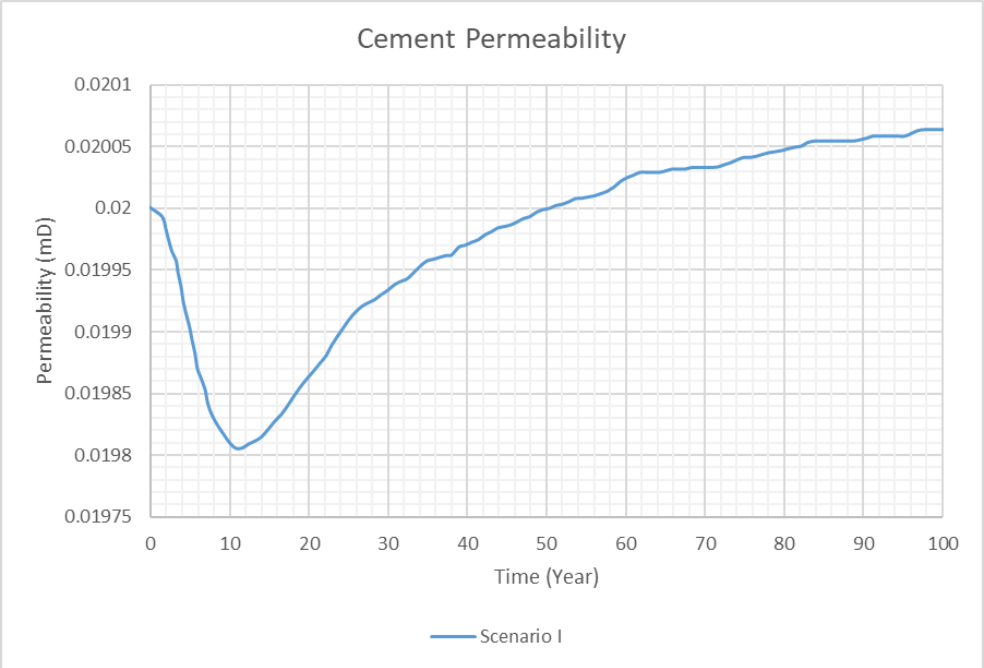

Figure 73. Cement permeability trend – Scenario I (150 degrees Fahrenheit)

It was however observed that the changes in porosity were very small (order of 10^{-4}). The changes in permeability were similarly very minor. These changes over such a long period

are an indication that the degradation of Portland cement is a very slow process that could take thousands of years to fully degrade a cement plug ten of meters long.

6.3.2 Scenario II

CO_2 was injected into a block with reservoir-like properties similar to the sedimentary carbonate reservoir previously simulated. It was injected at a steady rate of 0.001 kg/s for a period of 100 years and a temperature of 150 degrees Fahrenheit. This block was contacted with a 100-meter-long cement plug to see the effect of CO_2 on the degradation of wellbore cement in CO_2-rich environments. A micro-silica additive was added to the cement composition to observe its effect on CO_2 interaction with cement.

Results showed that the penetration of CO_2 saturated brine into the cement plug was less than in the previous scenario without any micro-silica additive. The CO_2 saturated brine had penetrated a distance of 10 meters after 100 years as shown in figure 74. This could be attributed to the plugging property of the micro-silica. It takes up spaces in some of the pores and pore throats thus effectively reducing the areas open to flow within the cement plug. Therefore, the CO_2 and CO_2 saturated brine penetrates less into the plug.

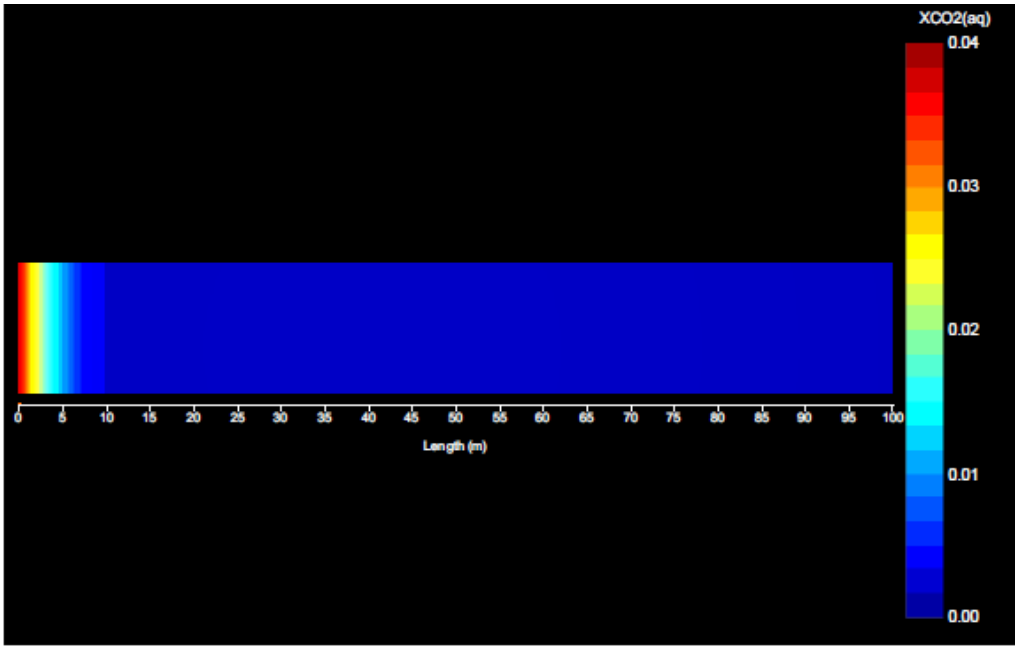

Figure 74. CO2 penetration into the cement plug after 100 years - 150 degrees Fahrenheit w/ micro-silica

There was less change in porosity and permeability of the cement plug in the presence of the micro-silica additive. A comparison between the trends of porosity and permeability of the first two scenarios is shown in figures 75 and 76 respectively.

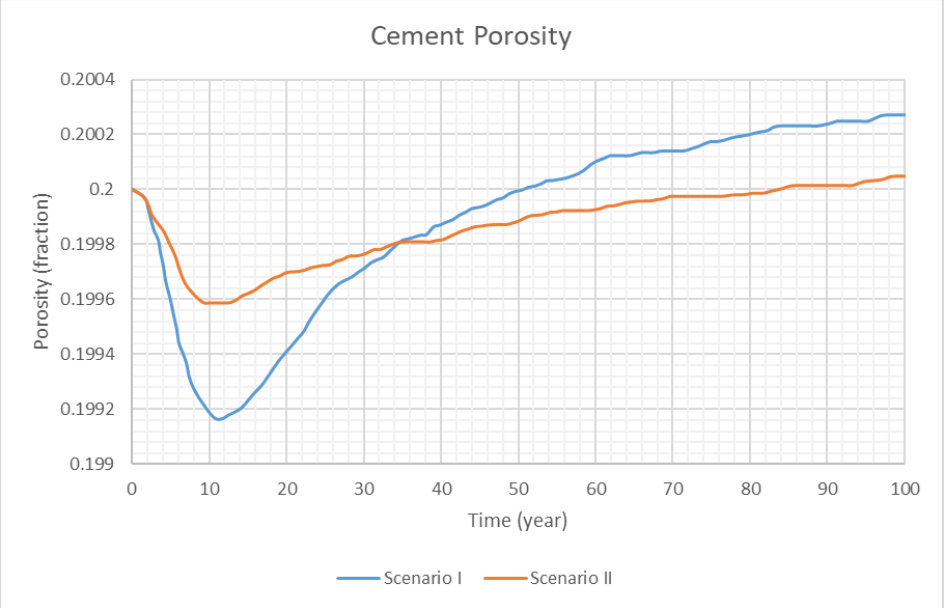

Figure 75. Cement porosity trend – Scenario I vs II comparison

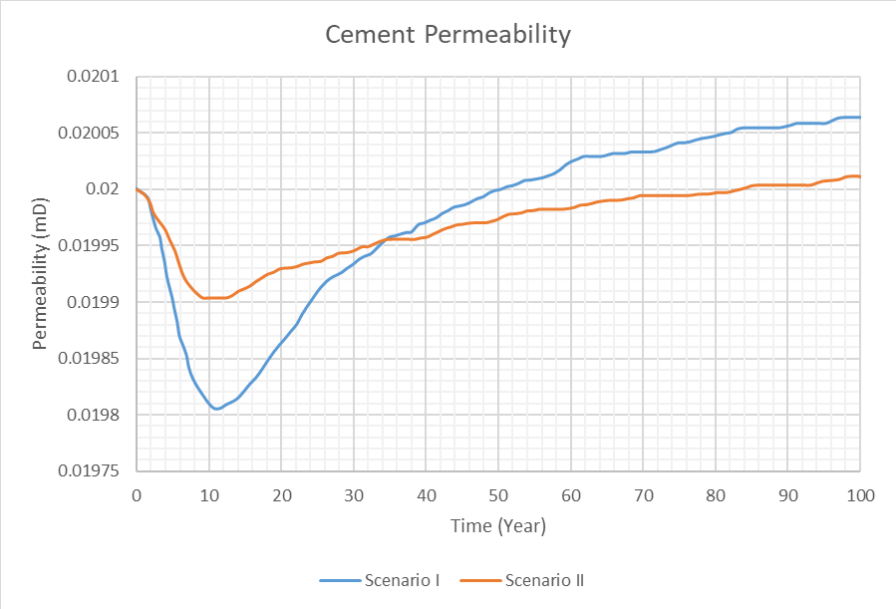

Figure 76. Cement permeability trend – Scenario I vs II comparison

6.3.3 Scenario III

CO_2 was injected into a block with reservoir-like properties similar to the metamorphic geothermal reservoir previously simulated. It was injected at a steady rate of 0.001 kg/s for a period of 100 years at a temperature of 468 degrees Fahrenheit. This block was contacted with a 100-meter-long cement plug to see the effect of CO_2 on the degradation of wellbore cement in high temperature CO_2-rich environments.

Results showed that there was significantly higher penetration of CO_2 into the plug in the high temperature conditions. CO_2-saturated brine reached a distance of 29 meters from the injection block after 100 years as shown in figure 77. Furthermore, there was a greater net increase in porosity after 100 years compared to the previous two scenarios as shown in figure 78. This is an indication that there was greater degradation of the cement in high temperature conditions.

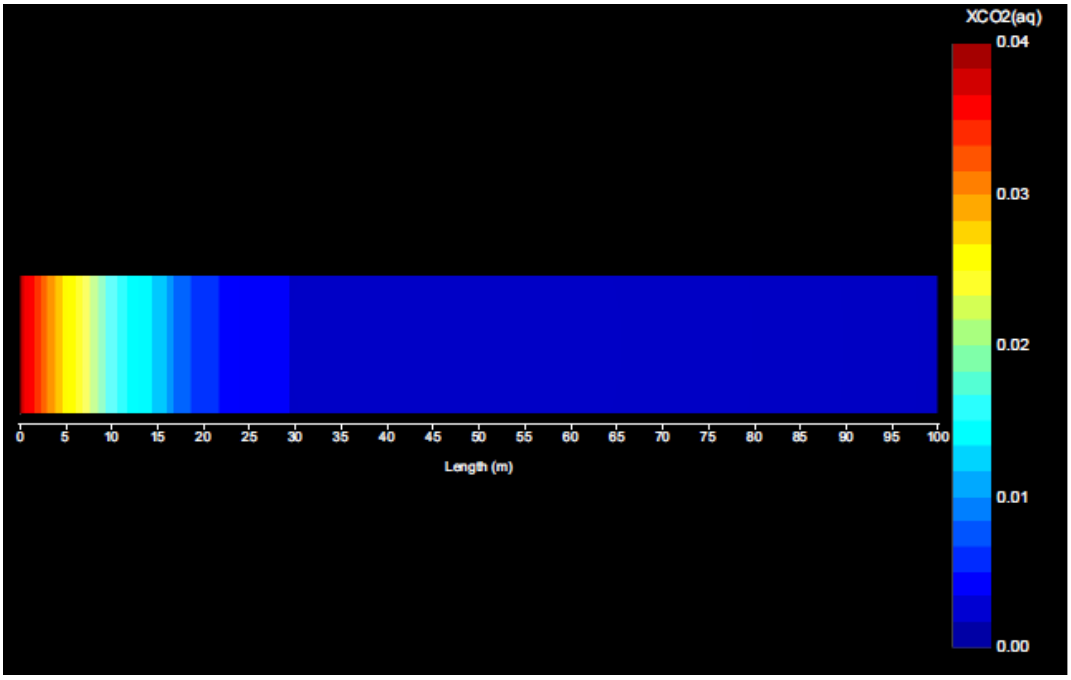

Figure 77. CO2 penetration into the cement plug after 100 years - 468 degrees Fahrenheit

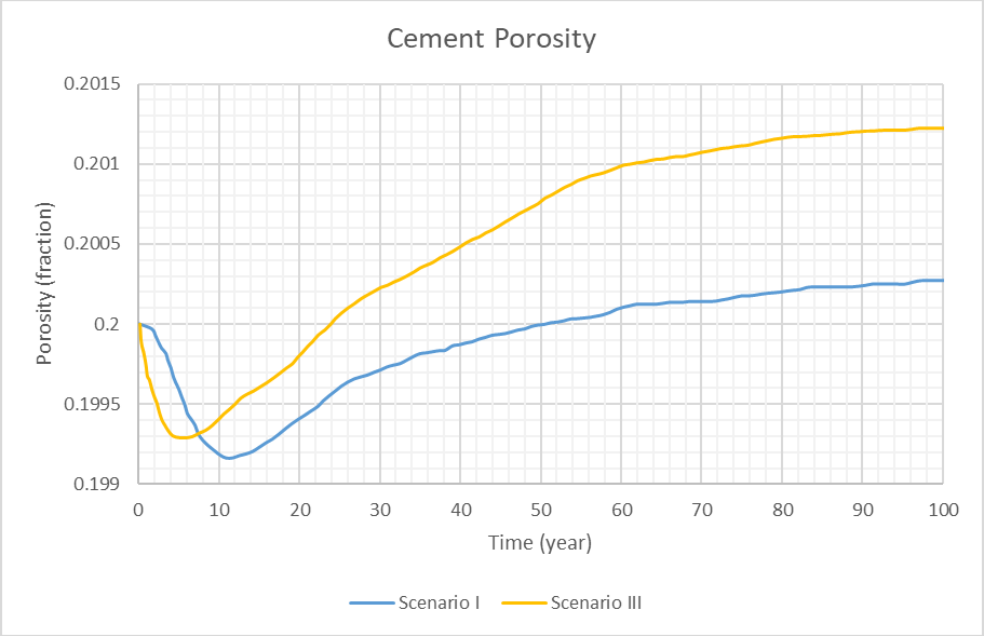

Figure 78. Cement porosity trend – Scenario I vs III comparison

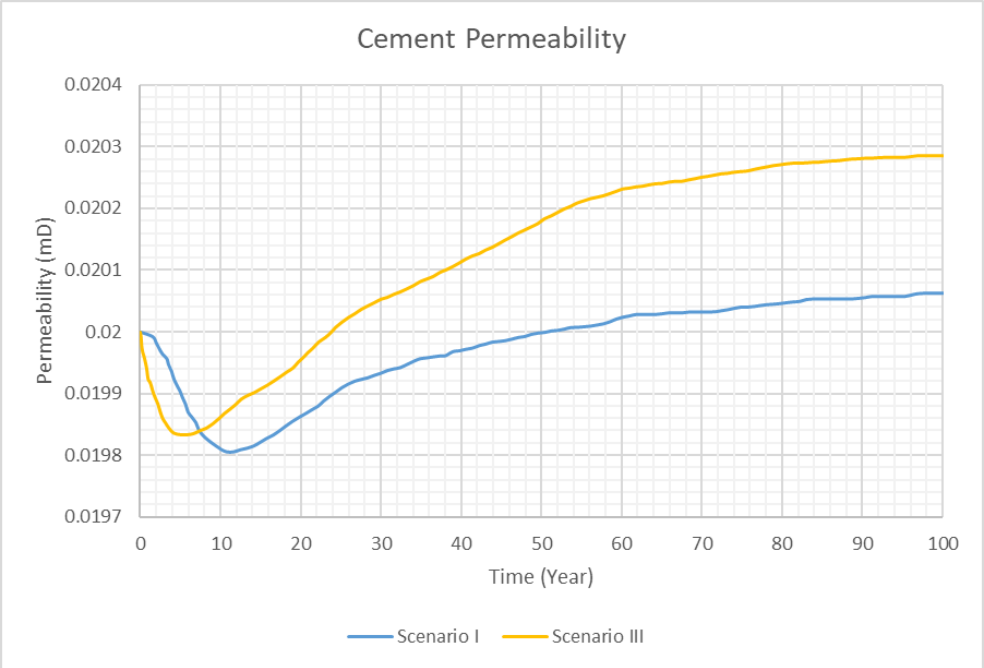

Figure 79. Cement permeability trend – Scenario I vs III comparison

CHAPTER 7

CONCLUSION

CO_2 is one of the biggest contributors to climate change. In efforts to mitigate climate change, reduction of CO_2 concentration in the atmosphere is one of the solutions being implemented. One of the methods to reduce CO_2 concentration in the atmosphere is by the long-term storage in deep geological formations. However, an issue of concern in such storage is the risk of leakage. Leakage can occur through the caprocks or wellbore cement therefore it is critical to understand the effect of CO_2 injection on the reservoir formation, caprock, and wellbore cement in order to ensure the safety and success of CO_2 sequestration at potential sequestration sites.

A numerical simulation study was conducted to investigate the effect of CO_2 injection on two potential CO_2 storage sites. One is a sedimentary-carbonate heavy oil reservoir, and the other is a metamorphic-marble geothermal reservoir. The effects of CO_2 injection on the mineral evolution, porosity and permeability, and trapping mechanisms were investigated. The effects of temperature and injection rates were also studied for the two respective reservoirs. The effects of CO_2 on the degradation of wellbore cement was also investigated. The numerical simulation was done using TOUGHREACT aided by PETRASIM used a pre- and post-processor.

Injection in the carbonate hydrocarbon reservoir showed major dissolution of calcite. This resulted in an initial increase in porosity and permeability. However, this was followed by precipitation of secondary minerals which caused a decrease in the porosity and permeability. This trend was similar in the shale caprock of the reservoir. The net decrease in porosity and permeability suggests an improvement in the sealing capacity of the caprock. CO_2 was mainly stored as a free phase under the caprock with some amount getting dissolved in the formation water and getting stored via solubility trapping. It was observed that high temperature conditions resulted in less dissolution of CO_2 and less distribution in the reservoir as a free phase. Higher temperatures seemed to inhibit the storage of CO_2 in such reservoirs.

Injection of CO_2 into the metamorphic geothermal reservoir resulted in major precipitation of calcite. This caused a decrease in porosity and permeability. Under low injection rates, all the injected CO_2 dissolved into the formation water and was mainly stored via solubility trapping. Some amounts of CO_2 also reacted with present ions to form stable carbonate compounds thus resulting in some mineral trapping. Under higher injection rates, some of the CO_2 remained as a free phase and thus the injected CO_2 was stored via solubility trapping, mineral trapping, and seal trapping under the impermeable seal layer at the top of the reservoir.

Investigation of the effects of CO_2 on wellbore cement showed that there was some degradation of the cement in the zones penetrated by CO_2 – saturated brine. Initially, there was a decrease in porosity and permeability due to carbonation followed by an increase. However, this degradation process seemed to be self-inhibiting as the decrease in porosity and permeability from the first step significantly slow down the second step. It was also observed that adding micro-silica to the cement composition reduces the cement degradation in the CO_2 rich environment. Furthermore, the cement degraded more in high temperature conditions compared to low temperature conditions. However, it was noted that the changes in porosity and permeability were very small and the cement degradation is a very slow process which could take hundreds or thousands of years to completely occur in plugs which are tens of meters in length. Nonetheless, proper cement bonding

must be ensured behind the casing because although the full degradation might take a long time, degradation of 20 – 30 meters might be enough to allow for the opening of a pathway for CO_2 between the injection formation and the formation above the caprock.

REFERENCES

Alsharhan, A. S., & Nairn, A. E. M. (2003). *Sedimentary Basins and Petroleum Geology of the Middle East*. Elsevier.

Arslan, I., Akin, S., Karakece, Y., & Korucu, O. (2007). Is Bati Raman Heavy Oil Field a Triple Porosity System? *SPE/EAGE Reservoir Characterization and Simulation Conference*. Abu Dhabi, UAE: Society of Petroleum Engineers. https://doi.org/10.2118/111146-MS

Babadagli, T., Sahin, S., Kalfa, U., Celebioglu, D., Karabakal, U., & Topguder, N. N. S. (2008). Development of Heavy Oil Fractured Carbonate Bati Raman Field: Evaluation of Steam Injection Potential and Improving Ongoing CO2 Injection. *SPE Annual Technical Conference and Exhibition*. Denver, Colorado, USA: Society of Petroleum Engineers. https://doi.org/10.2118/115400-MS

Barron, A. R., & Johnson, D. (n.d.). Portland Cement in the Energy Industry.

Bildstein, O., Kervévan, C., Lagneau, V., Delaplace, P., Crédoz, A., Audigane, P., … Jullien, M. (2010). Modélisation intégrée de l'intégrité des roches de couverture dans le contexte du stockage du CO 2 : Évolution des propriétés de transport et impact sur les performances et la s?reté du stockage. *Oil and Gas Science and Technology*, *65*(3), 485–502. https://doi.org/10.2516/ogst/2010006

Bouzalakos, S., & Maroto-Valer, M. M. (2010). Overview of carbon dioxide (CO2) capture and storage technology. *Developments and Innovation in Carbon Dioxide (Co*, *2*, 1–24. https://doi.org/10.1533/9781845699581.1

Bozkurt, E., & Oberhänsli, R. (2001). Menderes Massif (Western Turkey): structural, metamorphic and magmatic evolution–a synthesis. Springer.

British Geologic Survey. (2019). How Can CO2 be Stored? Retrieved December 11, 2019, from

http://www.bgs.ac.uk/discoveringGeology/climateChange/CCS/howCanCo2BeStored.html

Cao, P., Karpyn, Z. T., & Li, L. (2013). Dynamic alterations in wellbore cement integrity due to geochemical reactions in CO2-rich environments. *Water Resources Research*, *49*(7), 4465–4475. https://doi.org/10.1002/wrcr.20340

Carey, J. W., Wigand, M., Chipera, S. J., WoldeGabriel, G., Pawar, R., Lichtner, P. C., … Guthrie, G. D. (2007). Analysis and performance of oil well cement with 30 years of CO2 exposure from the SACROC Unit, West Texas, USA. *International Journal of Greenhouse Gas Control*, *1*(1), 75–85. https://doi.org/10.1016/S1750-5836(06)00004-1

Carroll, S., Carey, J. W., Dzombak, D., Huerta, N. J., Li, L., Richard, T., … Zhang, L. (2016). Review: Role of chemistry, mechanics, and transport on well integrity in CO2 storage environments. *International Journal of Greenhouse Gas Control*, *49*, 149–160. https://doi.org/10.1016/j.ijggc.2016.01.010

Dalkhaa, C. (2010). *Caprock Integrity in CO2 Storage (PhD Dissertation)*. Middle East Technical University.

Dalkhaa, C., & Okandan, E. (2013). 2-D numerical modeling of CO 2 -water-caprock interactions at a potential CO 2 storage site in Turkey. *Geochemical Journal*, *47*(5), 499–511. https://doi.org/10.2343/geochemj.2.0271

Duan, Z., & Sun, R. (2003). An improved model calculating CO2 solubility in pure water and aqueous NaCl solutions from 273 to 533 K and from 0 to 2000 bar. *Chemical Geology*, *193*(3), 257–271. https://doi.org/https://doi.org/10.1016/S0009-2541(02)00263-2

Duguid, A., & Scherer, G. W. (2010). Degradation of oilwell cement due to exposure to carbonated brine. *International Journal of Greenhouse Gas Control*, *4*(3), 546–560. https://doi.org/10.1016/j.ijggc.2009.11.001

Engineering ToolBox. (2018). Carbon Dioxide - Dynamic and Kinematic Viscosity. Retrieved December 18, 2019, from https://www.engineeringtoolbox.com/carbon-

dioxide-dynamic-kinematic-viscosity-temperature-pressure-d_2074.html

Gaus, I., Audigane, P., André, L., Lions, J., Jacquemet, N., Durst, P., … Azaroual, M. (2008). Geochemical and solute transport modelling for CO2 storage, what to expect from it? *International Journal of Greenhouse Gas Control*, *2*(4), 605–625. https://doi.org/10.1016/j.ijggc.2008.02.011

Gaus, I., Azaroual, M., & Czernichowski-Lauriol, I. (2005). Reactive transport modelling of the impact of CO2 injection on the clayey cap rock at Sleipner (North Sea). *Chemical Geology*, *217*(3-4 SPEC. ISS.), 319–337. https://doi.org/10.1016/j.chemgeo.2004.12.016

GECO/EU. (2019). Demo Sites. Retrieved December 14, 2019, from https://geco-h2020.eu/demo-sites/

Gherardi, F., Xu, T., & Pruess, K. (2007). Numerical modeling of self-limiting and self-enhancing caprock alteration induced by CO2 storage in a depleted gas reservoir. *Chemical Geology*, *244*(1–2), 103–129. https://doi.org/10.1016/j.chemgeo.2007.06.009

Güleç, N., & Hilton, D. R. (2016). Turkish geothermal fields as natural analogues of CO2 storage sites: Gas geochemistry and implications for CO2 trapping mechanisms. *Geothermics*, *64*, 96–110. https://doi.org/10.1016/j.geothermics.2016.04.008

Holubnyak, Y. I., Hawthorne, S. B., Mibeck, B. A. F., Miller, D. J., Bremer, J. M., Sorensen, J. A., … Harju, J. A. (2011). Modeling CO2-H2S-water-rock interactions at Williston Basin reservoir conditions. *Energy Procedia*, *4*, 3911–3918. https://doi.org/10.1016/j.egypro.2011.02.329

Huerta, N. J., Hesse, M. A., Bryant, S. L., Strazisar, B. R., & Lopano, C. L. (2013). Experimental evidence for self-limiting reactive flow through a fractured cement core: Implications for time-dependent wellbore leakage. *Environmental Science and Technology*, *47*(1), 269–275. https://doi.org/10.1021/es3013003

IPCC. (2005). *IPCC Special Report on Carbon dioxide Capture and Storage*. *Working Group III of the Intergovernmental Panel on Climate Change*.

https://doi.org/10.1021/es200619j

Karamanderesi. (2013). Characteristics of Geothermal Reservoirs in Turkey Goelogical Setting of Turkey and Menderes Massif.

Khalifeh, M., Hodne, H., Saasen, A., & Vralstad, T. (2013). Techniques and Materials for North Sea Plug and Abandonment Operations. https://doi.org/10.4043/23915-ms

Küçük, S. (2018). *SIMULATION OF GEOTHERMAL RESERVOIRS WITH HIGH AMOUNT OF CARBON DIOXIDE (MSc Thesis)*. Middle East Technical University.

Kutchko, B. G., Strazisar, B. R., Dzombak, D. A., Lowry, G. V., & Thauiow, N. (2007). Degradation of well cement by CO2 under geologic sequestration conditions. *Environmental Science and Technology*, *41*(13), 4787–4792. https://doi.org/10.1021/es062828c

Lagneau, V., Pipart, A., & Catalette, H. (2005). Reactive transport modelling of CO2 sequestration in deep saline aquifers. *Oil and Gas Science and Technology*, *60*(2), 231–247. https://doi.org/10.2516/ogst:2005014

Lindsey, R. (2018). Climate Change: Atmospheric Carbon Dioxide. Retrieved July 2, 2019, from https://www.climate.gov/news-features/understanding-climate/climate-change-atmospheric-carbon-dioxide

Liu, L., Suto, Y., Bignall, G., Yamasaki, N., & Hashida, T. (2003). CO2 injection to granite and sandstone in experimental rock/hot water systems. *Energy Conversion and Management*, *44*(9), 1399–1410. https://doi.org/10.1016/S0196-8904(02)00160-7

Lowry, G. V, & Dzombak, D. A. (2008). Rate of CO 2 Attack on Hydrated Class H Well Cement under Geologic Sequestration Conditions, *42*(16), 6237–6242.

Međimurec, N. G.-. (2018). The influence of CO2 on well cement utjecaj CO2 NA cementni kamen THE INFLUENCE OF CO 2 ON WELL CEMENT UTJECAJ CO 2 NA CEMENTNI KAMEN, (March).

NASA. (2019). What’s in a name? Weather, global warming and climate change.

Retrieved July 2, 2019, from https://climate.nasa.gov/resources/global-warming/

Olabode, A., & Radonjic, M. (2013). Experimental investigations of caprock integrity in CO2 sequestration. *Energy Procedia*, *37*, 5014–5025. https://doi.org/10.1016/j.egypro.2013.06.415

Pruess, K. (2005). ECO2N : A TOUGH2 Fluid Property Module for Mixtures of Water , NaCl , and CO2. *Contract*, (June), 1–76.

Randolph, J. B., & Saar, M. O. (2011). Coupling carbon dioxide sequestration with geothermal energy capture in naturally permeable, porous geologic formations: Implications for CO 2 sequestration. *Energy Procedia*, *4*, 2206–2213. https://doi.org/10.1016/j.egypro.2011.02.108

Rubin, E. S., Mantripragada, H., Marks, A., Versteeg, P., & Kitchin, J. (2012). The outlook for improved carbon capture technology. *Progress in Energy and Combustion Science*, *38*(5), 630–671. https://doi.org/10.1016/j.pecs.2012.03.003

Sahin, S., Kalfa, U., Celebioglu, D., & Corp, T. P. (2007). SPE 106575 Bati Raman Field Immiscible CO 2 Application : Status Quo and Future Plans. *Area*, 1–13.

Sahin, S., Kalfa, U., Celebioglu, D., Duygu, E., & Lahna, H. (2012). A Quarter Century of Progress in the Application of CO2 immiscible EOR Project in Bati Raman Heavy Oil Field in Turkey. https://doi.org/10.2118/157865-ms

Schütz, M. K., dos Santos, L. M., Coteskvisk, P. M., Menezes, S. C., Einloft, S., & Dalla Vecchia, F. (2019). Evaluation of CO2 attack in wellbore class G cement: influence of epoxy resins, composites and minerals as additives. *Greenhouse Gases: Science and Technology*, *12*(2019), 1–12. https://doi.org/10.1002/ghg.1928

Sengul, M. (2007). CO2 Sequestration - A Safe Transition Technology. https://doi.org/10.2118/98617-ms

Şimşek, Ş. (1985). Geothermal model of Denizli, Sarayköy-Buldan area. *Geothermics*, *14*(2–3), 393–417.

Şimşek, Ş., Parlaktuna, M., & Akın, S. (2009). Data Gathering and Evaluation of Kızıldere

Geothermal Field. *Report Prepared for Zorlu Energy*.

Tetiker, S., Akman, A. K., & Yalcin, H. (2018). Phyllosilicate / Clay Geochemistry of Mineralogy and Upper Cretaceous-Paleocene Germav Formation in Mardin-Dargeçit Area. *Geological Bulletin of Turkey*. https://doi.org/10.25288/tjb.468150

Thunderhead Engineering. (2017). PetraSim 2017, (April), 1–137.

United Nations. (2019a). The Paris Agreement. Retrieved July 2, 2019, from https://unfccc.int/process-and-meetings/the-paris-agreement/the-paris-agreement

United Nations. (2019b). What is the Kyoto Protocol? Retrieved July 2, 2019, from https://unfccc.int/kyoto_protocol

Vrålstad, T., Saasen, A., Fjær, E., Øia, T., Ytrehus, J. D., & Khalifeh, M. (2019). Plug & abandonment of offshore wells: Ensuring long-term well integrity and cost-efficiency. *Journal of Petroleum Science and Engineering*, *173*(September 2018), 478–491. https://doi.org/10.1016/j.petrol.2018.10.049

Xu, T., Sonnenthal, E., Spycher, N., & Pruess, K. (2008). TOUGHREACT User's Guide: A Simulation Program for Non-isothermal Multiphase Reactive Geochemical Transport in Variably Saturated Geologic Media, V1.2.1, (January). https://doi.org/10.2172/943451

Yücetaş, İ., Ergiçay, N., & Akın, S. (2018). Carbon dioxide injection field pilot in umurlu geothermal field, Turkey. *Transactions - Geothermal Resources Council*, *42*(October), 2285–2291.

Zhang, L., Ezekiel, J., Li, D., Pei, J., & Ren, S. (2014). Potential assessment of CO2 injection for heat mining and geological storage in geothermal reservoirs of China. *Applied Energy*, *122*, 237–246. https://doi.org/10.1016/j.apenergy.2014.02.027

APPENDICES

APPENDIX A – Comparison of CO_2 injection Under Low-Temperature and High Temperature Conditions

A.1 Supercritical CO_2 Transport (Saturation)

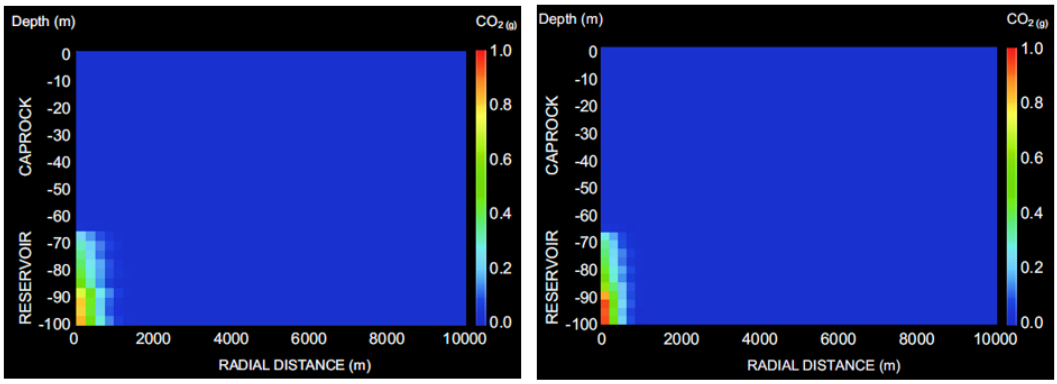

Figure 80. Low T (left) vs High T (right) - 2 years

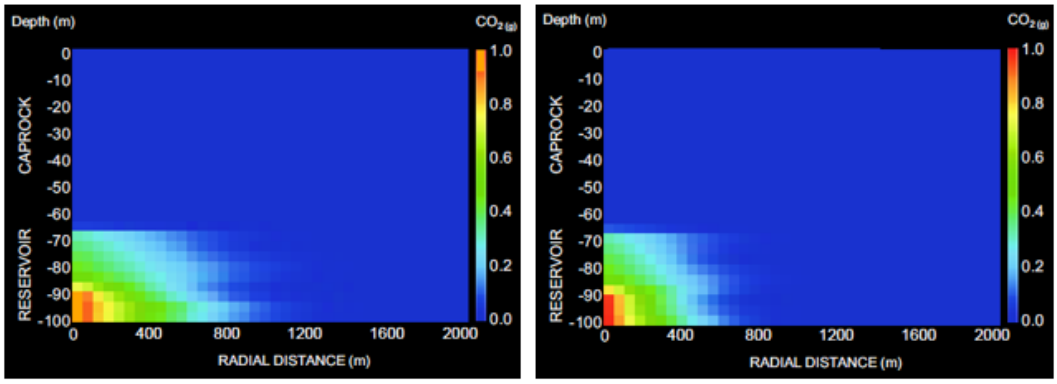

Figure 81. Low T (left) vs High T (right) - 2 years [zoomed in]

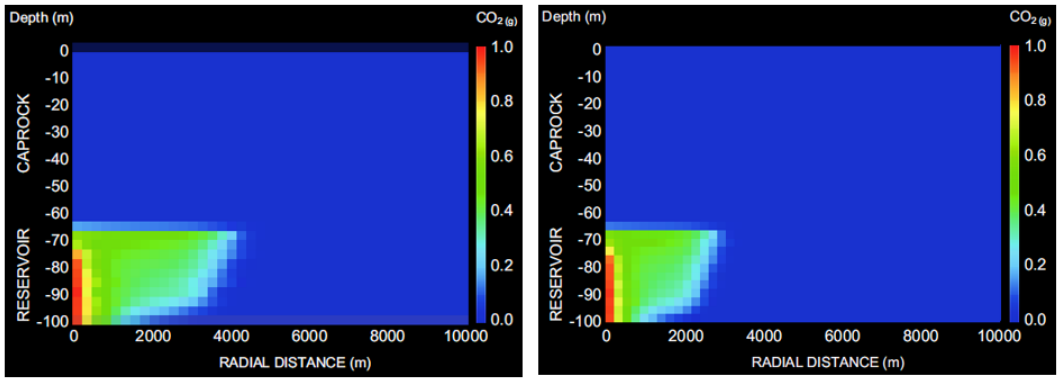

Figure 82. Low T (left) vs High T (right) - 100 years

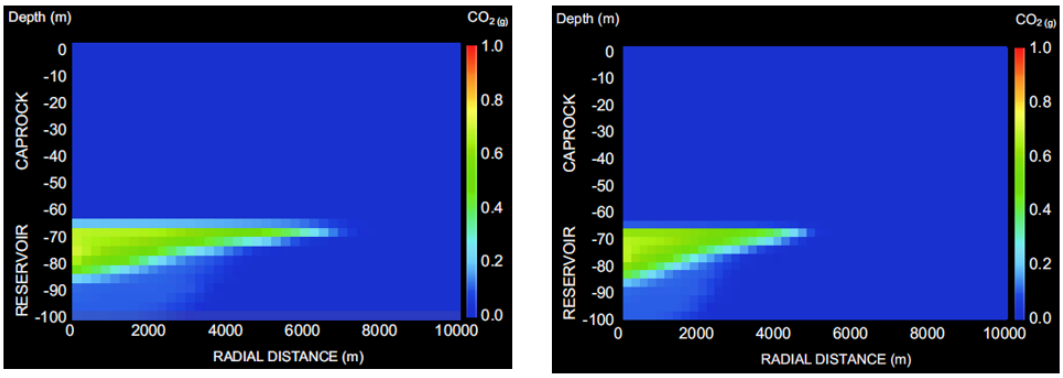

Figure 83. Low T (left) vs High T (right) - 500 years

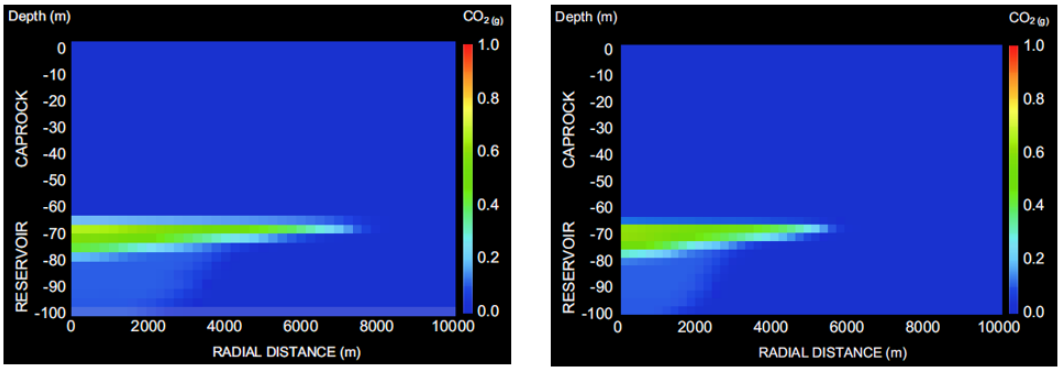

Figure 84. Low T (left) vs High T (right) - 1000 years

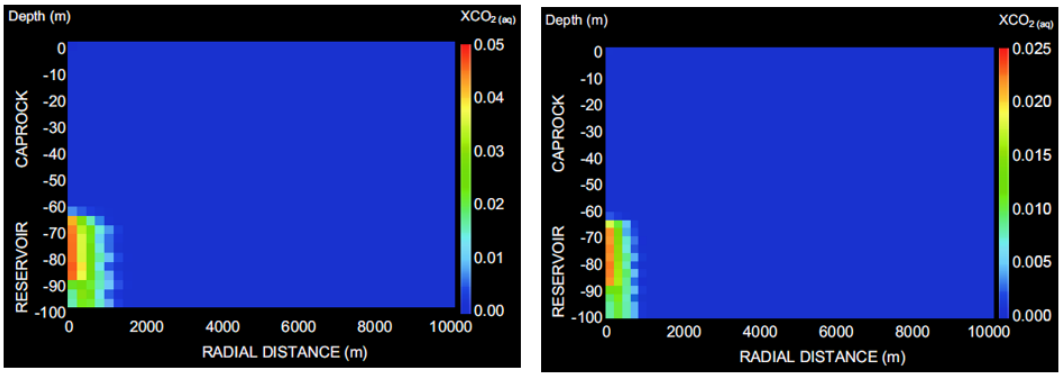

Figure 85. Low T (left) vs High T (right) - 2 years

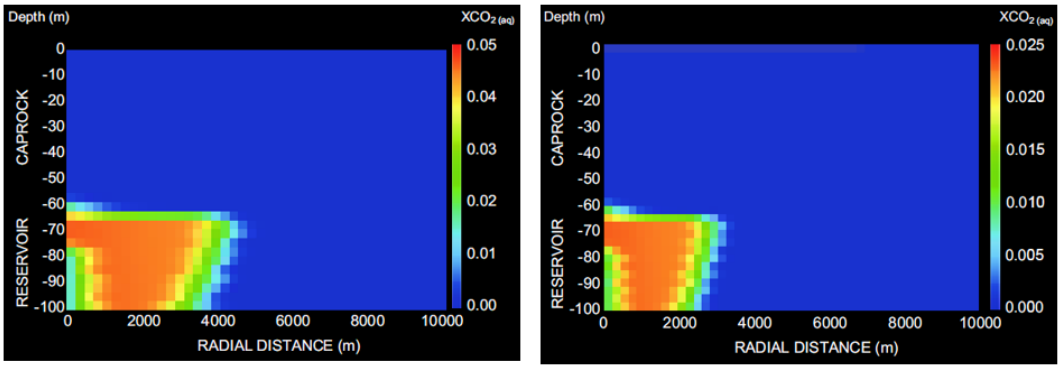

Figure 86. Low T (left) vs High T (right) - 100 years

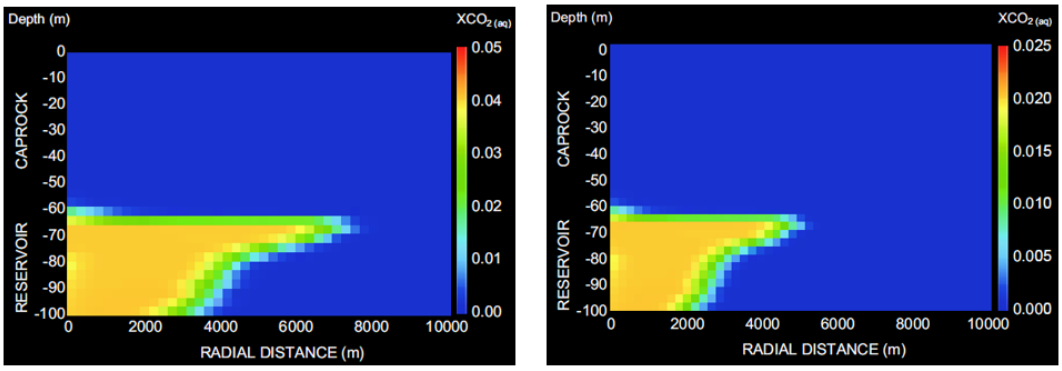

Figure 87. Low T (left) vs High T (right) - 500 years

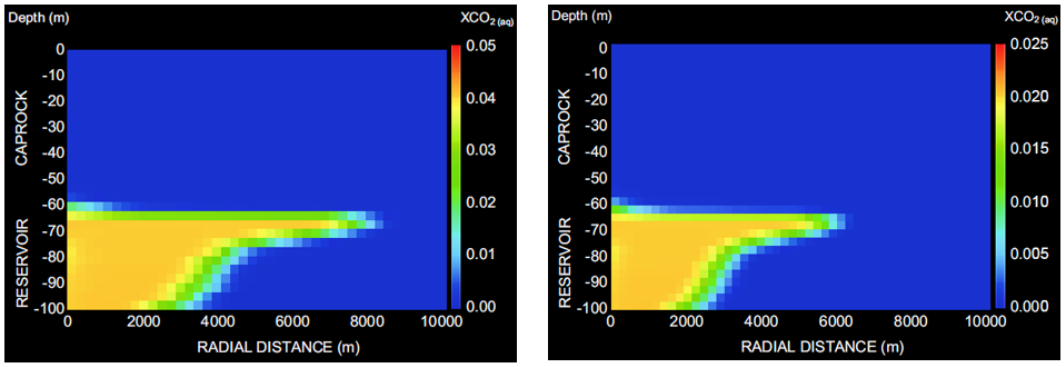

Figure 88. Low T (left) vs High T (right) - 1000 years

A.3 Evolution of Calcite (Volume Change)

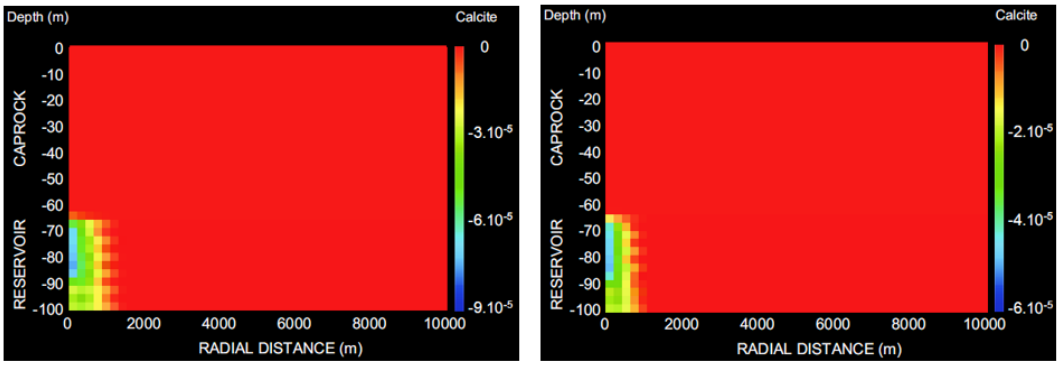

Figure 89. Low T (left) vs High T (right) - 2 years

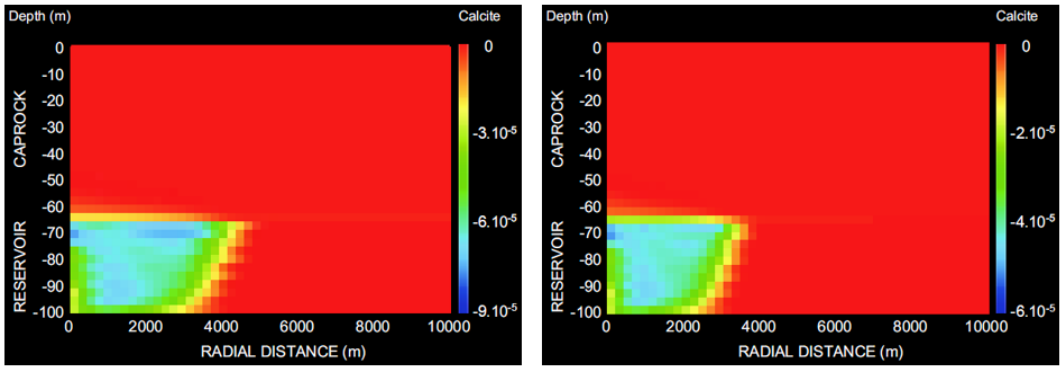

Figure 90. Low T (left) vs High T (right) - 100 years

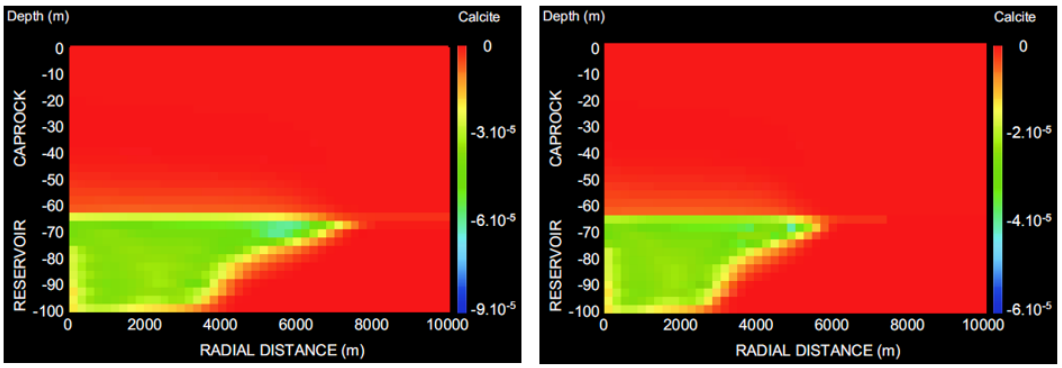

Figure 91. Low T (left) vs High T (right) - 500 years

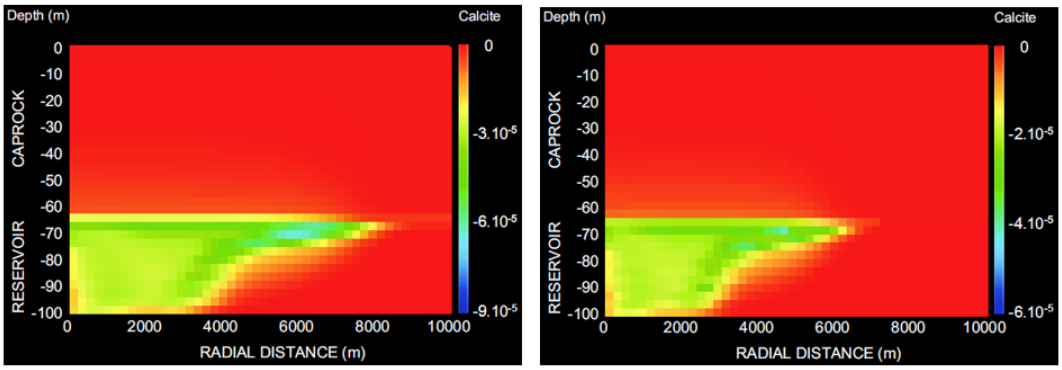

Figure 92. Low T (left) vs High T (right) - 1000 years

A.4 Ca^{2+} Ion Concentration (Mol/Kg)

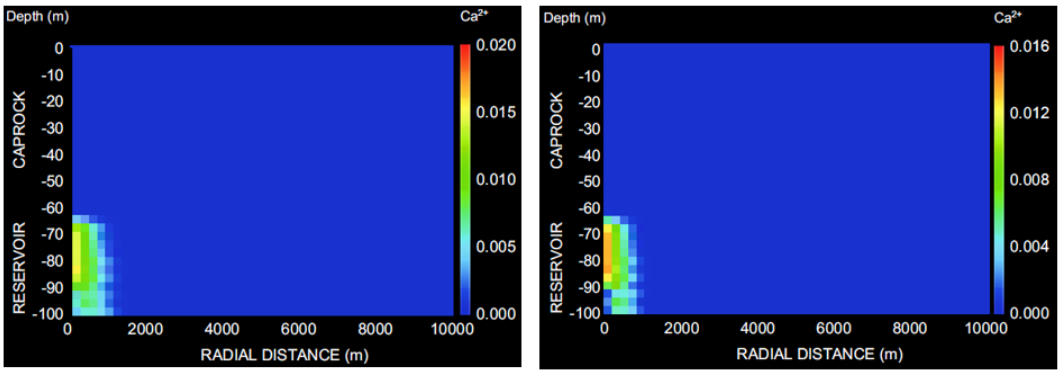

Figure 93. Low T (left) vs High T (right) - 2 years

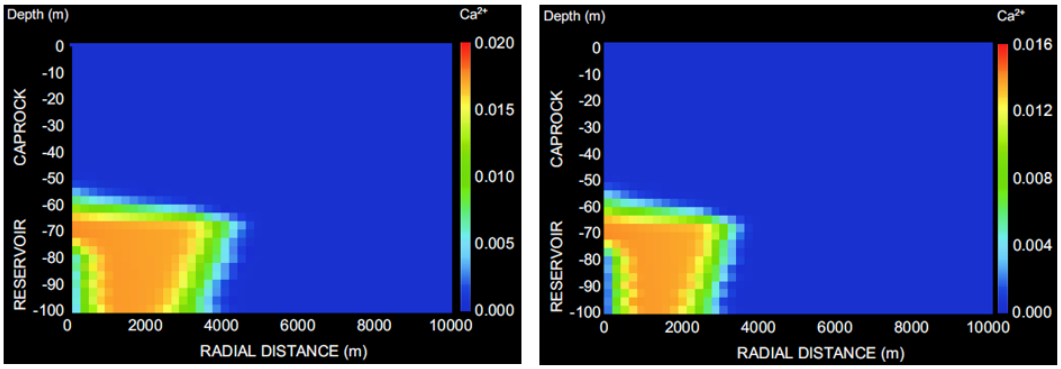

Figure 94. Low T (left) vs High T (right) - 100 years

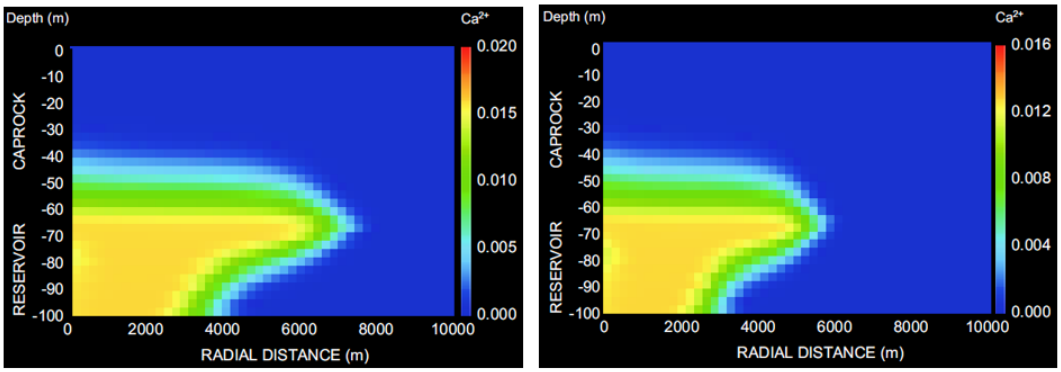

Figure 95. Low T (left) vs High T (right) - 500 years

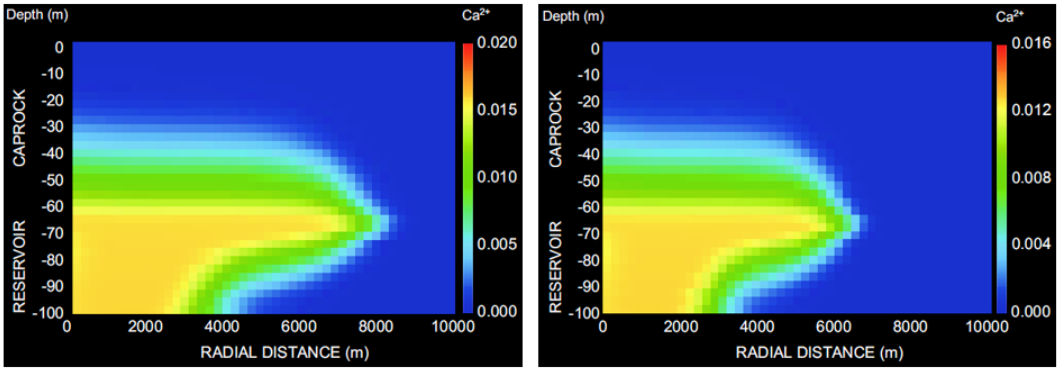

Figure 96. Low T (left) vs High T (right) - 1000 years

A.5 HCO_3^- Ion Concentration (Mol/Kg)

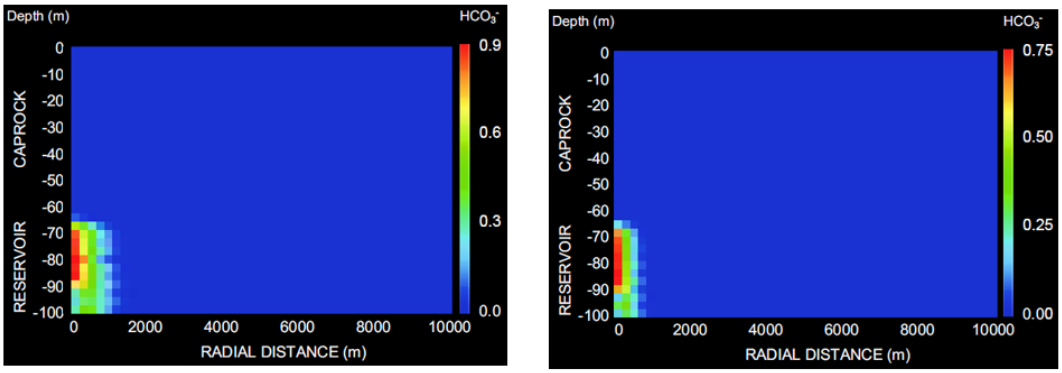

Figure 97. Low T (left) vs High T (right) - 2 years

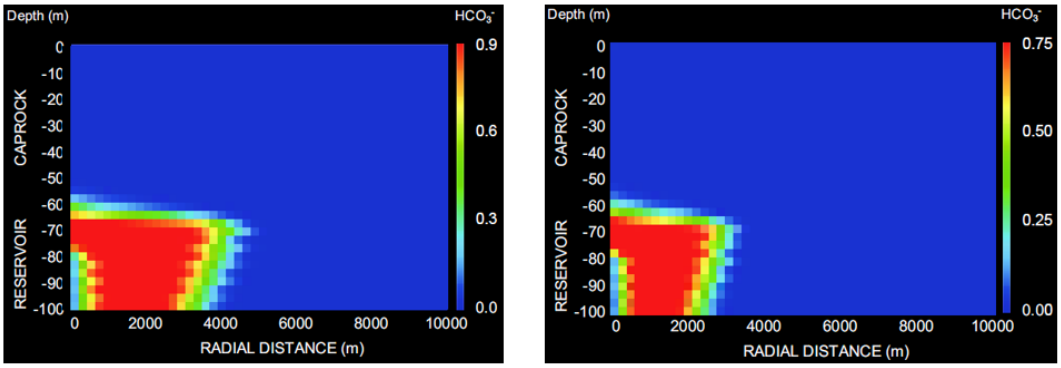

Figure 98. Low T (left) vs High T (right) - 100 years

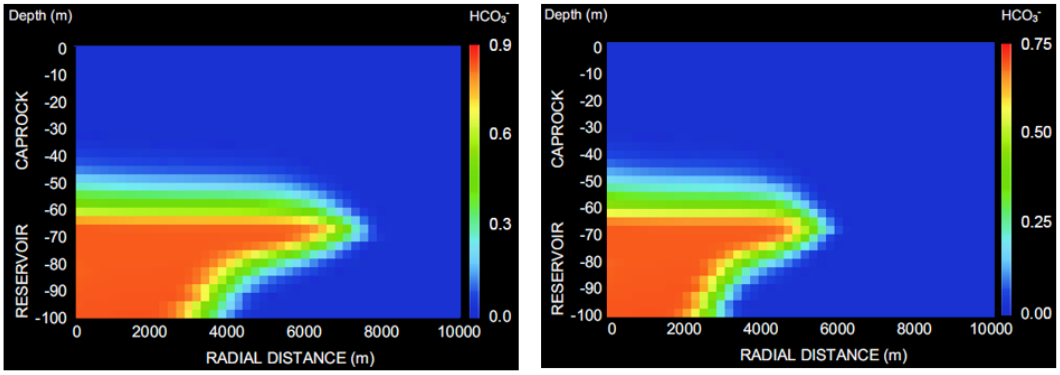

Figure 99. Low T (left) vs High T (right) - 500 years

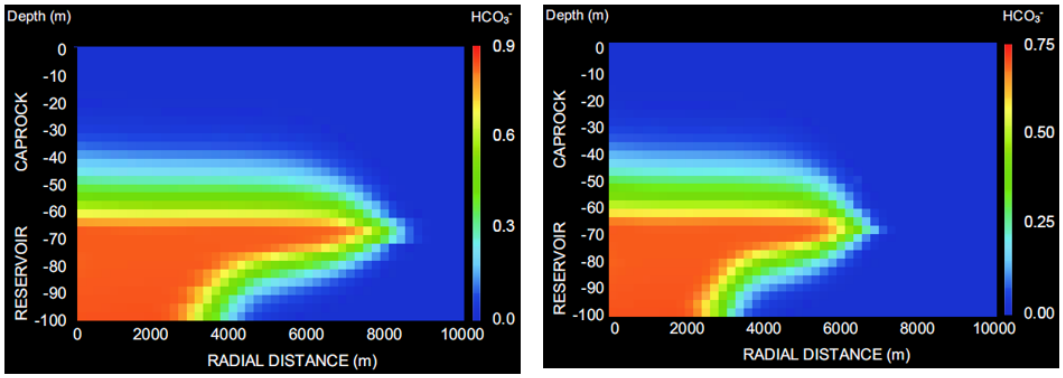

Figure 100. Low T (left) vs High T (right) - 1000 years

A.6 Formation Water pH

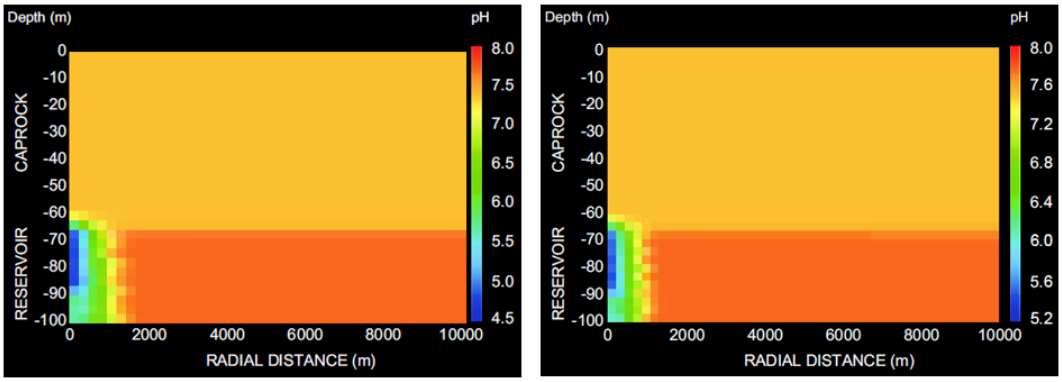

Figure 101. Low T (left) vs High T (right) - 2 years

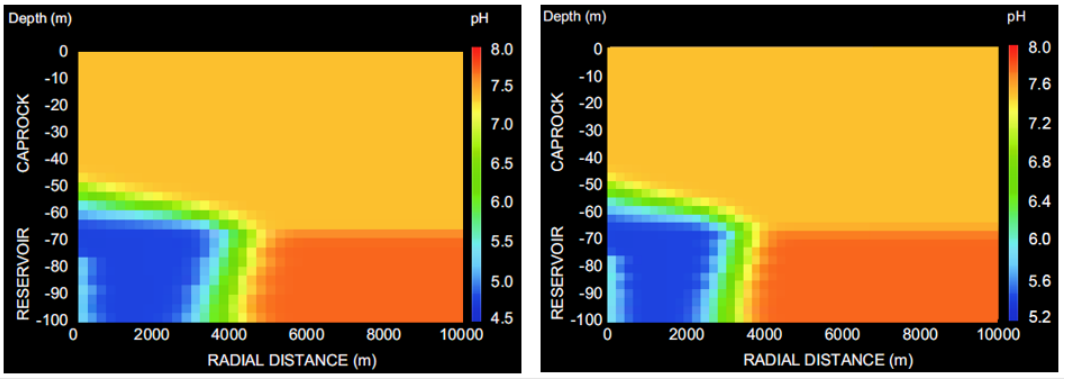

Figure 102. Low T (left) vs High T (right) - 100 years

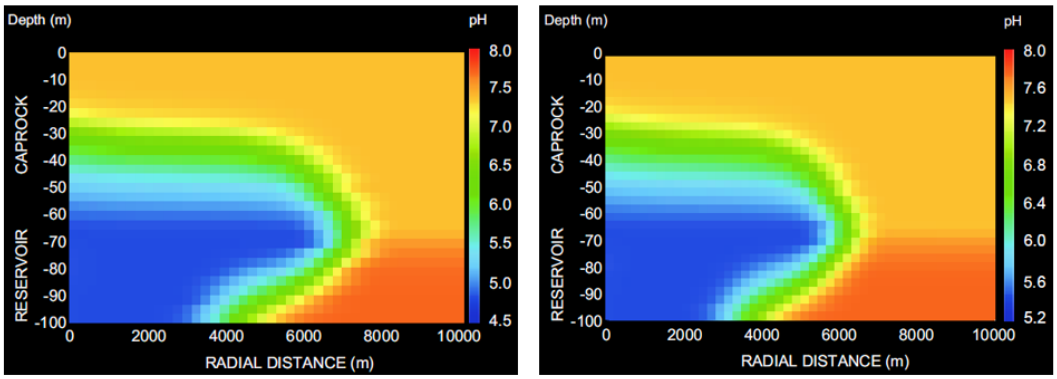

Figure 103. Low T (left) vs High T (right) - 500 years

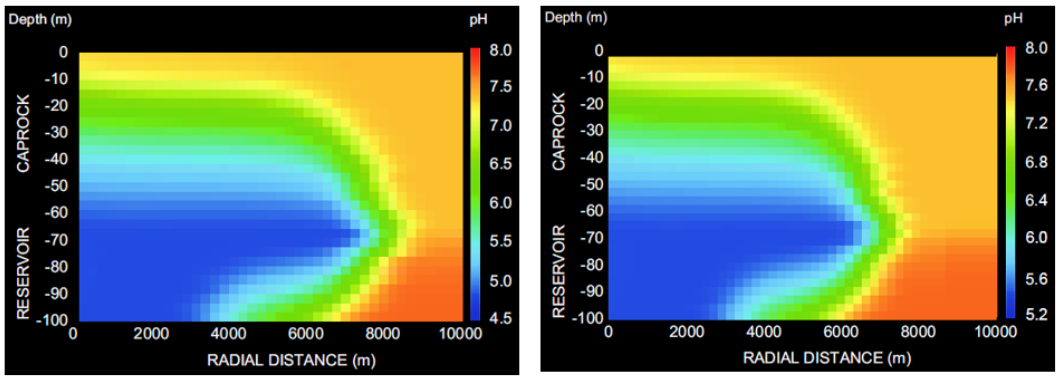

Figure 104. Low T (left) vs High T (right) - 1000 years

A.7 Caprock Porosity (Fraction *10^{-2})

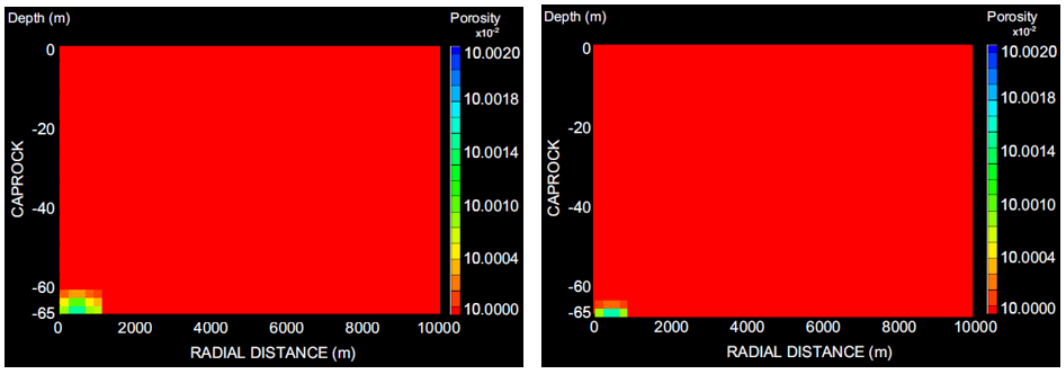

Figure 105. Low T (left) vs High T (right) - 2 years

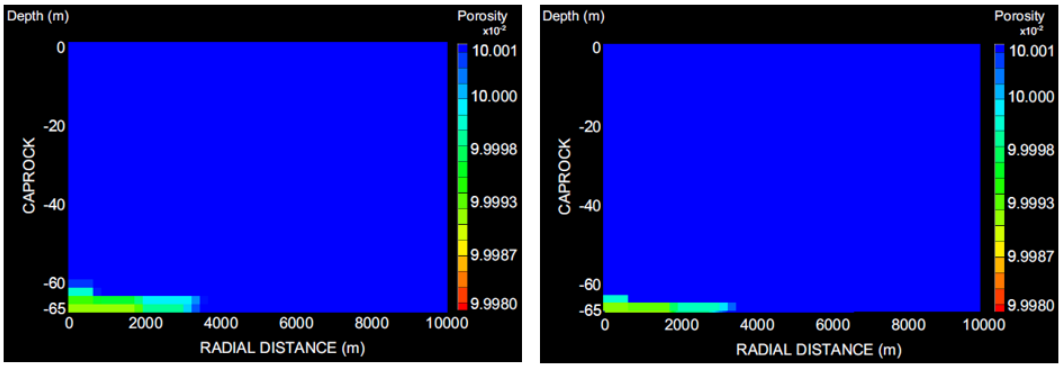

Figure 106. Low T (left) vs High T (right) - 100 years

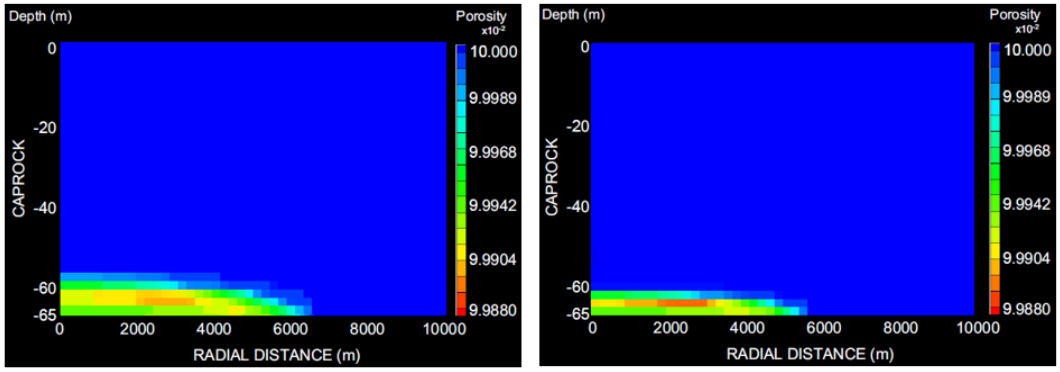

Figure 107. Low T (left) vs High T (right) - 500 years

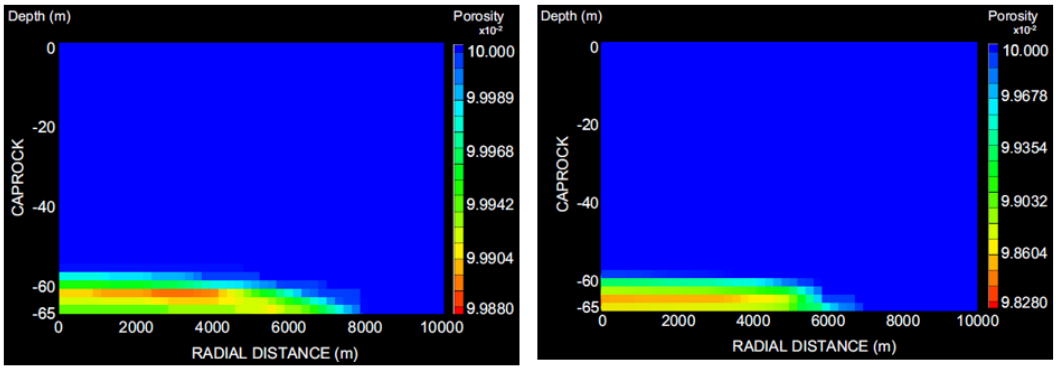

Figure 108. Low T (left) vs High T (right) - 1000 years

A.8 Caprock Permeability ($m^2 *10^{-17}$)

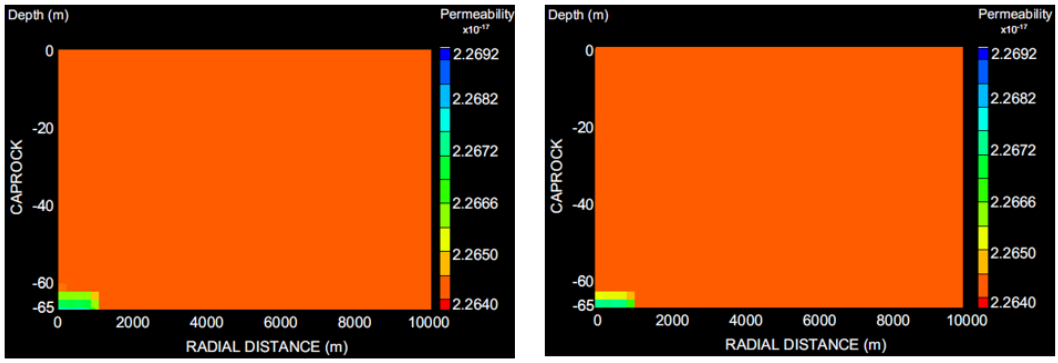

Figure 109. Low T (left) vs High T (right) - 2 years

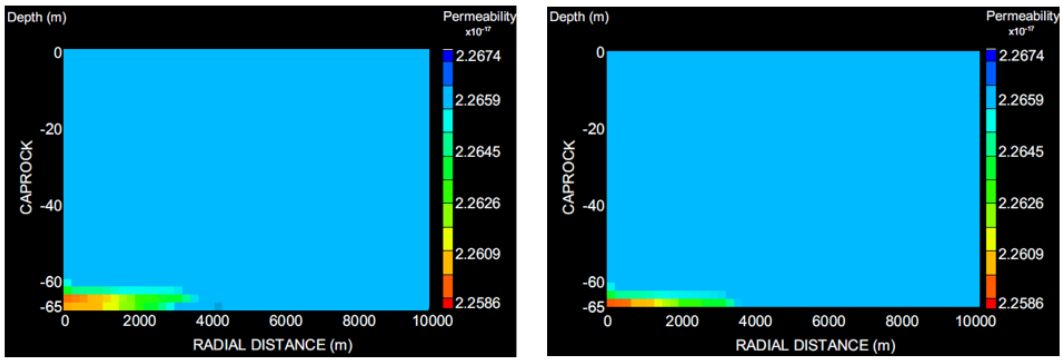

Figure 110. Low T (left) vs High T (right) - 100 years

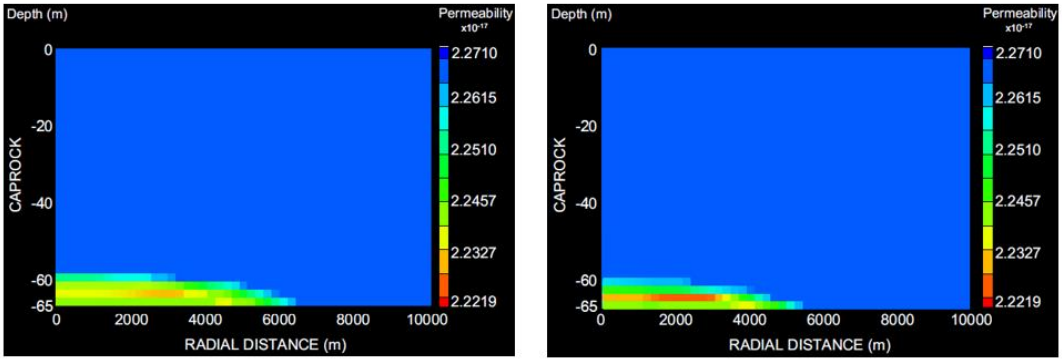

Figure 111. Low T (left) vs High T (right) - 500 years

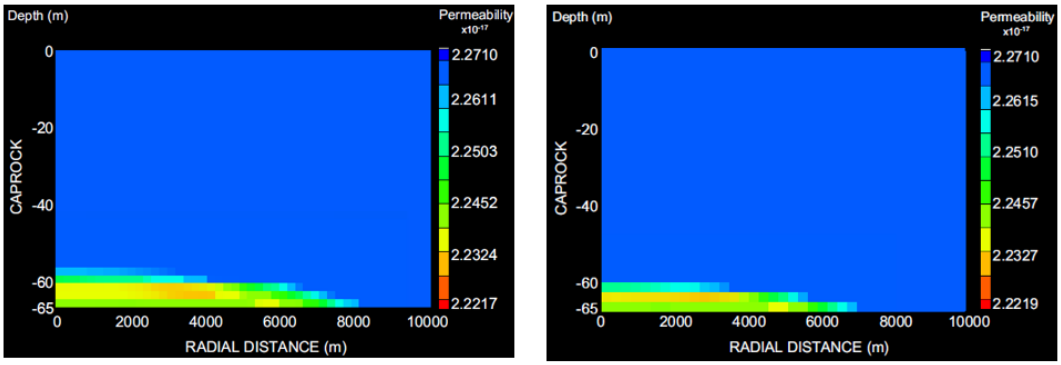

Figure 112. Low T (left) vs High T (right) - 1000 years

APPENDIX B – Comparison of CO_2 Injection at 37.2 kg/s and 120 kg/s into a Geothermal Reservoir

B.1 Supercritical CO_2 Transport (Saturation)

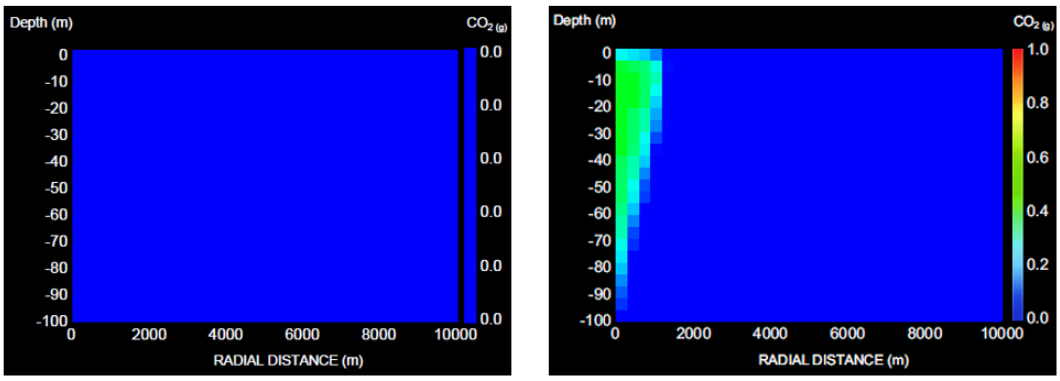

Figure 113. 37.2 kg/s (left) vs 120 kg/s (right) - 2 years

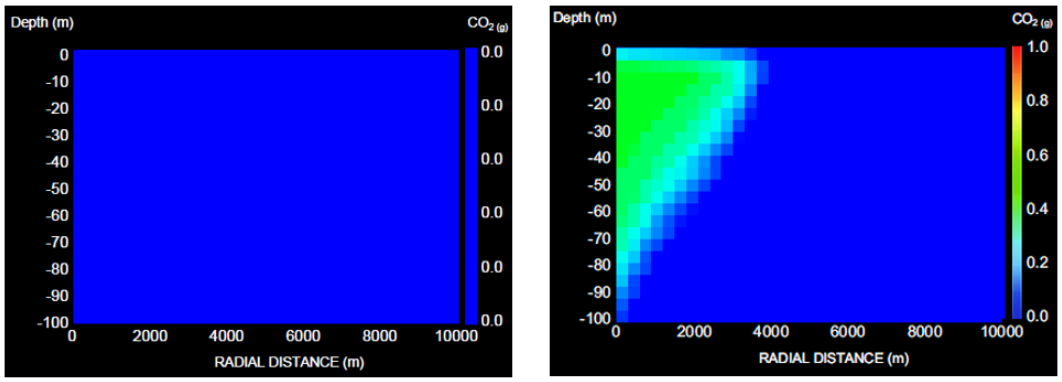

Figure 114. 37.2 kg/s (left) vs 120 kg/s (right) - 100 years

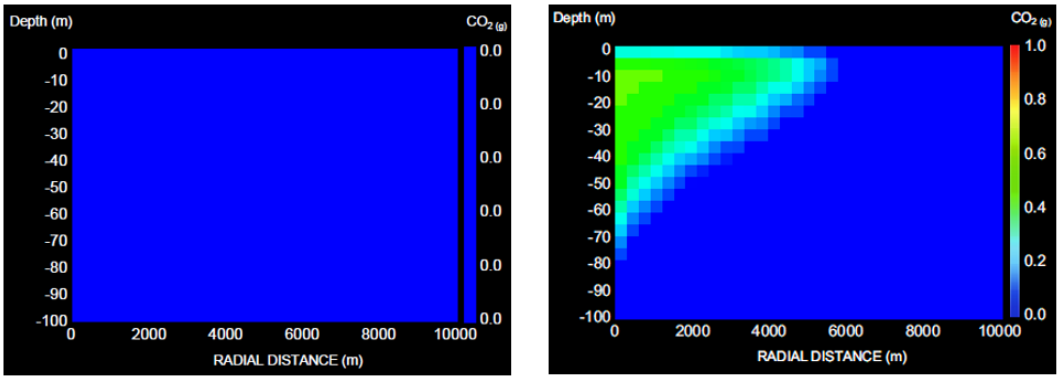

Figure 115. 37.2 kg/s (left) vs 120 kg/s (right) - 500 years

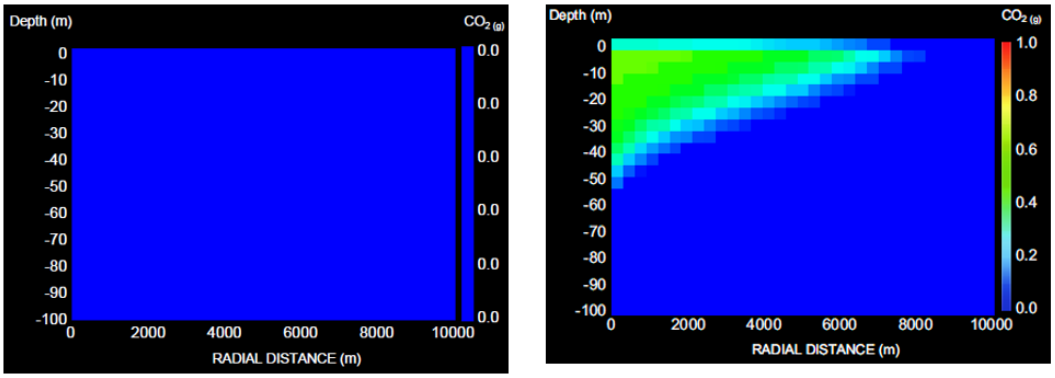

Figure 116. 37.2 kg/s (left) vs 120 kg/s (right) - 1000 years

B.2 Dissolved CO_2 Transport (Mass Fraction)

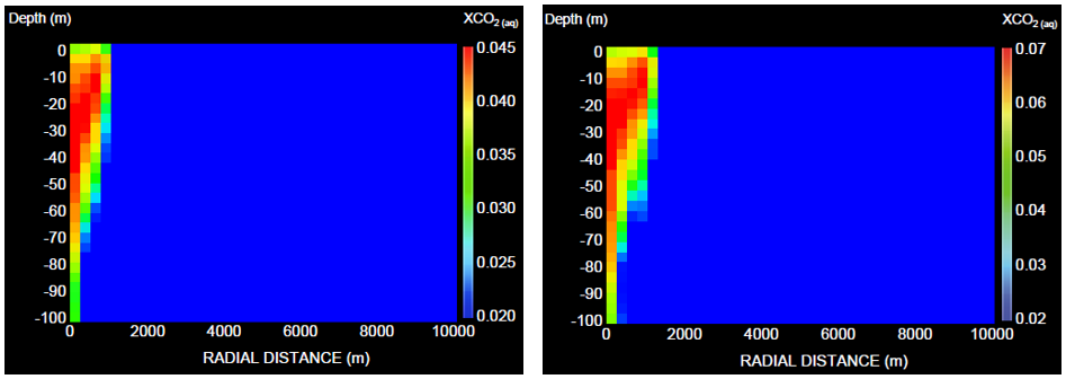

Figure 117. 37.2 kg/s (left) vs 120 kg/s (right) - 2 years

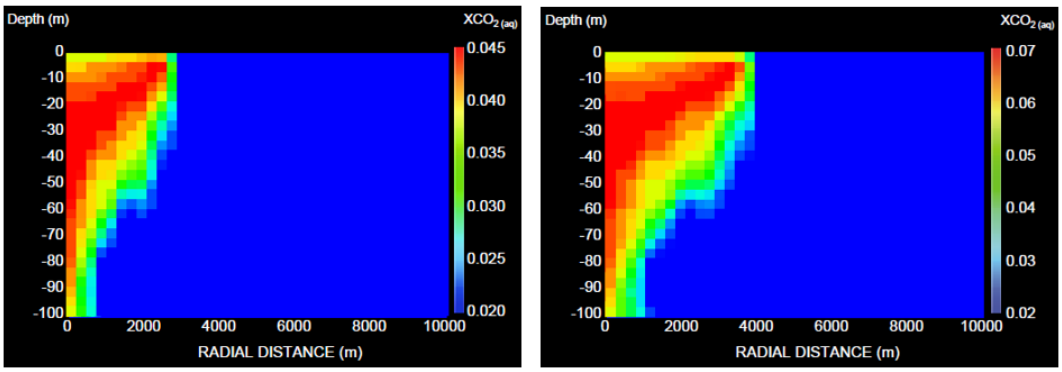

Figure 118. 37.2 kg/s (left) vs 120 kg/s (right) - 100 years

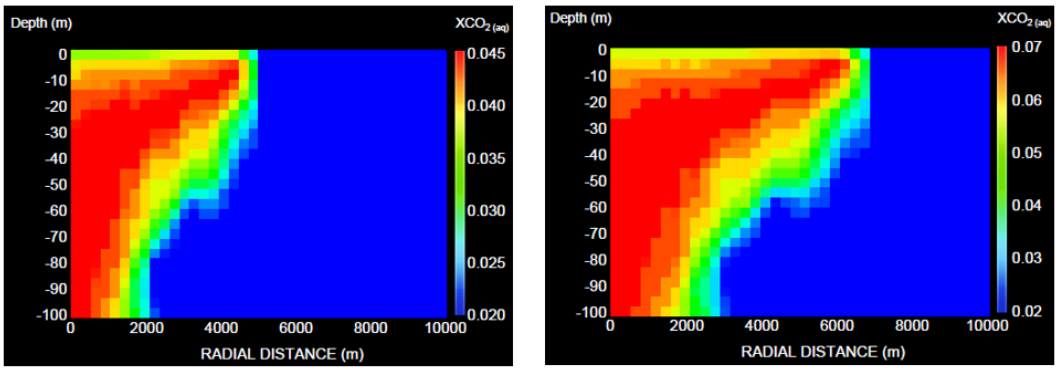

Figure 119. 37.2 kg/s (left) vs 120 kg/s (right) - 500 years

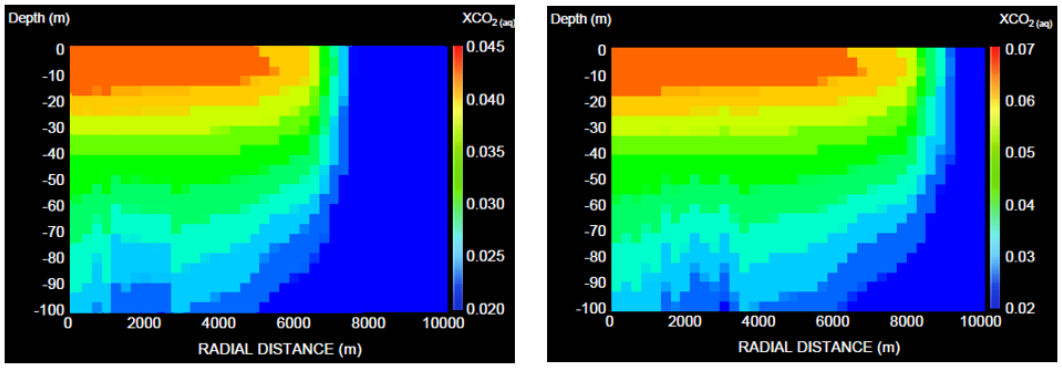

Figure 120. 37.2 kg/s (left) vs 120 kg/s (right) - 1000 years

B.3 Evolution of Calcite (Volume Change)

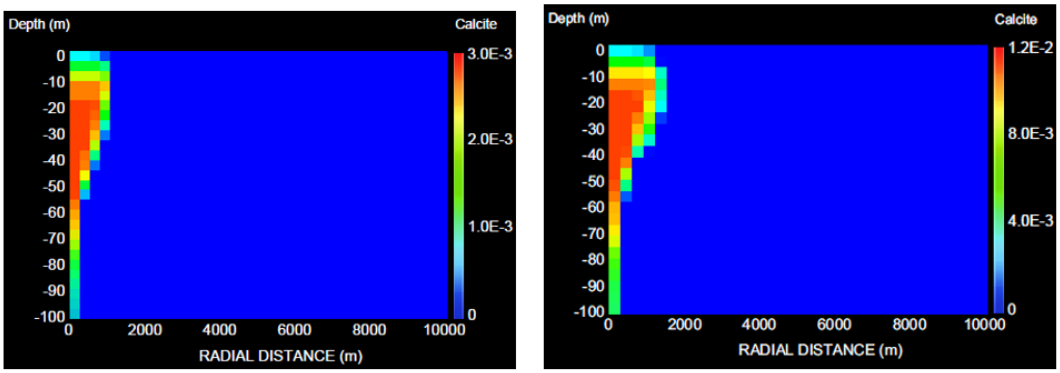

Figure 121. 37.2 kg/s (left) vs 120 kg/s (right) - 2 years

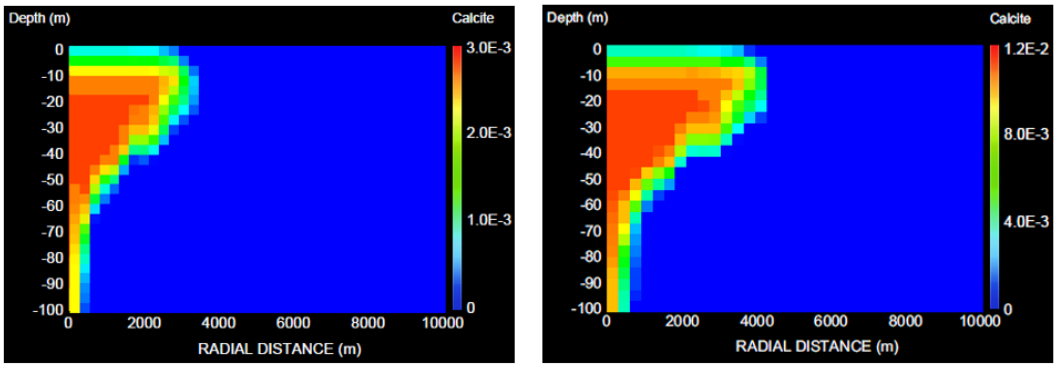

Figure 122. 37.2 kg/s (left) vs 120 kg/s (right) - 100 years

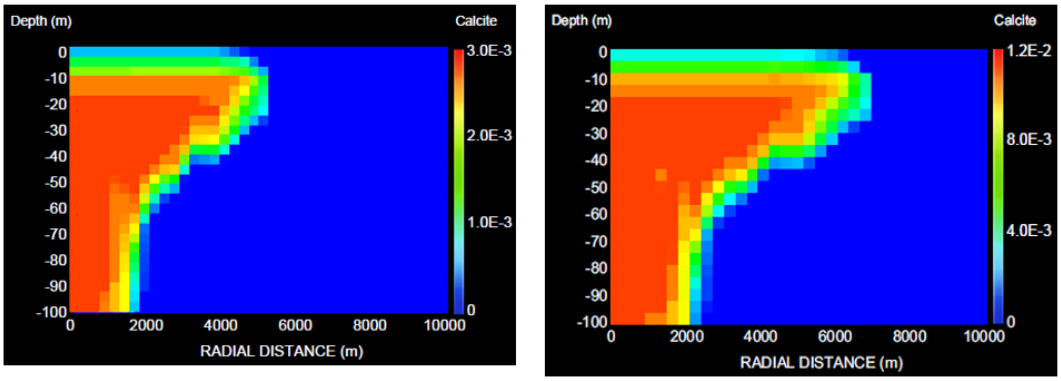

Figure 123. 37.2 kg/s (left) vs 120 kg/s (right) - 500 years

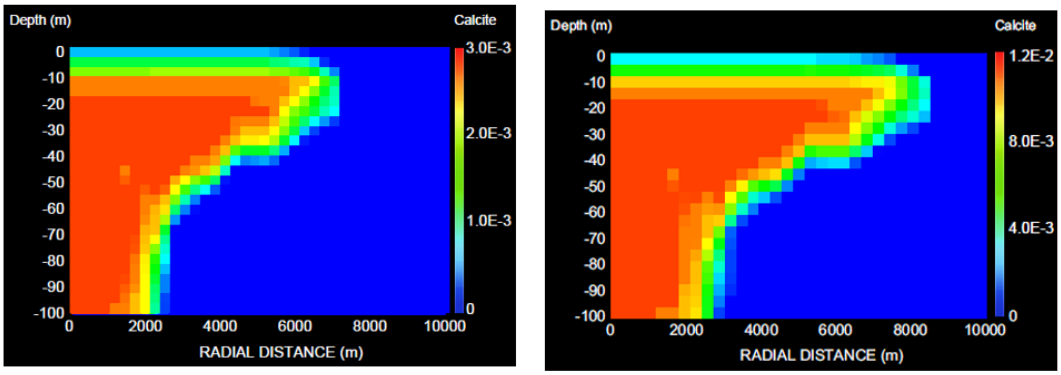

Figure 124. 37.2 kg/s (left) vs 120 kg/s (right) - 1000 years

B.4 Porosity (Fraction *10^{-2})

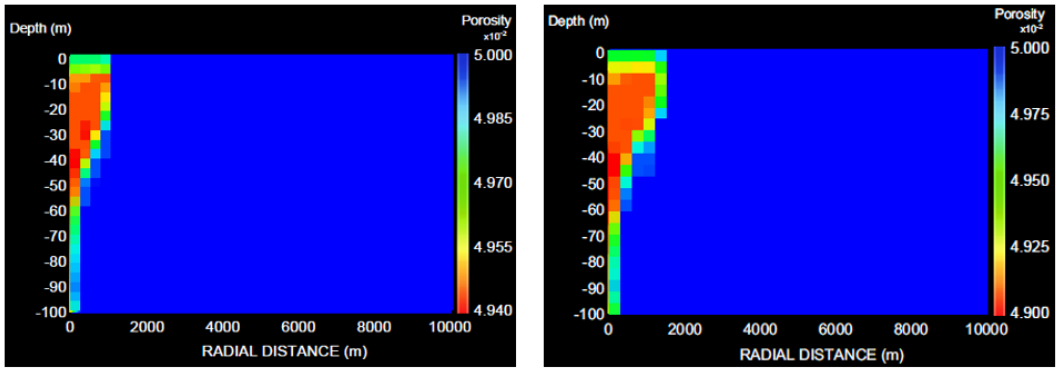

Figure 125. 37.2 kg/s (left) vs 120 kg/s (right) - 2 years

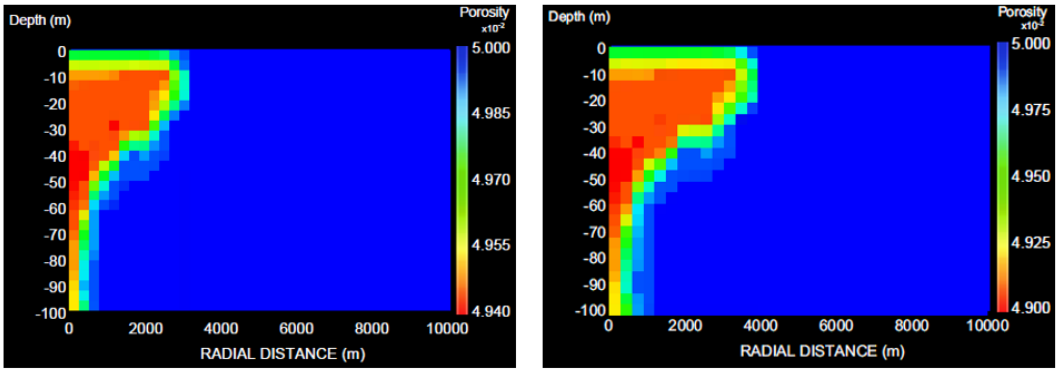

Figure 126. 37.2 kg/s (left) vs 120 kg/s (right) - 100 years

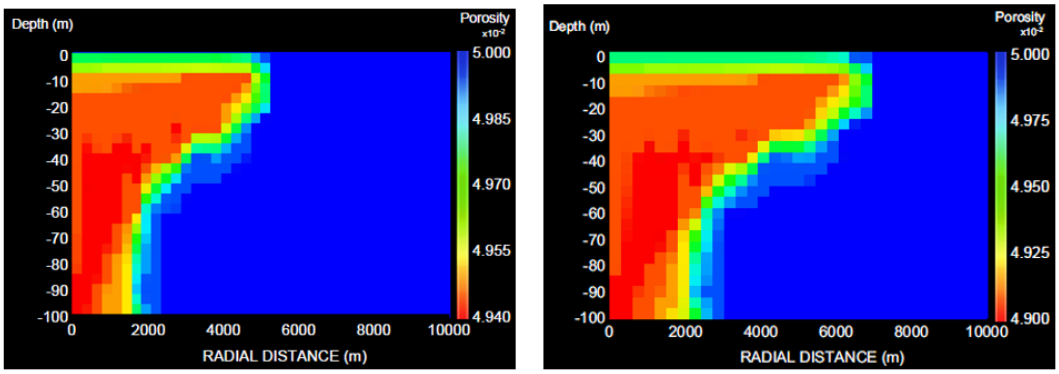

Figure 127. 37.2 kg/s (left) vs 120 kg/s (right) - 500 years

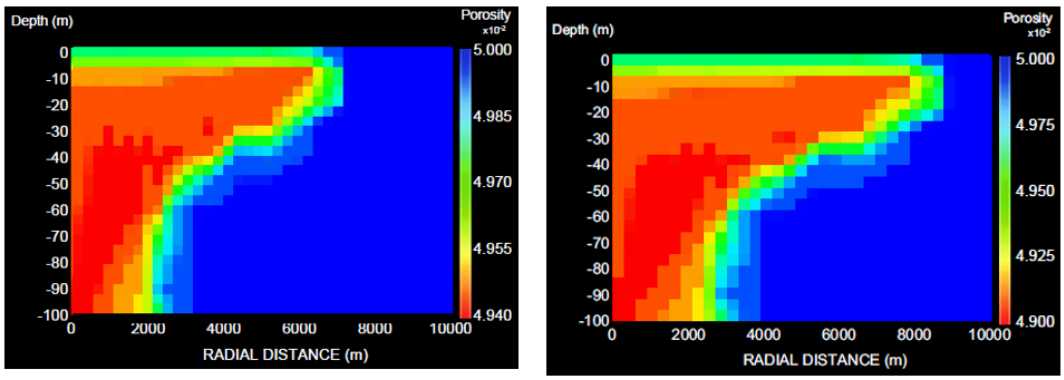

Figure 128. 37.2 kg/s (left) vs 120 kg/s (right) - 1000 years

B.5 Permeability ($m^2 * 10^{-14}$)

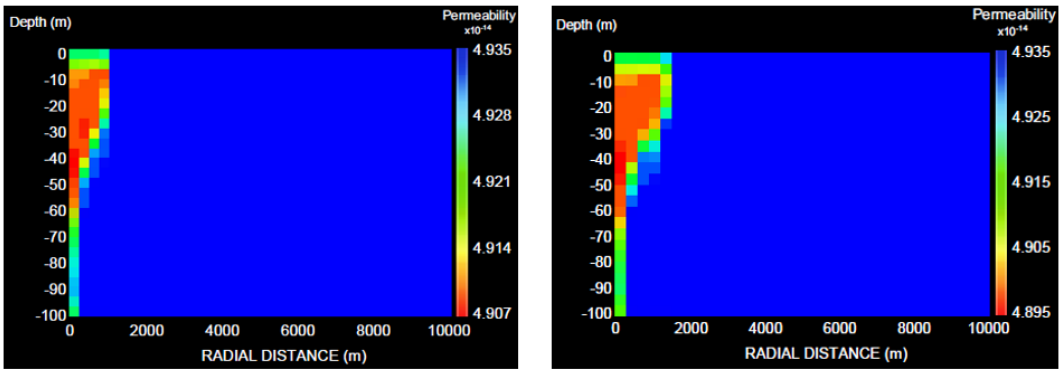

Figure 129. 37.2 kg/s (left) vs 120 kg/s (right) - 2 years

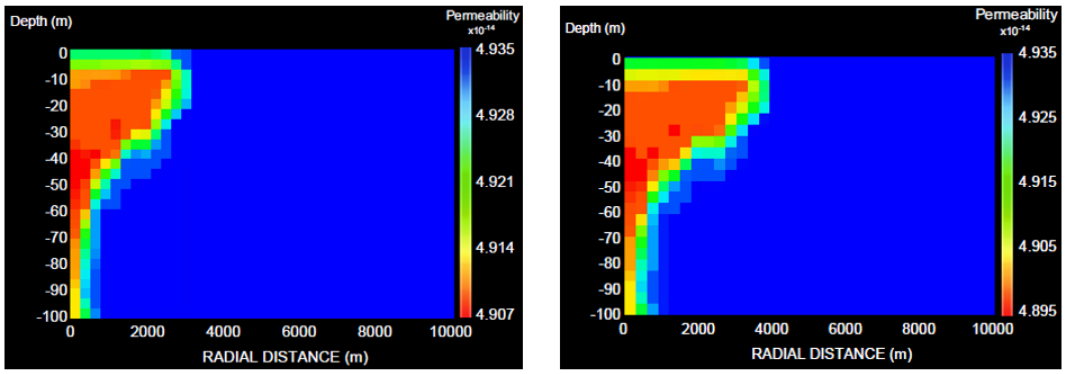

Figure 130. 37.2 kg/s (left) vs 120 kg/s (right) - 100 years

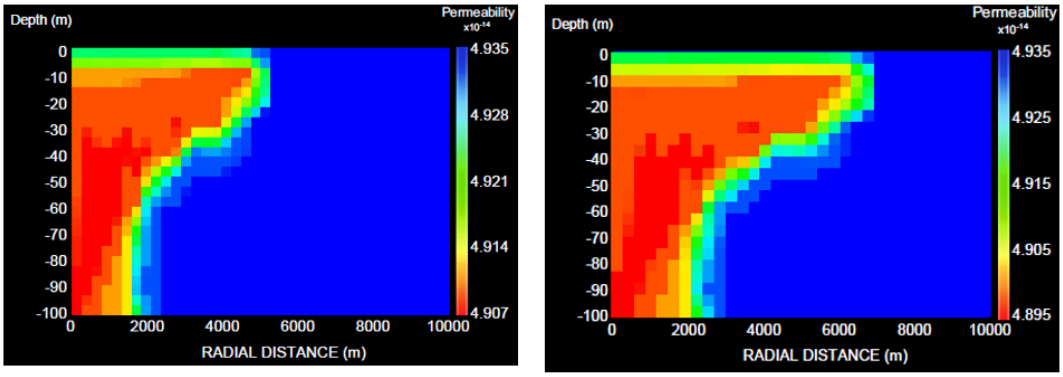

Figure 131. 37.2 kg/s (left) vs 120 kg/s (right) - 500 years

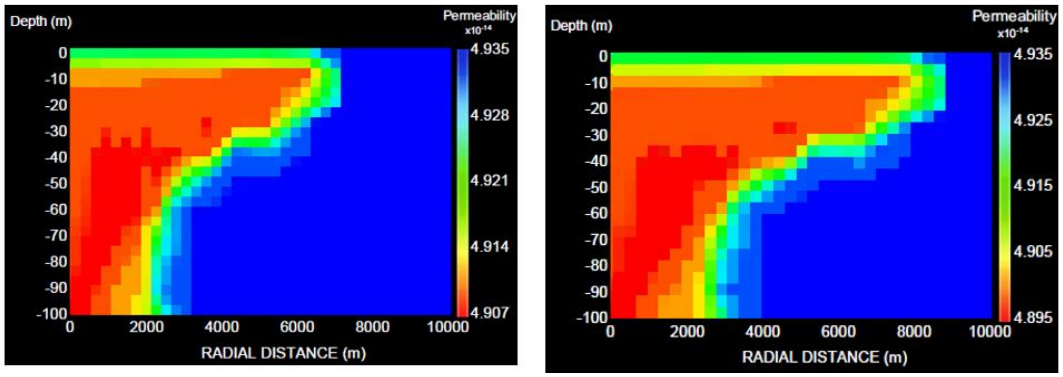

Figure 132. 37.2 kg/s (left) vs 120 kg/s (right) - 1000 years